



University
of Glasgow

Ghods, Hoda (2011) *Constraining non-standard cosmological models*.
PhD thesis.

<http://theses.gla.ac.uk/2998/>

Copyright and moral rights for this thesis are retained by the author

A copy can be downloaded for personal non-commercial research or
study, without prior permission or charge

This thesis cannot be reproduced or quoted extensively from without first
obtaining permission in writing from the Author

The content must not be changed in any way or sold commercially in any
format or medium without the formal permission of the Author

When referring to this work, full bibliographic details including the
author, title, awarding institution and date of the thesis must be given



Constraining Non-Standard Cosmological Models

Hoda Ghodsi B.Sc.

Astronomy & Astrophysics Group
School of Physics & Astronomy
University of Glasgow

Thesis submitted for the Degree of Doctor of Philosophy to
University of Glasgow

© Hoda Ghodsi, September 2011

Abstract

Current observational evidence does not yet exclude the possibility that dark energy could be in the form of phantom energy. A universe consisting of a phantom constituent will be driven toward a drastic end known as the ‘Big Rip’ singularity where all the matter in the universe will be destroyed. Motivated by this possibility, other evolutionary scenarios have been explored by e.g. Barrow, including the phenomena which he called Sudden Future Singularities (SFS). In a model consisting of such events it is possible to have a blow up of the pressure occurring at sometime in the future evolution of the universe while the energy density would remain unaffected. The particular evolution of the scale factor of the universe in this model that results in a singular behaviour of the pressure also admits acceleration in the current era. In this thesis we will present the results of our confrontation of one example class of SFS models with the available cosmological data from high redshift supernovae, baryon acoustic oscillations (BAO) and the cosmic microwave background (CMB). We then discuss the viability of the model under consideration in light of the data.

More importantly however in this pursuit, we will make the case that the cosmological constraints employed in this analysis were not blindly applied to the non-standard model in question, which is not unfortunately the practice that is always followed in the cosmology community. This applicability issue is a very important one which if neglected could potentially result in biased and unreliable outcomes. Hence, although we have worked on one example non-standard cosmological model in this thesis, this work could be viewed as a demonstration of a thought through process of testing one’s model against observations which can be applied to every other preferred model.

Contents

Abstract	1
List of Figures	8
Declaration	9
Acknowledgements	10
Foreword	11
1 A Brief Review of Modern Cosmology	12
1.1 The Journey...	13
1.2 Some essential General Relativity	14
1.3 Cosmological Models	17
1.3.1 Cosmological Parameters	24
1.4 The Celebrated Observations	36
1.4.1 Type Ia Supernovae	38
1.4.2 Cosmic Microwave Background	39
1.4.3 Baryon Acoustic Oscillations	41
1.5 Concordance Cosmology	43
1.5.1 Λ CDM Problems	47
1.5.2 Conclusions	48
2 The Exotic World	50
2.1 The Fate of the Universe and Exotic Singularities	51

2.2	Sudden Future Singularities	65
2.2.1	Sudden Singularities	65
2.2.2	Sudden Future Singularity Models	77
2.2.3	Conclusions	84
3	Data Analysis Methodology	85
3.1	Bayesian Inference	87
3.1.1	Parameter Estimation	90
3.1.2	Maximum Likelihood and χ^2 Fitting	91
3.2	Markov Chain Monte Carlo	97
3.3	Conclusions	100
4	Cosmological Constraints	102
4.1	SNe Ia Luminosity Distance-Redshift Relation	102
4.2	Cosmic Microwave Background Distance Priors	108
4.2.1	Acoustic Scale, l_a	108
4.2.2	Shift Parameter, R	109
4.3	Baryon Acoustic Oscillations Distance Parameter	115
4.4	Age of the Universe	116
4.5	Hubble Constant	117
4.6	Conclusions	118
5	Results with Fixed m	119
5.1	Fixing y_0	121
5.2	Fixing δ	133
5.3	Conclusions	142
6	Results with Varied m	144
6.1	Conclusions	152
7	Concluding Remarks	153

List of Figures

1.1	Variation of luminosity distance vs. redshift relation for different density parameters	31
1.2	Curvature of the universe seen through CMB sky map .	34
1.3	Hubble diagram	37
1.4	Supernova Cosmology Project Hubble diagram	40
1.5	CMB fluctuation map	41
1.6	SDSS redshift survey showing BAO characteristic scale	43
1.7	SNe Ia, CMB and BAO credible regions on $(\Omega_M, \Omega_\Lambda)$ space	45
1.8	SNe Ia, CMB and BAO credible regions on (Ω_M, w) space	46
2.1	Distance modulus vs. redshift comparison of SFS and concordance models from Dabrowski et al. [1]	64
3.1	$\Delta\chi^2$ values table	96
3.2	MCMC example plot	99
4.2	Distance modulus vs. redshift comparison between SFS and concordance models	107
4.3	Shift parameter definition	110
4.4	The evolution of w_{eff} as a function of redshift	114
5.1	Conditional credible regions in (n, δ) space at $y_0 = 0.99936$	122
5.2	Conditional credible regions in (n, δ) space at $y_0 = 0.999$	123

5.3	Conditional credible regions in (n, δ) space at $y_0 = 0.99$	123
5.4	Conditional credible regions in (n, δ) space at $y_0 = 0.9$	124
5.5	Conditional credible regions in (n, δ) space at $y_0 = 0.8$	124
5.6	Conditional credible regions in (n, δ) space at $y_0 = 0.7$	125
5.7	Conditional credible regions in (n, δ) space at $y_0 = 0.9999$	127
5.8	Conditional credible regions in (n, δ) space at $y_0 =$ 0.99999	128
5.9	Conditional credible regions in (n, δ) space at $y_0 =$ 0.999999	128
5.10	2D credible regions in (n, δ) plane marginalised over y_0	129
5.11	Superposition of 2D credible regions in (n, δ) plane marginalised over y_0	130
5.12	Projection effect	131
5.13	Marginalised and unmarginalised SNe Ia credible re- gions in (n, δ) space	132
5.14	Conditional credible regions in (n, y_0) for $\delta = -0.7$. . .	135
5.15	Conditional credible regions in (n, y_0) for $\delta = -1$	138
5.16	Conditional credible regions for $\delta = -1.5$	139
5.17	Superimposed conditional credible regions of all probes in (n, y_0)	140
5.18	The impact of physical conditions on credible regions. .	141
5.19	Excluded regions of (n, y_0) spaces at $\delta = -0.7$, $\delta = -1$ and $\delta = -1.5$	142
5.20	Superposition of excluded areas in (n, y_0) spaces at $\delta =$ -0.7 , $\delta = -1$ and $\delta = -1.5$	143
6.1	Multiplet of marginalised MCMC chains for the SNe Ia, CMB, R and BAO probes	148
6.2	Separated out marginalised MCMC chains in (m, y_0) plane	149

6.3	Multiplet of “thinned” marginalised MCMC chains for the SNe Ia and BAO probes together with the top 68% of the CMB, R chain	150
6.4	Multiplet of marginalised MCMC chains for the SNe Ia, CMB, R and l_a and BAO probes	151

Declaration

This thesis is my own composition except where indicated in the text.

September 1, 2011

Acknowledgements

My PhD journey like any other's has had its ups and downs but with the support of my loving family by my side through it all I have managed to get past many obstacles along the way. Therefore, first and foremost I would like to thank my family for always being there. I would then like to express my deepest gratitude towards Martin Hendry, my ever helpful and supportive supervisor. He was the light at the end of the tunnel at difficult times and has taught me invaluable lessons. I will always remember his helpful 'learn to unlearn' motto for data analysis!

I would also like to thank the astro group who have always been very helpful. In particular I would like to thank Norman Gray who always solved everything!

I must also thank Iain Sim who helped me greatly with my (never ending) IT problems.

Many thanks to Prof Reza Mansouri who kindly gave me the opportunity to spend time at the IPM School of Astronomy in the summer of 2010. I look forward to starting my first postdoc at IPM.

Thanks to our collaborators Mariusz Dabrowski and Tomek Denkwicz for the work we did (and still have to do) together.

And last but not least I want to thank my dear friends who made my PhD life easier for me.

Finally I would like to thank the university for the scholarship. I would also like to thank the department for funding my conference trips.

Foreword

This thesis is a result of the work undertaken at the University of Glasgow during the period from September 2007 to September 2011. I present this work in seven chapters which are organised as follows:

Chapter 1 presents a brief overview of modern cosmology and the standard model while in addition it detours into the non-standard world regarding the ultimate fate of the universe which is relevant to the non-standard cosmological model investigated.

Chapter 2 details the Sudden Future Singularity (SFS) model at length by providing a thorough review of the relevant literature.

Chapter 3 discusses the data analysis methodology and techniques employed in testing the SFS model.

Chapter 4 provides an account of all the cosmological probes utilised in our model investigations and their confrontation with the data.

Chapter 5 & 6 report the results of our investigations of the SFS model which are divided into two separate sections corresponding to two different paths of investigation.

Chapter 7 concludes the thesis by summarising this work and discussing future directions.

Chapter 1

A Brief Review of Modern Cosmology

Cosmology is itself a modern science. Despite that truth that the skies have always caused humankind to wonder about its bewildering mysteries and our place within it, it was not until the 1960s that (as Douglas Scott [2] puts it) cosmology transformed from an armchair activity in people's free time to a proper science. What began as such an armchair activity has now given us the Standard Cosmological Model which could be considered as one of the greatest scientific achievements of the 20th century. Cosmology, this "bold endeavour" as Andrew Liddle [3] puts it, has come to progress so remarkably through advances made in the technology of observations and the mathematical machinery. With ever more precise observations that are being made now we should interpret modern cosmology really as "precision cosmology", a term first coined by Michael Turner [4].

We will now take a very brief look at what one might refer to as a *cosmological* journey of thought, considering the scales involved, that has taken us to where we are now.

1.1 The Journey...

Throughout history one observes humankind's desire for seeking special stances in the universe from Ptolemy's Earth-centred to Copernicus' Sun-centred universes. Even after the Herschels discovered the Milky Way in the 1700s, they thought that we are located at the centre of this cosmic structure. Not to disappoint this expectation, the works of Shapley and Baade in early 1900s and 1952 respectively showed that we are in fact located at some two thirds of the distance from the centre of the galaxy and that our Milky Way galaxy is a typical galaxy in the universe [3]. We have therefore come a long way to comprehend that we occupy a not so special place in this fantastically vast universe.

What we perceive as modern cosmology today has its roots laid down in the *Copernican Principle* which states that the Earth is not in any special and centred position and rather it revolves around the Sun together with the other planets. Nicolaus Copernicus brought back to life the idea of a heliocentric universe in 16th century some 1800 years after its first proposition by Aristarchus whose idea could not overcome Ptolemy's geocentric model at the time. Copernicus' motivation for his model was to do with explaining the apparent retrograde motions of the planets in the sky. He demonstrated that one can do away with Ptolemy's complicated epicycle system which was proposed to explain the observed apparent reversing of the motion of the planets in the sky.

Generalising the Copernican Principle to the whole universe, we arrive at a much more powerful assumption known as the *Cosmological Principle*, which states that the universe is homogeneous and isotropic on sufficiently large scales. *Homogeneity* implies that the universe looks

the same at every point in space and *isotropy* means that the universe looks the same in all directions. We think the minimum scale above which the cosmological principle starts to hold is about 100 Mpc, which is the scale of the largest structures observed in galaxy redshift surveys. This scale is still very small compared to the size of the observable universe.

Now to see how the Cosmological Principle shapes a standard model for us, we require a basic foundation of General Relativity.

1.2 Some essential General Relativity

Einstein's theory of General Relativity (GR) forms the basic foundation of modern cosmology as we know it today. It is an essential tool in understanding our expanding universe. The theory of GR, which was published in 1916 relates the curvature of the universe to the force of gravity. Gravity is included in the *metric* of the space-time under consideration. This metric is what provides us with invariant, observer independent distances. Indeed this observer/coordinate independency is the beauty of GR and it implies that all laws of physics are unchanged from one coordinate system to another. In our 4-dimensional universe (comprised of 3 spatial and 1 time coordinates) the invariant interval between space-time events is written as:

$$ds^2 = \sum_{\mu, \nu=0}^3 g_{\mu\nu} dx^\mu dx^\nu, \quad (1.1)$$

where the indices μ and ν run over 0 to 3 corresponding to time ($dx^0 = dt$) and the 3 other spatial coordinates and $g_{\mu\nu}$ is the metric which is a symmetric matrix. As an example, Special Relativity as

described by the flat Minkowski space-time has the metric, $g_{\mu\nu}=\eta_{\mu\nu}$ which is:

$$\eta_{\mu\nu} = \begin{pmatrix} -1 & 0 & 0 & 0 \\ 0 & 1 & 0 & 0 \\ 0 & 0 & 1 & 0 \\ 0 & 0 & 0 & 1 \end{pmatrix}, \quad (1.2)$$

where the signature $(- + + +)$ has been used. Since we already have gravity included in the metric we need not to consider gravity as an external force which would require to be accounted for separately and instead we can imagine a distorted or curved space-time where particles move freely on what are known as *geodesics*. A geodesic is the shortest path a particle would follow in a space-time when not acted upon by any forces. The way geodesics behave is therefore dictated by the form of the metric adopted.

More specifically two point particles starting to move in parallel lines will deviate from straight lines in a curved space-time dictated by a curved metric. This curvature is mathematically given by the amount of deviation of the point particles' geodesics known as *geodesic deviation*. More precisely, curvature is mathematically related to the acceleration of geodesic deviation that occurs in a non-uniform gravitational field. Hence this shows the equivalent treatment of gravity and acceleration in GR and how the metric includes gravity.

In an expanding universe, the proper distance between two points is scaled by the universe's expansion. That is if the universe is scaled up according to a scale factor, $a(t)$, distances will be multiplied by this factor too. Therefore, if we take the space-time in the universe to be flat as in the Minkowski space-time for now, the metric would take

the form of:

$$g_{\mu\nu} = \begin{pmatrix} -1 & 0 & 0 & 0 \\ 0 & a^2(t) & 0 & 0 \\ 0 & 0 & a^2(t) & 0 \\ 0 & 0 & 0 & a^2(t) \end{pmatrix}. \quad (1.3)$$

This metric is the famous *Friedmann-Lemaitre-Robertson-Walker* (FLRW) metric which is the general form of the metric satisfying the Cosmological Principle. We will generalise this metric later on in §1.3 to account for the curvature of the universe as well.

Energy and matter as the sources of gravity have not entered the discussion thus far. This is where *Einstein's field equations* come in. In the theory of GR it is the Einstein's field equations that relate the curvature of space-time to the matter/energy that it contains. These equations can be written as:

$$G_{\mu\nu} + \Lambda g_{\mu\nu} = \frac{8\pi G}{c^4} T_{\mu\nu}, \quad (1.4)$$

where $G_{\mu\nu}$ is the Einstein tensor, which encodes information about the curvature of the universe, Λ is the non-zero cosmological constant, $g_{\mu\nu}$ is the metric of the space-time, G is Newton's gravitational constant, $T_{\mu\nu}$ is the energy-momentum tensor which relates to the matter content of the universe and c is the speed of light. Einstein first introduced Λ in his equations to create a static solution which was believed to be the model of the universe at that time. But after the discovery of the expansion of the universe by Hubble's observation in 1929 [5] that demonstrated that galaxies are receding away from us at a rate proportional to their distance from us, Einstein reasoned that Λ should be set to zero and famously referred to this mistake as his "greatest

blunder”. After some 50 years however, cosmologists discovered that direct and indirect observations (which shall be discussed later) all call for the return of a positive cosmological constant [6].

The other component of the Einstein equations is the energy-momentum tensor. The Cosmological Principle’s assumptions of homogeneity and isotropy of the universe on large scales means that we can therefore treat the cosmological fluid as a perfect fluid which has an energy-momentum tensor of the form:

$$T_{\mu\nu} = (p + \rho)u_{\mu}u_{\nu} + pg_{\mu\nu}, \quad (1.5)$$

where, ρ is the mean density, p is the isotropic pressure, u_{μ} is the 4-velocity of the fluid element and $g_{\mu\nu}$ is the metric tensor describing the geometry of the background space-time.

Equipped now with the necessary GR tools that we require, in the next section we will see how cosmological models are constructed from the GR foundations set out here.

1.3 Cosmological Models

It is not possible to solve Einstein’s equations analytically without making some simplifying symmetrical assumptions. The Cosmological Principle provides us with such assumptions. As talked about earlier, it implies that the universe is homogeneous and isotropic on sufficiently large scales. The best evidence for this assumption comes from the uniformity of the temperature of the *Cosmic Microwave Background* (CMB) radiation to a high degree across the sky (which will be explained in more detail in §1.4.2). Putting this and the fact that we

occupy no special place in the universe (the Copernican Principle) together we see that the Cosmological Principle is indeed a well-justified assumption (on large scales).

The metric describing a homogeneous and isotropic space-time is the FLRW metric. We introduced the FLRW metric for a flat space-time in §1.2. We now generalise that for a space-time with any curvature which can be written in the form:

$$ds^2 = -c^2 dt^2 + a^2(t) \left(\frac{dr^2}{1 - kr^2} + r^2 d\theta^2 + r^2 \sin^2 \theta d\phi^2 \right), \quad (1.6)$$

where $a(t)$ is the scale factor, which measures the expansion of the universe, (r, θ, ϕ) are the so-called *comoving* spatial coordinates and k is the curvature constant which can be scaled to take up discrete values of 0, -1 and +1 corresponding to flat, open and closed models. In a comoving coordinate system, observers are “attached” to the expanding background and hence the coordinate distance between them does not change with the expansion. To work out the *proper distance* between these observers we use the scale factor at the required moment in time: $d = a(t)s$, where d is the proper distance at time t between two observers separated by the comoving distance, s .

Now with the metric of the underlying space-time and the energy-momentum tensor specified through simplifying assumptions of the Cosmological Principle we can solve Einstein’s field equation. Alexander Friedmann first solved these equations in 1922 and arrived at the most important equations in cosmology, the well-known *Friedmann equations* which describe the evolution of the scale factor in an expanding universe:

$$\left(\frac{\dot{a}}{a}\right)^2 = \frac{8\pi G}{3}\rho - \frac{kc^2}{a^2} + \frac{\Lambda c^2}{3} \quad (1.7)$$

and

$$\left(\frac{\ddot{a}}{a}\right) = -\frac{4\pi G}{3}\left(\rho + \frac{3p}{c^2}\right) + \frac{\Lambda c^2}{3}, \quad (1.8)$$

where a is the scale factor, an overdot denotes derivative with respect to cosmic time, ρ and p are the energy density and the pressure, G is Newton's gravitational constant and Λ is the cosmological constant.

Now to be able to solve these equations we need to know how the matter content evolves in the universe. This is given by the fluid equation which can be derived through requiring the conservation of energy in an expanding universe:

$$\dot{\rho} + 3\frac{\dot{a}}{a}\left(\rho + \frac{p}{c^2}\right) = 0. \quad (1.9)$$

Furthermore, the other ingredient needed for solving Friedmann equations is a relation between the energy density, ρ and the pressure, p . This is known as the *equation of state*:

$$w = \frac{p}{\rho c^2}, \quad (1.10)$$

where, w is called the equation of state parameter. For pressure-less (non-relativistic) matter $w = 0$ and for radiation $w = 1/3$. Moreover, in general for a fluid with an equation of state parameter of w , from Equation 1.9 we have:

$$\rho = \rho_0 \left(\frac{a_0}{a} \right)^{3(1+w)}, \quad (1.11)$$

where the subscript 0 denotes the present day value, here and throughout. Therefore, for non-relativistic matter we have: $\rho \propto a^{-3}$, which is as expected; density drops as the volume expands. And for radiation the relation is: $\rho \propto a^{-4}$, which is also to be expected. That is, in the case of radiation which has both pressure and energy density, in addition to the drop in density due to the expansion, the wavelength of radiation is stretched by the scale factor and hence $\rho \propto a^{-3}a^{-1} = a^{-4}$.

This phenomenon of the stretching of the wavelength of electromagnetic radiation due to the expansion of the universe is called the *cosmological redshift*. The name arises from the fact that the stretching of a wavelength makes it longer and hence towards the red end of the electromagnetic spectrum. We define redshift, z , by the change in the wavelength of light divided by the emitted wavelength:

$$z = \frac{\lambda_{\text{obs}} - \lambda_{\text{em}}}{\lambda_{\text{em}}} = \frac{a_0}{a}, \quad (1.12)$$

where λ_{obs} and λ_{em} correspond to the observed and emitted wavelengths respectively.

We now define the parameter known as *the critical density* to be the density required for the universe, with $\Lambda = 0$, to be flat. Setting $k = \Lambda = 0$ in Equation 1.7 corresponding to a flat universe with no cosmological constant we get:

$$\rho_{\text{crit}} = \frac{3H^2}{8\pi G}, \quad (1.13)$$

where we define the Hubble parameter, H , as the rate of expansion

as:

$$H = \frac{\dot{a}}{a}, \quad (1.14)$$

where again an overdot represents derivative with respect to cosmic time. We write today's Hubble parameter as:

$$H_0 = 100h \text{ km s}^{-1}\text{Mpc}^{-1}, \quad (1.15)$$

where the dimensionless, h parameterises our lack of certainty in the Hubble parameter. However we do know that $0.5 \leq h \leq 1$ and the latest observations by the Hubble Space Telescope suggest that $h = 0.738 \pm 0.024$ [7]. We can now write the current critical density, $\rho_{\text{crit},0}$ as:

$$\rho_{\text{crit},0} = \frac{3H_0^2}{8\pi G} = 1.88h^2 \times 10^{-29} \text{ g cm}^{-3}, \quad (1.16)$$

where $G = 6.67 \times 10^{-11} \text{ m}^3 \text{ kg}^{-1} \text{ s}^{-2}$ has been used. The critical density is used to define the useful dimensionless *density parameter*, Ω which is easier to work with than actual physical values:

$$\Omega = \frac{\rho}{\rho_{\text{crit}}}. \quad (1.17)$$

Writing the first Friedmann equation (1.7) in terms of today's value of the critical density we have:

$$H^2 = \frac{8\pi G}{3} \rho_{\text{crit},0} \Omega_M - \frac{kc^2}{a^2} + \frac{\Lambda c^2}{3} = H_0^2 \Omega_M - \frac{kc^2}{a^2} + \frac{\Lambda c^2}{3}. \quad (1.18)$$

Here Ω_M represents the matter and radiation constituents of the energy budget of the universe. That is, $\Omega_M = \Omega_m + \Omega_r$, where Ω_m and Ω_r are the matter and radiation density parameters. Dividing Equation (1.18) through by H_0^2 we get:

$$E^2(z) = \frac{H^2}{H_0^2} = \Omega_M - \frac{kc^2}{a^2 H_0^2} + \frac{\Lambda c^2}{3H_0^2}, \quad (1.19)$$

where $E(z)$ was first introduced in Peebles' books and papers (e.g. [8]) and has been later called the "Hubble function". It is straightforward to show that the Friedmann equation can be written in the useful form:

$$E(z) = \sqrt{\Omega_{m,0}(1+z)^3 + \Omega_{r,0}(1+z)^4 + \Omega_{k,0}(1+z)^2 + \Omega_{\Lambda,0}}, \quad (1.20)$$

where, $\Omega_{m,0}$ and $\Omega_{r,0}$ are the current dimensionless matter and radiation density parameters respectively and we define $\Omega_{k,0}$ and $\Omega_{\Lambda,0}$, the respective current curvature and cosmological constant density parameters, as:

$$\Omega_{k,0} = -\frac{kc^2}{a_0^2 H_0^2} \quad \text{and} \quad \Omega_{\Lambda,0} = \frac{\Lambda c^2}{3H_0^2}. \quad (1.21)$$

While Ω_k does not have anything to do with the actual physical density of the universe, Ω_Λ can be interpreted as the energy density of vacuum in the particle physics world. We will go on to explain these density parameters along with some other cosmological parameters in more detail in §1.3.1.

With the Friedmann equation written in the form of Equation 1.20 we can see how the evolution of the universe depends on its various matter

constituents and its curvature. In particular we can see that as we go back in time to the early universe, i.e. as $a \rightarrow 0$ which is equivalent to $z \rightarrow \infty$ the dominant term in Friedmann equation becomes the radiation term with the highest power for the redshift. We call this era in the universe's evolution the *radiation-dominated* era where the expansion of the universe is described as $a \propto t^{1/2}$. But the higher power for the redshift in the radiation term also means that it loses energy more rapidly than the pressure-less matter (the cosmological constant density parameter is negligible in the early universe). Hence there will come a time when the densities of radiation and matter will equal each other. We refer to this epoch as the *matter-radiation equality* epoch. Continuing this trend we will eventually reach the so-called *matter-dominated* era where it can be shown that $a \propto t^{2/3}$. After that the *curvature-dominated* era follows (although since it appears that curvature is zero, this era is not usually considered) and finally we get to the present Λ -*dominated* era. A universe dominated by Λ will continue its expansion into an exponential phase where $a \propto \exp(Ht)$.

A flat ($k = 0$), matter-dominated ($\Omega_M = 1$) universe is known as the *Einstein-de Sitter* universe. This type of universe is different from the *de Sitter* universe, which is the name given to the exponentially expanding Λ -dominated universe.

The different phases of the universe talked about above are possible in universes that are flat or open as the scale factor is constantly increasing. However, if the universe has positive curvature and is indeed closed, it might not even make it to the matter-dominated phase and recollapse on itself in a *Big Crunch* before reaching this phase.

Furthermore, provided Λ is not too large, a universe with matter, radiation and cosmological constant will always start from a *Big Bang*

singularity. This forms the basis for hot Big Bang models. The ‘hot’ comes from the fact that we know the temperature of radiation evolves as $T \propto a^{-1}$, hence as $a \rightarrow 0$ the universe becomes hotter and hotter ultimately culminating in a Big Bang singularity.

We now look at some of the parameters in the standard model of cosmology which are most relevant to the work in this thesis.

1.3.1 Cosmological Parameters

As in every model attempting to describe a certain physical phenomenon, any cosmological model also consists of a set of free parameters which are to be determined by observations. Moreover, indeed for any model to be testable against observations, free parameters are generally required. Here in this section we take a brief look at some of the most important cosmological parameters defined to shape the standard cosmological model.

The Hubble parameter

Perhaps the most fundamental cosmological parameter is the Hubble parameter, H , which measures the rate of expansion of the universe. This parameter is named after Edwin Hubble who first discovered the expansion of the universe in 1929 [5] through observation of distant galaxies. The current value of the Hubble parameter is known as the ‘Hubble constant’, H_0 , which measures the current rate of expansion of the universe. From Hubble’s law, which (as will be described more fully later) states that the rate of recession of galaxies is proportional to their distance from us, we know that: $v = H_0 d$, where v is the velocity and d the distance. From this relation we see that we need to determine velocities and distances of galaxies for determining H_0 .

We measure velocities through the redshift of spectral lines which is easily done today, but with the knowledge that we need to go to great distances to overshadow what are known as the *peculiar velocities* of galaxies, which are not to do with the expansion of the universe, we are faced with difficulty. Peculiar velocities of galaxies result from their motions relative to one another due to the gravitational pull of their neighbouring massive galaxies. Peculiar velocities are of order a few hundred km s^{-1} and from the cosmological principle we know that this range of values should be the same throughout the universe (i.e. they do not increase with distance as the velocity due to expansion does). With the redshift method only resulting in radial velocity measurement of galaxies we therefore need to use other distance indicators to measure the distances to these galaxies to be able to subtract off their peculiar velocities. For an accuracy limit of about 10% (which is the limit currently achievable) using redshift-independent distance indicators, we need to go to distances of about tens of Mpc to overshadow peculiar velocities. For such great distances we need to use *standard candles*, which are objects with a narrow range of luminosities everywhere in the universe, such as Cepheid variable stars and Type Ia supernovae (SNe Ia).

Cepheid variable stars are pulsating stars for which the period of luminosity is related to their absolute brightness providing us with a very useful standard candle. These objects are found in the Local Group which means that they can be well-calibrated for use at larger distances. And SNe Ia (as will be discussed further in §1.4.1) are exploding white dwarf stars which reach the Chandrasekhar limit through mass accretion from a binary companion. Therefore since the underlying mechanism for their creation is the same, their absolute magnitudes could be assumed to be constant hence yielding a standard

candle.

By measuring the apparent brightnesses of SNe Ia we should hence be able to infer their relative distances from us provided we know their absolute magnitude, which is not trivial to determine. For this we need to calibrate the distance to SNe Ia host galaxies using some other relatively closer objects like Cepheid variable stars. Prior to the launch of the Hubble Space Telescope (HST) we could only observe Cepheids up to a distance of about 4 Mpc, but after this space telescope went live the team led by Wendy Freedman [9] extended our distance measurements to about 20 Mpc through the so-called HST Key Project to determine the Hubble constant to be $H_0 = 72 \pm 8 \text{ km s}^{-1} \text{ Mpc}^{-1}$. This then allowed us to calibrate SNe Ia as secondary distance indicators and to therefore go much farther to about 400 Mpc. Such difficult long distance determinations therefore demonstrate why we parameterise the Hubble parameter as shown in Equation 1.15, where we set the dimensionless h as the placeholder for the true value [3]. As quoted before the latest observations of HST give $h = 0.738 \pm 0.024$ [7].

Density Parameters

Earlier we saw how the Friedmann equation could be written in a format where its dependence on the various density parameters corresponding to different mass-energy components in the universe could be seen clearly. This showed that the Friedmann equation describes the evolution of the universe depending on the material it contains. Here we will expand on each mass-energy component, reviewing the most important aspects of each in turn.

Matter

By matter we mean any kind of non-relativistic and pressure-less material which in cosmology is referred to as “dust”. Considering the

fully relativistic energy equation, $E^2 = m^2c^4 + p^2c^2$, for non-relativistic matter we have: $pc \ll mc^2$ which means that the energy is dominated by the mass.

We can divide the types of matter we have in the universe into the two types: *baryonic* and *non-baryonic dark matter*. Therefore we can write the matter density parameter as: $\Omega_m = \Omega_b + \Omega_{dm}$, where Ω_b and Ω_{dm} are the baryon and dark matter density parameters respectively. We will expand on these two matter components below:

- *Baryonic Matter*: This type of matter includes any form of luminous (like stars) or non-luminous matter (like low mass stars and brown dwarfs) made up of baryons. By baryons we mean protons and neutrons, which are the most stable types of baryons. Furthermore, cosmologists also traditionally include electrons in this class while they are not really baryons. While baryonic matter is the only type of “ordinary matter” we expect to see in the universe, observations suggest otherwise. Specifically, the observed rotation curves of spiral galaxies showed that instead of the velocity of objects falling off as $\frac{1}{\sqrt{r}}$, where r is the distance from the centre of the galaxy, they remain almost constant as one moves towards the edge of the galaxy. This situation calls for a greater gravitational pull from the matter inside the galaxy, which could hold these high speed objects bound to the galaxy than could be provided by the luminous matter we observe. The same kind of observations have been made in the case of the motion of galaxies in clusters and clusters of galaxies in superclusters. Naturally, one might think that the required extra gravitational pull could come from non-luminous baryonic matter. But this option has been ruled out through construction of models based on non-luminous baryonic matter. Some kind of non-baryonic dark matter must

therefore be present.

- *Dark Matter*: This type of non-baryonic matter does not interact with electromagnetic radiation (neither absorbs nor emits) and hence cannot be directly detected but only through its gravitational effects as was discussed in the case of baryonic matter. While we have firmly established the fact that non-baryonic matter must be present through gravitational considerations, we have other lines of evidence to support this claim.

The density of baryons is determined through various different ways, from the gas between galaxies in galaxy groups to the anisotropies in the cosmic microwave background. Remarkably however, all these techniques agree with each other pretty well [10]. Currently the baryon density parameter is estimated to be about 0.02 which makes up about 4-5% of the total energy budget of the universe. This upper bound on the baryon density is indeed much lower than that required to explain the gravitational considerations discussed earlier. Furthermore, as we will see later on in this section the cosmic microwave background data suggest that we live in a nearly flat universe with a total matter density nearly equal to 1. Putting these data together we end up with strong evidence for the existence of non-baryonic dark matter.

Moreover, we usually mean the collision-less, slow moving Cold Dark Matter (CDM) when we refer to dark matter as opposed to Hot Dark Matter (HDM) which has a large pressure and is not desirable for structure formation. More specifically, by HDM we mean light dark matter particles which were relativistic ($v \approx c$) at the time when they decoupled from baryons and photons of the early universe (noting that dark matter interacted more strongly with matter at early times), such as neutrinos with mass

of order a few eV. And by CDM we mean the kind of heavy dark matter particles that were moving slowly ($v \ll c$) when decoupled from baryons and photons such as neutralinos. CDM particles have masses in the range of 10 to 1000 GeV. There is also the Warm Dark Matter (WDM) which had speeds intermediate between those of HDM and CDM with mass of order 1-10 keV.

Similar to baryon density, various methods for measuring dark matter agree well with one another. For instance, dark matter estimates from galaxy redshift surveys and cosmic microwave background fluctuations observations (which we will discuss in §1.4.2) yields a value of about 25% of the total density for this matter constituent corresponding to $\Omega_{dm} \simeq 0.25$.

Many experiments are now underway to try and detect the dark matter particles through the effects of their hopefully non-gravitational interaction with ordinary matter. It is believed that in this case dark matter particles interact through the weak nuclear force with ordinary matter. These hypothetical dark matter particles are therefore called Weakly Interacting Massive Particles (WIMPs)“ one example of which was given above, the neutralino. WIMPs are predicted by supersymmetric extensions to the standard model of particle physics. Other exotic particles hypothesised as CDM candidates are the axions, WIMPzillas, photinos and gravitinos.

Radiation

Once the dominant form of energy in the universe, radiation density is almost negligible today. The dominant portion of radiation in the universe in all wavelengths is found in the Cosmic Microwave Background (CMB) which is the relic radiation left over from the Big Bang

and fills up the whole universe. We will expand on this later in §1.4.2 but for now we will mention that the energy density of radiation can be calculated from the temperature of the CMB, $T = 2.7\text{K}$, to be:

$$\Omega_r = 2.47 \times 10^{-5} h^{-2}. \quad (1.22)$$

Therefore we can see that it is much smaller compared to the matter density today but not completely negligible.

Dark energy

The realisation of the existence of this energy component came through two sets of evidence. Firstly, when it was shown theoretically through inflation and observationally through the CMB (as will be discussed in §1.4.2) that the universe is very nearly flat with a total density equal to the critical density, there appeared a deficiency in the total energy budget of the universe. The observations of matter had corresponded to only about 1/3 of the critical density. Therefore, cosmologists reasoned that the rest must be in a kind of as yet unknown energy, dubbed *dark energy*. And the second evidence laid in the observed distance-redshift relation as probed by SNe Ia [11], [12]. To see how exactly this was done, we can write the luminosity distance, $d_L(z)$, in an expanding universe as:

$$d_L(z) = \frac{c(1+z)}{H_0} \int_0^z \frac{dz'}{E(z')}, \quad (1.23)$$

where the integral is from now ($z = 0$) to the redshift of the object, z , c is the speed of light, H_0 is the Hubble constant and $E(z)$ is the Hubble function as defined before. Considering a flat universe with negligible radiation density, the luminosity distance reduces to:

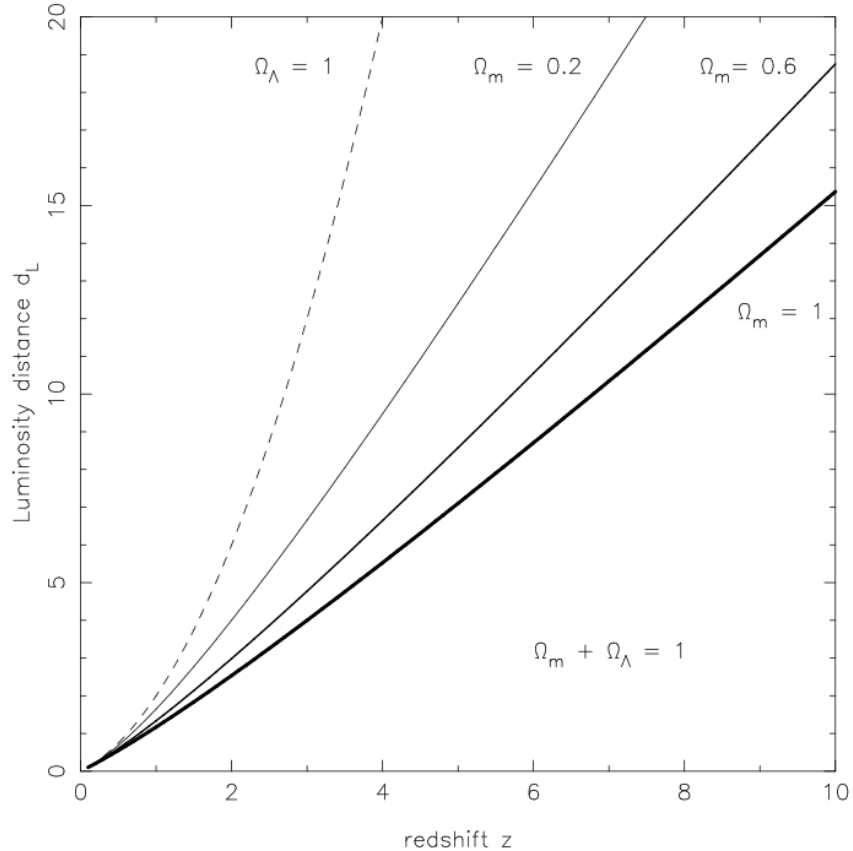


Figure 1.1: The plot shows the variation of the luminosity distance, d_L , (in units of the Hubble radius, cH_0^{-1}) as a function of redshift, z , for varying matter and cosmological density parameters in a flat model ($\Omega_M + \Omega_\Lambda = 1$, which follows from Equation 1.20 by neglecting the radiation term today). Figure from [13].

$$d_L(z) = \frac{c}{H_0} \int_0^z \frac{dz'}{\sqrt{\Omega_m(1+z')^3 + \Omega_\Lambda}}, \quad (1.24)$$

where, Ω_m and Ω_Λ are the usual matter and cosmological constant density parameters. Hence, we can see how the luminosity distance is dependent on the expansion of the universe through Ω_m and Ω_Λ . Figure 1.1 shows different luminosity distance-redshift relations for varying matter and cosmological constant contents.

Through observations of distant SNe Ia cosmologists therefore concluded that – at least within the standard model – there must be other forms of energy present in the universe. We now know that

dark energy must fill up about 70% of the total energy density of the universe corresponding to $\Omega_\Lambda \simeq 0.7$.

Dark energy in the standard model is in the form of the cosmological constant, Λ , which has negative pressure and constant energy density. For the cosmological constant therefore $w = -1$.

The cosmological constant can be physically interpreted as the energy density of vacuum which fills space-time in the absence of any particles. However, there is a large discrepancy between the observed energy density of this effective fluid and the value derived for it by particle physicists. The difference is of order a mere 10^{120} ! This is known as the *cosmological constant problem*. Therefore, even though cosmological observations are generally consistent with a dark energy in the form of Λ as we will see in §1.5, cosmologists have been looking for alternatives to it, which include varying equation of state ($w = w(t)$) dark energy known as quintessence to phantom energy with super negative equation of state ($w < -1$). It can be shown easily that in general in order to have acceleration we need to have $w < -1/3$. Furthermore, one can now rewrite the Friedmann equation (1.20) in the more general form:

$$E(z) = \sqrt{\Omega_{m,0}(1+z)^3 + \Omega_{r,0}(1+z)^4 + \Omega_{k,0}(1+z)^2 + \Omega_{de,0}(1+z)^{3(1+w)}}, \quad (1.25)$$

where, $\Omega_{de,0}$ would be the current value of the dark energy density parameter and w is its constant equation of state parameter.

The consequences of different dark energy candidates for the final fate of the universe (as will be discussed in §2.1) are immense and yet current observations cannot still distinguish between these options.

Indeed finding the source of the enigmatic dark energy is one of the biggest mysteries facing cosmologists today.

To clarify further the situation we are in with this mysterious dark energy, here we briefly mention some of the possible dark energy candidates proposed to date. As mentioned above dark energy equation of state can vary in time hence it could take the form of a scalar field similar to that which drove inflation. Several scalar-field dark energy model have been proposed such as the abovementioned quintessence and phantom fields. There are also the K-essence [14, 15] and tachyonic models [16]. As mentioned previously the phantom field corresponds to $w < -1$ and K-essence also could have this equation of state. This is an unusual property which requires a negative kinetic energy term as will be discussed in Chapter 2. Furthermore, the problem of explaining the current acceleration of the universe could be solved by questioning the general relativistic gravity of Einstein. In other words, the other approach to solving the dark energy problem is by modifying the general relativistic Friedmann evolution equations for the universe. Such investigation is done in theories such as f(R) gravity theories which modify the Einstein's GR field equations.

Curvature

As was mentioned before, curvature is presented in the form of a density parameter while it bears no physical meaning related to the actual physical density of the universe. Therefore, it is usually expressed as:

$$\Omega_k = 1 - \Omega, \tag{1.26}$$

where $\Omega = \Omega_m + \Omega_r + \Omega_\Lambda$ is the total density of the universe. Equation 1.26 follows directly from the Friedmann equation (1.7). In the same

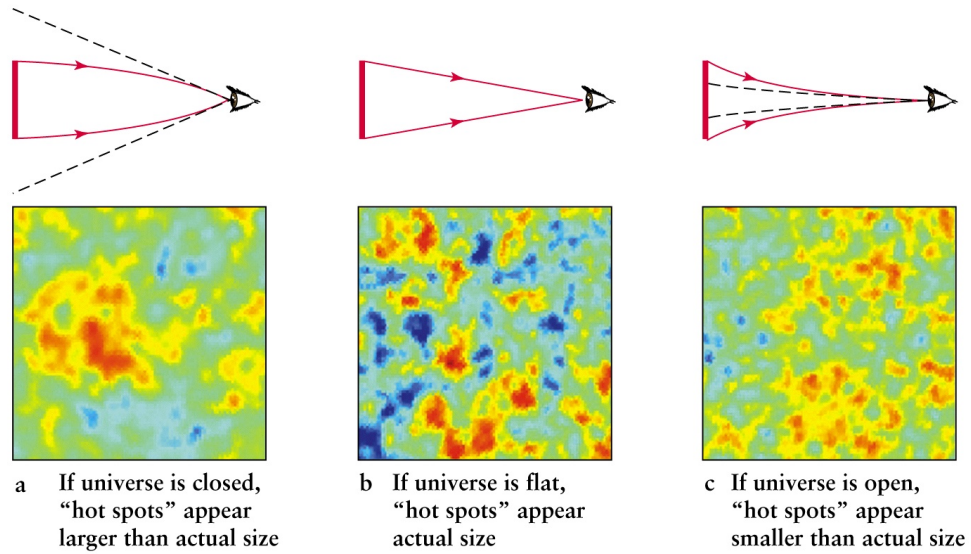


Figure 1.2: As the description under every section reads, the sizes of the spots of temperature variation in the CMB sky will be the same as the original size, smaller or larger than the actual size in flat, open and closed universes respectively. This results from the fact that light rays follow geodesics. Figure from: <http://find.spa.umn.edu/~pryke/teaching/natsci102/spring-2005/cmbmaplab/>.

way as we can use the total sum of the interior angles of triangles to work out the curvature in 2-dimensional flat, spherical and hyperbolic spaces, we can determine the curvature of the space-time manifold in our universe using light rays. This is because in GR light rays follow geodesic paths. We can use the CMB for this task. The basic principle follows that we can compare the observed sizes of hot and cold patches in the CMB sky created through temperature anisotropies (as will be discussed in §1.4.2) with the theoretically predicted sizes for universe with different curvatures. Figure 1.2 shows a schematic representation of the argument.

The observed value of the curvature is found in this way to be very close to 0 and hence we believe that we are living in a flat universe.

Current constraints from SNe Ia redshift-magnitude relation observations, baryon acoustic oscillation (BAO) (as will be discussed in Chapter 4) and the cosmic microwave background (CMB) (again as

will be discussed in Chapter 4) on Ω_M , Ω_k and the equation of state parameter, w , could be summarised as shown in Table 1.1.

Table 1.1: Current constraints on Ω_M , Ω_k and w from SNe Ia, BAO and CMB. These results are taken from the latest SNe data release in [17] which incorporate the latest results for the CMB [18] and the BAO [19].

	Ω_M	Ω_k	w
SNe Ia + BAO + CMB	$0.281^{+0.016}_{-0.015}$	-0.005 ± -0.007	$-1.026^{+0.055}_{-0.059}$

Deceleration parameter

After the discovery of the expansion of the universe, the deceleration parameter was introduced to measure the deceleration of the universe which was a logical expectation from the universe consisting of only gravitating matter. In such a universe surely gravity would win over the expansion one day and result in a decelerating universe which is doomed to recollapse. To the great astonishment of cosmologists however it was found through observations of high redshift supernovae that the universe is indeed accelerating [11], [12]. The name “deceleration” parameter has nevertheless historically remained unchanged since. We now require the deceleration parameter to be negative to imply acceleration.

To derive the deceleration parameter, consider a Taylor series expansion of the scale factor about the current time:

$$a(t) = a(t_0) + \dot{a}(t_0)[t - t_0] + \frac{1}{2}\ddot{a}(t_0)[t - t_0]^2 + \dots \quad (1.27)$$

Dividing through by $a(t_0)$ yields:

$$\frac{a(t)}{a(t_0)} = 1 + H_0[t - t_0] - \frac{q_0}{2}H_0^2[t - t_0]^2 + \dots, \quad (1.28)$$

where the current deceleration parameter will be defined by:

$$q_0 = -\frac{a(t_0)\ddot{a}(t_0)}{\dot{a}^2(t_0)}. \quad (1.29)$$

Using the Friedmann equations, (1.7) and (1.8) and the definition of the critical density in Equation 1.13, it can be shown that for a universe with matter and cosmological constant:

$$q_0 = \frac{\Omega_0}{2} - \Omega_\Lambda, \quad (1.30)$$

where Ω_0 is the total current matter density parameter and Ω_Λ is the cosmological constant density parameter. If we assume a flat universe this equation reduces to $q_0 = 3\Omega_0/2 - 1$, which means that we will have acceleration, provided $\Omega_\Lambda > 1/3$.

As a final note in this section, we go back to the comment we made regarding the relevance of the parameters discussed here to our model at the end of §1.2. The particular model we investigate in this thesis is built through kinematical considerations. That is, as we will see, the feature of the model is a specific form for the scale factor of the universe. Now the parameters discussed here are relevant in the sense that they are either kinematical parameters themselves i.e. H and q or related to kinematical considerations i.e. the density parameters. As we saw in §1.2 the density parameters appear in the Friedmann equation (1.20) which describes the evolution of the scale factor of the universe which is hence relevant to our purpose.

1.4 The Celebrated Observations

Unsurprisingly, this section must start with perhaps the most renowned cosmological observation of all time: the Hubble's discovery of the

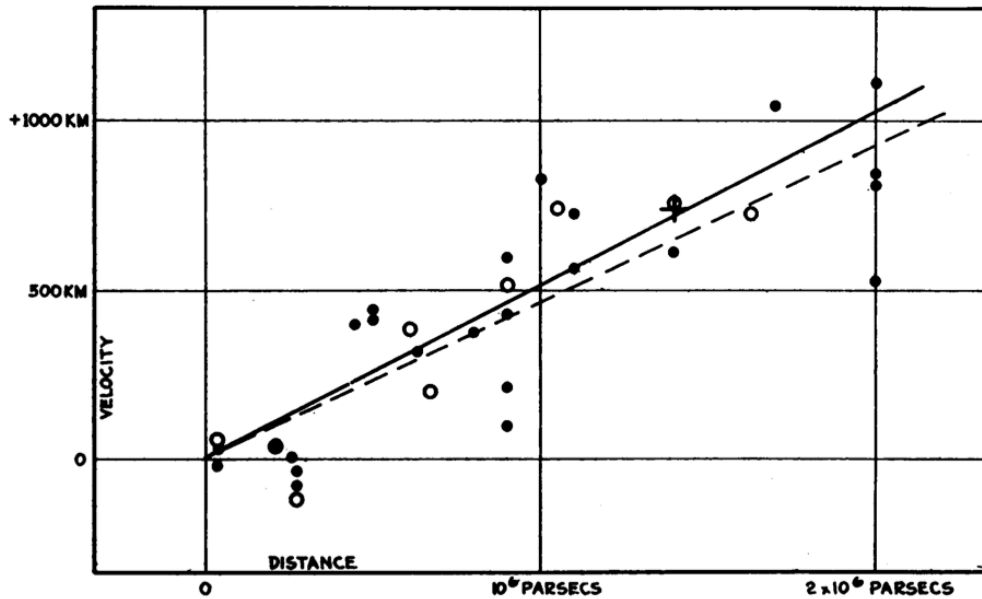


Figure 1.3: The original Hubble diagram made by Edwin Hubble himself in 1929 displaying the velocities of distant galaxies versus distance. Velocity unit should read km s^{-1} . Figure from [5].

expansion of the universe. Figure 1.3 shows the famous and revolutionary plot of velocity against distance of distant galaxies made by Edwin Hubble himself in 1929. Through the data presented in this plot he demonstrated that the velocities of galaxies are proportional to their distances from us and hence established the law of expansion of the universe which became known as *Hubble's law*:

$$v = H_0 d, \quad (1.31)$$

where v is the velocity of object, d is the distance to the object and H_0 is the constant of proportionality known as the Hubble constant, which measures the current rate of expansion of the universe.

Subsequent revolutionary observational discoveries followed the work of Hubble. We will discuss some of these below.

1.4.1 Type Ia Supernovae

After the discovery of the expansion of the universe, this expansion was further probed using Type Ia supernovae (SNe Ia) which are ideal astronomical objects for distance determination. These objects are created through the explosion of accreting white dwarf stars when they reach the Chandrasekhar limit. Therefore since they all have the same progenitors and are triggered through a consistent underlying mechanism we can assume that they have constant absolute magnitude and can hence use them as standard candles. Although SNe Ia are not perfect standard candles as they exhibit an intrinsic scatter in their absolute magnitude which could be the result of e.g. the evolution of their progenitors with redshift.

Furthermore, these objects possess a characteristic correlation between their maximum brightness and the rate at which this brightness fades. Again the intrinsic scatter of SNe Ia results in slight variations in their light curves but putting this correlation together with the almost constant absolute magnitudes of SNe Ia we arrive at an improved standard candle.

The extreme brightness of SNe Ia which may temporarily exceed that of their host galaxy can be viewed from great distances and the fact that they have almost the same absolute magnitudes make them ideal standard candles with which to probe the distances to far away galaxies. Indeed it was the observations of SNe Ia that culminated in the discovery of the acceleration of the universe by two independent teams of Riess et al. [11] and Perlmutter et al. [12]. This was understandably a shocking discovery. After all, how could a universe governed solely by the attractive force of gravity accelerate? As we saw earlier such an unexpected behaviour has therefore been attributed to

a form of as yet unknown dark energy. Figure 1.4 shows the SNe Ia redshift-magnitude relation observed by the Supernova Cosmology Project (SCP) [20] (the team led by Saul Perlmutter), which clearly indicates that the best-fit flat cosmology (solid curve) includes a form of dark energy in the standard model.

1.4.2 Cosmic Microwave Background

About 300,000 years after the Big Bang, the universe cooled to a temperature of about $kT \simeq 0.3$ eV (where k is the Boltzmann constant) at which point Thomson scattering between electrons and protons which held the cosmic plasma ionised stopped as it was no longer favourable. This allowed protons and electrons to form neutral atoms in a process known as *recombination*. This event in turn set the photons free from their interaction with matter and hence they began propagating throughout the universe from the *surface of last scattering* at a redshift of about 1100. We now observe this Big Bang remnant as the Cosmic Microwave Background (CMB) radiation as the wavelength of this primordial radiation has now been stretched (as a result of energy loss due to the expansion of the universe) to the microwave part of the spectrum. The CMB was first predicted by George Gamow and colleagues in 1948 [22] and the observational evidence for it was first found by Penzias and Wilson in 1965 [23], who measured the temperature of this radiation to be $T = 3.5$ K. Later in 1992 the Cosmic Background Explorer (COBE) satellite found the temperature of the CMB to be $T = 2.7$ K with a spectrum described by a black-body extremely well [24].

The next step in the CMB exploration is the discovery of spatial temperature anisotropies in the CMB. It was again the COBE satellite [24]

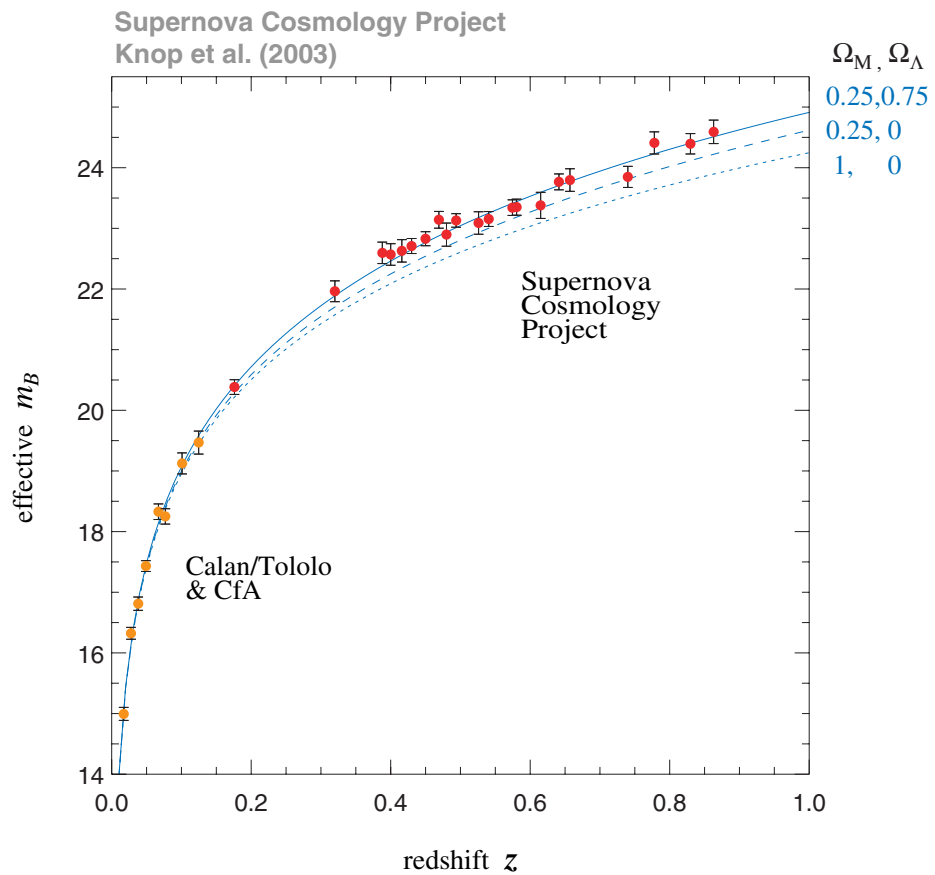


Figure 1.4: This Hubble diagram shows the high-redshift SNe Ia of the SCP. Clearly the best-fit model is the flat cosmology with a cosmological constant dark energy (solid curve). Other models (dashed curves) have been shown for comparison. Figure from [21].

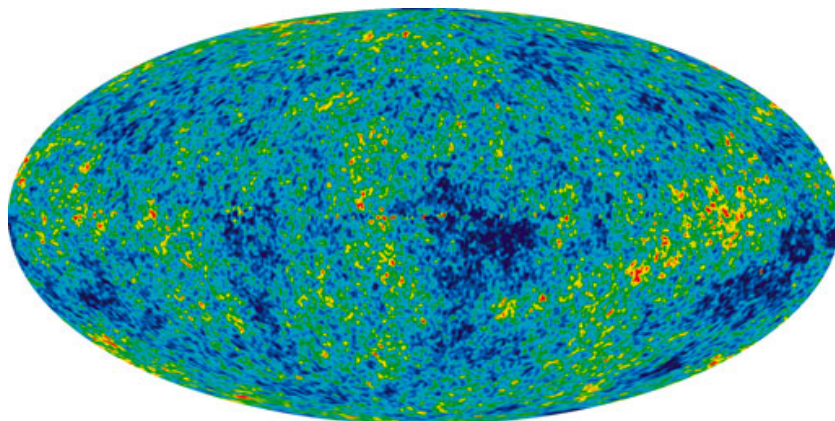


Figure 1.5: The sky map of temperature fluctuations in the cosmic microwave background as seen by WMAP over 7 years. Figure from: <http://map.gsfc.nasa.gov/news/>.

which first measured these temperature fluctuations to be of order 1 part in 100,000. Figure 1.5 shows the CMB temperature fluctuation sky map. These anisotropies, which are thought to have been generated by small density perturbations, are filled with valuable information about the cosmological parameters. After COBE, the Wilkinson Microwave Anisotropy Probe (WMAP) satellite [25] measured these anisotropies with higher accuracy and today the Planck satellite [26] is pushing the accuracy of these measurements to the limit, hence providing us with ever so precise cosmological parameters.

We will be returning to the CMB in Chapter 4, where we will discuss the two associated distance priors, namely the *shift parameter*, R and the *acoustic scale*, l_a in relation to the application of the CMB data to constraining cosmological models.

1.4.3 Baryon Acoustic Oscillations

Another important observational discovery is the Baryon Acoustic Oscillations (BAO) which arise from the same density perturbations that cause the anisotropies in the CMB temperature. As talked about in

the CMB section, in the early pre-recombination universe photons and baryons were tightly coupled to each other through Thomson scattering. In that epoch perturbations resulted in the creation of gravitational instability in the “photon-baryon” fluid and the collision-less dark matter. These gravitational instabilities continued to grow in the dark matter part but the baryons could not collapse under the force of gravity as the radiation pressure of photons would oppose this. This is basically the mechanism that holds a star together but in the case of a star the two opposite forces are balanced. In the early universe plasma however there is an imbalance between the forces leading to oscillations in the photon-baryon fluid like sound waves in spherical shells. After recombination photons free-stream, and these acoustic oscillations leave their imprint both on the CMB and the distribution of matter. Of course the oscillations occur at many different wavelengths but there will be a characteristic resonant wavelength, which we can measure. This distance scale has grown with the universe’s expansion which means that we observe it in the distribution of galaxies today to be about 100 Mpc. This length scale translates into about 1 degree between the hot and cold patches of the CMB sky. Putting these two information together we can thus use this natural “standard ruler” to trace the universe’s expansion history back to the time when the CMB was emitted. The BAO was first convincingly detected in 2005 by two international teams, namely the Two degree Field Galaxy Redshift Survey (2dFGRS) [27] and the Sloan Digital Sky Survey (SDSS) [28]. Figure 1.6 shows an SDSS map of galaxy distribution, where the arrows point towards increasing redshift. The red bullseye on the map shows the characteristic scale set by the BAO in the early universe which can now be detected in redshift surveys.

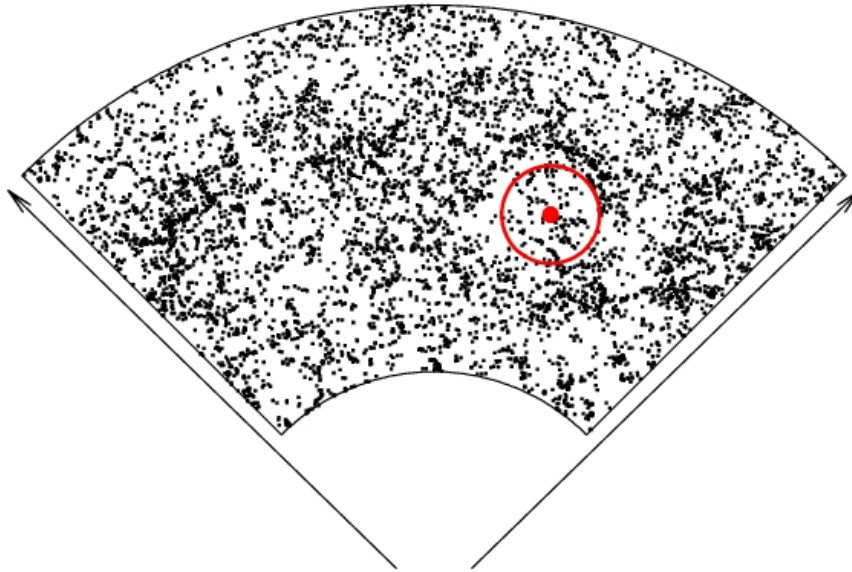


Figure 1.6: An SDSS map of distribution of galaxies with a bullseye indicating the characteristic scale of the Baryon Acoustic Oscillations in the early universe imprinted on the distribution. Figure from [29].

1.5 Concordance Cosmology

The best picture of the universe we have at the current time constructed through observations, some of which were discussed in §1.4 is known as the Concordance Cosmology or the Standard Model of Cosmology. This model is based on the hot Big Bang model which is outstandingly successful at explaining the abundance of light elements and the origin of cosmic microwave background. We have discussed the CMB earlier but the former corresponds to the abundance of light elements created through *Big Bang nucleosynthesis* in the early universe as it expanded and cooled, which can be accurately calculated in the hot Big Bang theory. Furthermore, the resulting required baryon density from such calculations is precisely what we deduce from CMB data.

In addition to the above, the standard model includes an early period

of inflation (extremely rapid expansion) which is needed to account for the production of density perturbations which serve as seeds for the creation of the large scale structure that we observe today. Moreover, the standard model contains CDM and a positive cosmological constant, Λ to be able to satisfy observations like the ones we have seen earlier, and therefore is given the nomenclature Λ CDM.

Current constraints on the Λ CDM parameters deduced from the latest 7-year CMB observations of the WMAP satellite known as the WMAP7 results [18] together with the latest (at the time when WMAP7 data were interpreted) H_0 measurements [30] and the latest BAO data [19] gives baryon density, $\Omega_b = 0.0458 \pm 0.0016$, dark matter density $\Omega_{dm} = 0.229 \pm 0.015$ and cosmological constant density, $\Omega_\Lambda = 0.725 \pm 0.016$. In Figure 1.7 we see the famous $(\Omega_M, \Omega_\Lambda)$ plot with cosmological constraints from the latest SNe Ia observations [17] together with the latest CMB and BAO data.

The drawback of Figure 1.7 is that it allows for too much freedom in the values that the matter and dark energy densities can take. That is, the flatness condition corresponding to $\Omega_M + \Omega_\Lambda = 1$ is only satisfied on the designated diagonal line. In comparison Figure 1.8 shows the same constraints on the (Ω_M, w) plane while assuming flat universes throughout.

An important feature of Figure 1.8 is that in addition to showing that the cosmological constant gives a good fit to the data, it also clearly allows for dark energy with an equation of state of less than -1 . This means that phantom energy with $w < -1$, leading to a Big Rip singularity is indeed still currently a legitimate candidate for dark energy. At a Big Rip, which will be explained further in §2.1 the universe is literally ripped apart down to its smallest constituents.

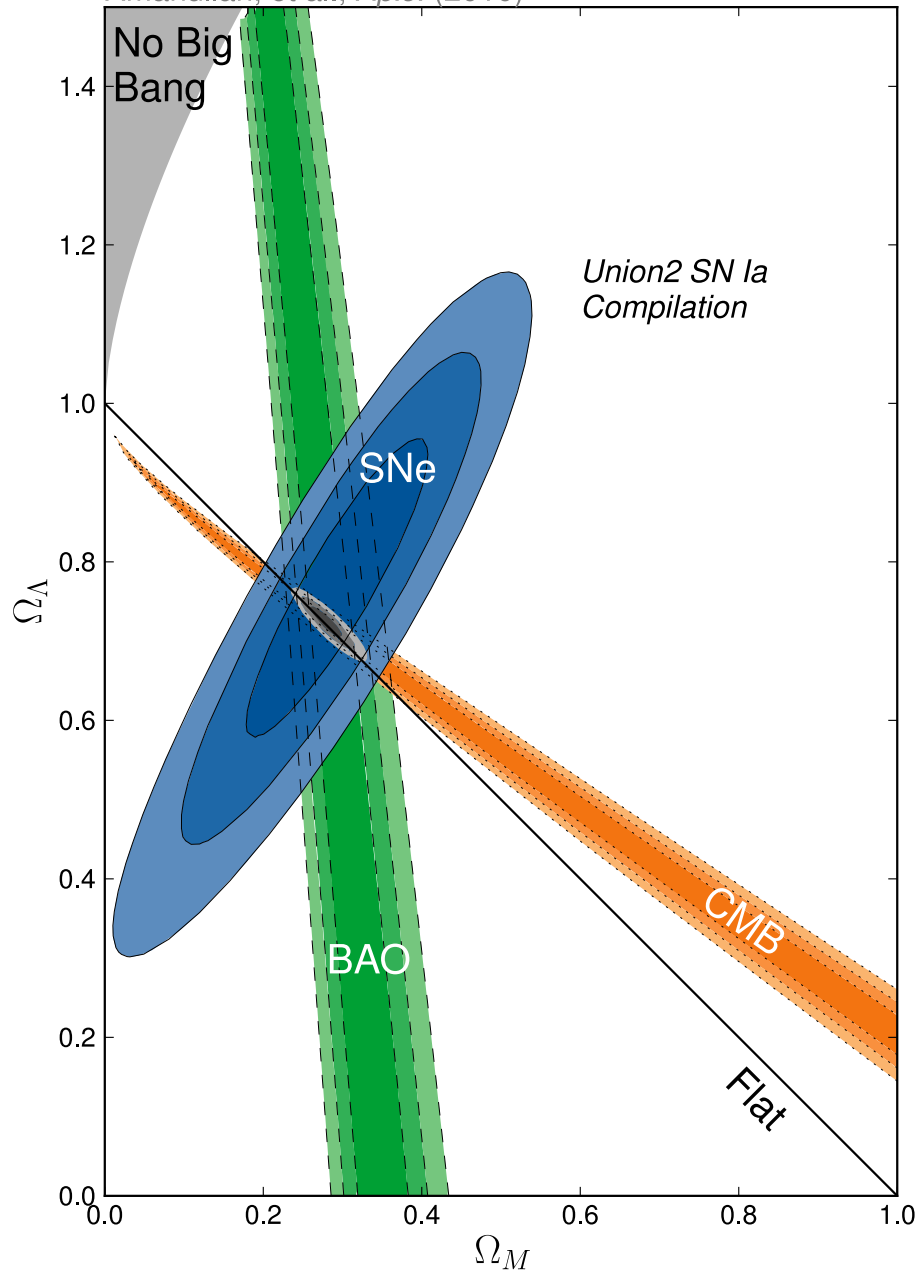


Figure 1.7: The contours show 68%, 95% and 99% credible regions in the $(\Omega_M, \Omega_\Lambda)$ space calculated using SNe Ia, CMB and BAO data. Dark energy is assumed to be the cosmological constant with $w = -1$ as in the concordance model. Figure from [17].

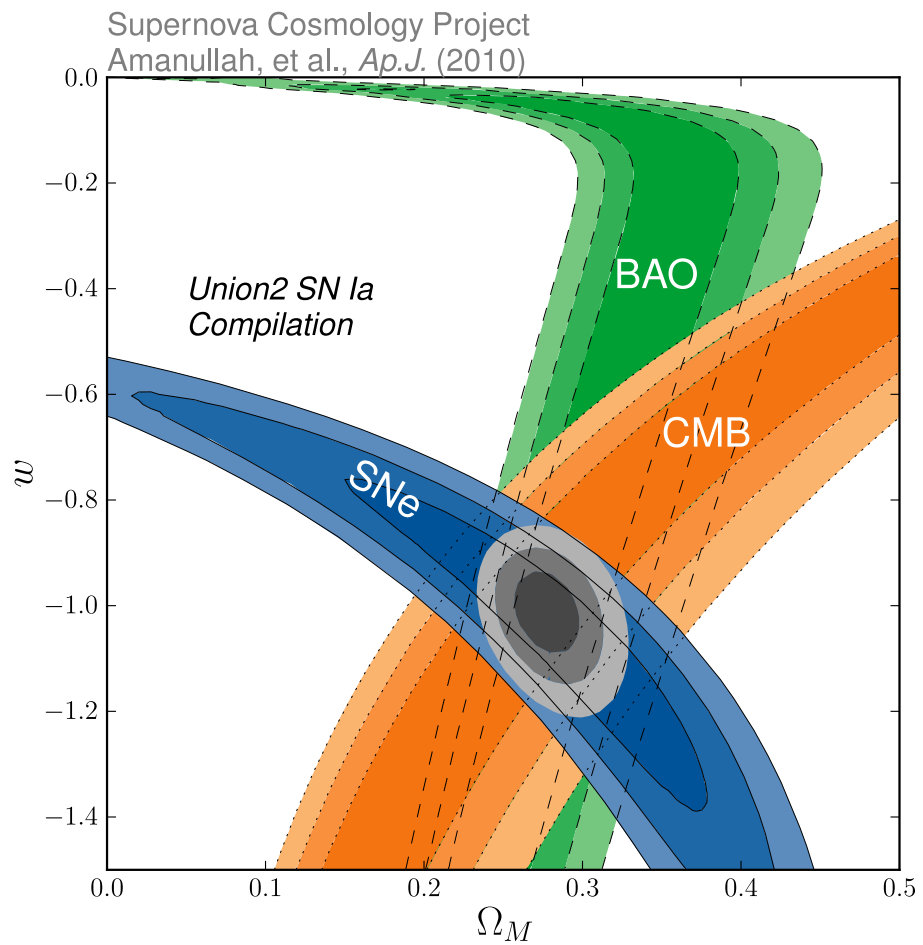


Figure 1.8: The contours show 68%, 95% and 99% credible regions in the (Ω_M, w) space calculated using SNe Ia, CMB and BAO data. It can be seen that $w < -1$ is allowed. Figure from [17].

1.5.1 Λ CDM Problems

Despite its remarkable successes at describing the various available observational data, there are also fundamental problems with the concordance model. For example, as mentioned before there is a large discrepancy between the observed and predicted values for the energy density of vacuum which is what the cosmological constant is thought to be interpreted as. This is the famous *cosmological constant problem* as introduced before. This problem therefore naturally calls for alternatives to the cosmological constant to be sought for where as discussed the equation of state of dark energy is different from that of the cosmological constant, $w = -1$ and instead varies with time, $w = w(t)$.

Furthermore, the problem known as the *flatness problem*, basically questions the very nearly flat curvature of the universe in Λ CDM as observed through the CMB data. The reason for this is that, a flat universe must have either always been flat or extremely fine tuned at early times. Any deviations from this fine-tuning would grow in time to result in a non-flat model. The way to see this is by writing the Friedmann equation (1.20) in the form:

$$|\Omega - 1| \equiv |\Omega_k| = \frac{|k|c^2}{a^2 H^2}, \quad (1.32)$$

where we are assuming $\Lambda = 0$, which is a reasonable assumption for the most part of the history of the universe's evolution. In this decelerating universe, H is constantly decreasing and the scale factor is effectively increasing as $a \propto t^{2/3}$ (assuming a matter-dominated universe which is also a good approximation for the majority of the universe's evolution). We can see that the term on the right hand side is constantly increasing

as a function of time. Thus, if $k \neq 0$, a small deviation can grow to result in a significantly non-flat model today.

Another example is the *horizon problem*. We can work out the angle subtended by the horizon at the time when the CMB was emitted. Today this is about 1 degree on the sky. This means that two patches on the CMB sky further than about 1 degree apart must not have been in causal contact with each other, yet we see that the whole of sky (about 40,000 square degrees) has the same temperature. That is, these patches could not have communicated with one another to reach an equilibrium to give us the isotropic CMB that we observe today.

And of course there is the problem with the dark matter and dark energy in the standard model introduced to account for observations. The unknown nature of these dominating components is a major problem with the Λ CDM.

Hence, for the problems listed here and also some others that are not considered here, many other non-standard models for the universe have been sought which attempt to explain observations as well as Λ CDM is able to, while at the same time resolve the issues with this standard model. In the next chapter where we discuss the future state of the universe and the particular model we have investigated, we come across some non-standard cosmologies proposed to serve as alternatives to the standard Λ CDM model.

1.5.2 Conclusions

In this first chapter we have laid the theoretical foundations of our investigations to follow in later chapters. We talked about the standard Λ CDM cosmological model and the observational evidence supporting it. However, we also argued how in some circumstances the observa-

tions also allow for theories that are considered beyond the standard model such as phantom dark energy. As we will see in Chapter 2, this has encouraged new paths of investigations to be followed by cosmologists.

Chapter 2

The Exotic World

Having become familiar with the standard cosmological paradigm in Chapter 1, in this chapter we will start our journey into the world of exotics, which will take us to the specific model that we investigated in this thesis. Arguably, the definition of “exotic” is not fixed. Until about a decade ago we could not have imagined to have to consider a negative pressure energy component to dominate the total energy budget of the universe and yet now this does not seem as bizarre perhaps. Therefore, more correctly we present here some ideas which are considered to be exotic *now*.

Seeing as our model of interest, as we will see, concerns a possible future evolution for the universe, we will discuss some of the possibilities for the fate of the universe in non-standard models first.

Throughout this chapter references have been made to some papers in the literature where the contents of these works have only been very briefly touched upon in the text just to convey an impression of the subjects discussed. The reason for the inclusion of these references is mainly to demonstrate the place occupied by the model of interest, Sudden Future Singularities, within the literature. More detailed descriptions of these investigations lie beyond the scope of this work.

2.1 The Fate of the Universe and Exotic Singularities

“*Some say the world ends in fire, some say in ice*” [31]. Although perhaps other thoughts served as Robert Frost’s motivation for writing this poem in 1916, he unknowingly summarised our understanding of the end of the universe in his later years to come pretty well. Until the late nineties of the twentieth century the only kinds of possible fates for the universe in Big Bang models were considered to be the two cases of eternal expansion in an open or a flat universe or an eventual recollapse known as a Big Crunch in a closed model. The universe would start out from a Big Bang in all these models but would end in one of the possible fates depending on the curvature of the universe.

When in early- to mid-1990’s astronomers set out to discover by how much the expansion of the universe was decelerating, due to the gravitational attraction of all the matter within it, by observing standardisable candles such as Type Ia supernovae the least they could imagine to find was that the universe was indeed accelerating! Later this result was supported by other cosmological observations such as the anisotropies in the cosmic microwave background radiation and the baryon acoustic oscillations.

Geometry no longer determined destiny after this discovery since now with the inclusion of an extra component in the mass-energy content of the universe, which causes this speeding up of the expansion of the universe, a closed universe could expand indefinitely and an open universe could recollapse [32]. More specifically, the equation of state of this extra, dominant mass-energy constituent of the universe, the so-called *dark energy* which acts against gravity will determine its ultimate fate. Hence the search for the nature of this mysterious

cosmological fluid now thought to be making up about 70% of the mass-energy content of the universe began.

If we look at the second Friedmann equation (or the acceleration equation) in Equation 1.8 we notice that in order to obtain acceleration, when $\Lambda = 0$, we necessarily need a substance that has negative pressure. Various forms of negative-pressure components have been proposed since the discovery of acceleration to account for this repulsive force. As we have seen earlier, in the standard concordance cosmology the dark energy responsible for this behaviour is the cosmological constant, Λ with an equation of state parameter, $w = -1$. A Λ -dominated universe will continue to expand exponentially into an empty de Sitter type universe.

As talked about in Chapter 1, another leading candidate is quintessence with $w < -1/3$ which varies in time and space. Phantom energy [33, 34] with $w < -1$ is a special case of quintessence whose energy density increases with time. Phantom energy is indeed very unusual as mentioned in Chapter 1. The way to see this is by noting that the pressure and density of a scalar field, ϕ are defined as:

$$p = \frac{1}{2}\dot{\phi}^2 - V(\phi) \quad (2.1)$$

and

$$\rho = \frac{1}{2}\dot{\phi}^2 + V(\phi) \quad (2.2)$$

where $\frac{1}{2}\dot{\phi}^2$ is the kinetic energy and $V(\phi)$ is the potential energy of the scalar field. Now to have $w = \frac{p}{\rho c^2} < -1$ would require the introduction of a negative kinetic energy term. This is where the abnormality of phantom energy comes from.

A phantom-dominated universe will expand towards a Big Rip singularity [35] where all the matter in the universe will also take part in

the expansion and will hence be torn apart. The Big Rip singularity violates all energy conditions of GR (which will be discussed in §2.2.1).

While current cosmological data are consistent with a dark energy in the form of a cosmological constant, they are not yet able to rule out other more exotic candidates, including most intriguingly phantom energy which drives the universe towards a Big Rip singularity. This has encouraged the study of the possibility of the occurrence of other non-standard events in the future evolution of the universe which could be stemming from various other kinds of matter. And indeed at the same time that the inclusion of a negative pressure dark energy would be a solution to the acceleration problem, cosmologists have also been looking at other ways to modify Einstein's theory of gravity to achieve this goal.

These studies have brought a zoo of new cosmological singularities to the table which are different from the standard singularities of Big Bang and Big Crunch. Not all of these extremal events mark the end of the universe however and the evolution of the universe may continue beyond some of them [36, 37, 38]. Here I aim to provide a list of the most important possible non-standard fates for the universe discovered by now.

Exotic extremal events have been classified in different ways in a number of works. Nojiri et al. [39] first produced a classification of cosmological singularities in terms of the three quantities of the scale factor, a , the density, ρ and the pressure, p . In this classification, which remains the basic and classic one to date, we have four types of singularities:

- Type I (“Big Rip”): For $t \rightarrow t_s$, $a \rightarrow \infty$, $\rho \rightarrow \infty$ and $|p| \rightarrow \infty$

-
- Type II (“Sudden”): For $t \rightarrow t_s$, $a \rightarrow a_s$, $\rho \rightarrow \rho_s$ and $|p| \rightarrow \infty$
 - Type III: For $t \rightarrow t_s$, $a \rightarrow a_s$, $\rho \rightarrow \infty$ and $|p| \rightarrow \infty$
 - Type IV: For $t \rightarrow t_s$, $a \rightarrow a_s$, $\rho \rightarrow 0$ and $|p| \rightarrow 0$ and higher derivatives of H diverge.

In the above, a_s , ρ_s and p_s are constants and also $a_s \neq 0$. I will now explain these types of singularities further detail below:

Type I, Big Rip: As mentioned before these singularities happen in phantom dark energy models with $w < -1$ [33, 34]. In such a universe the very negative equation of state parameter results in a super negative pressure (resulting in super acceleration following the second Friedmann equation (1.8)) of the dominating dark energy component which together with its ever increasing energy density dissociate everything in the universe. Starting from the largest structures of super clusters of galaxies and continuing to the smallest constituents of matter, namely nuclei and nucleons. This drastic end to the universe has not been ruled out by observations of Type Ia supernovae, the CMB and large scale structure which seem to allow for a dark energy with $w < -1$ [18, 19, 17]. And indeed this very discovery has been a great encouragement for searching for other exotic possible fates for the universe.

Dabrowski and Denkiewicz in [40], make an estimate of the time at which this singularity may occur in the future. They report this time to be about 20 Gyr.

Type II, Sudden: Sudden singularities were first discovered by Barrow

[41] as pressure singularities which are accompanied by the divergence of the second derivative of the scale factor. In fact Barrow [41] first put forward the idea of Sudden *Future* Singularities and constructed a class of models which could accommodate such extremal events. Since then almost all the research done on the subject has been concerned with future events. Throughout this work therefore when I talk about sudden singularities I really mean sudden future singularities. Just to mention an interesting viewpoint here, Cattoen and Visser [42] regard the discussion of a past sudden singularity as implying an alternative beginning for the universe and they comment that this would form “the most unusual and disturbing” beginning that could be envisaged for the universe.

Furthermore, when Barrow’s particular sudden singularity model is meant, the term Sudden Future Singularity is used, as the name has in a way become a trademark for Barrow’s finding. Strictly speaking however, all the singularities discussed here belong to the sudden singularities group since they all occur at some finite time in the future. Barrow chose the name “sudden” for his discovery to translate finite-time. And sudden singularities has indeed been used in the literature (e.g. in Copeland et al. [43]) to mean finite-time singularities in general .

Type III: This type of extremal event was first discovered by Nojiri et al. [44]. Later it was found by Bouhmadi-lopez et al. [45] in phantom models where the universal fluid is expressed as generalised Chaplygin gas (GCG). In this work the singularity has been dubbed *Big Freeze*. The fluid considered by Bohmadi-lopez has come to be known as phantom generalised chaplygin gas (PGCG). Dual phantom fluids [46], which result in two Big Rip singularities both in the past and in the future, have been considered in this context as well [47]. In this

case the fluid is known as a dual phantom generalised Chaplygin gas (DPGCG). Both PGCG and DPGCG are referred to more simply as GCG and DGCG. To briefly go through GCG and DGCG definitions, we start from the Chaplygin gas which is a perfect fluid that obeys an exotic equation of state of the type:

$$p = -\frac{A}{\rho}, \quad (2.3)$$

where p is the pressure, ρ the energy density and A a positive constant. This type of fluid has been named after the Russian mathematician and mechanical engineer, Sergey Chaplygin following his works in aerodynamics. He proposed the above relation as a mathematical approximation for measuring the lifting force on the wings of an airplane.

The energy density of the Chaplygin gas is positive and it has been shown that such a fluid would naturally provide the transition from a decelerating matter-dominated epoch to an accelerating epoch as Kamenshchik et al. show in [48]. In this work, the authors further introduce the GCG which takes on the following form for its equation of state:

$$p = -\frac{A}{\rho^\alpha}, \quad (2.4)$$

with $0 \leq \alpha \leq 1$. This has been studied in [49]. The same evolution from early deceleration to acceleration at late times is achievable with this fluid but in this case a cosmological constant will be mimicked at the current accelerating epoch.

At a Big Freeze singularity the phantom energy density diverges, filling the whole of the universe which means that nothing can move any

further. This fact led the authors to call this standstill state a Big Freeze singularity. This nomenclature may not be confused with the big freeze that occurs in an open or a flat universe where there is an obvious cooling of the universe due to the dilution of the matter it contains as a result of the expansion. (Strictly speaking closed models with a sufficient amount of dark energy could expand to end up in a similar fate as open and flat models.) Bouhmadi-lopez et al. in [45] further show that in models with GCG and DGCG fluid types such described Big Freeze singularity is what replaces and hence avoids the Big Rip singularity. Moreover, Yurov, Astashenok and Gonzalez-Diaz [50] confronted these models against observational data and showed that the only way these models could match current observations is by including an amount of dark matter.

Another name for a type III singularity is the Finite Scale Factor (FSF) singularity as given by [40]. In this work, the authors confront the FSF model they consider with the Riess et al. Gold supernovae data [51]. This way they show that an FSF could occur in less than 0.3 Gyr in the future in the model they studied.

Type IV: Such singularities which were first discovered in the tachyonic cosmological model studied by [52] were named Big Brake singularities. They are regarded as a subclass of sudden singularities as they also feature an infinite deceleration of the universe at some time in the future evolution of the universe. What distinguishes Big Brake singularities from sudden singularities is the fact that the first time derivative of the scale factor is zero at this singularity whereas this quantity is finite in the case of the sudden singularity. Therefore, at a Big Brake singularity the universe stops its evolution to zero speed while at a sudden singularity this final speed is finite. To better make sense of the situation with the Big Brake and the sudden singularity

we use the analogy of a moving car. At the Big Brake singularity the situation would be like when the driver pushes on the brakes suddenly and brings the car to a complete halt but in the case of the sudden singularity the driver pushes suddenly on the brakes just to reduce the speed to a lower value. It should be noted that as Copeland et al. [43] describe, type IV singularities also include singularities with finite values for the density, the pressure or both.

Big Brake singularities also take place in models with the exotic fluid in the form of the so-called anti-Chaplygin gas which has an equation of state of the same form as the Chaplygin gas but with the opposite sign: $p = \frac{A}{\rho}$, where A is a positive constant [52]. This is the only type of equation of state that can be considered for singularities of this sort [40]. As will be discussed in full detail later on in this chapter, sudden singularities do not admit any type of an equation of state. While the Big Brake would be the only fate possible in anti-Chaplygin gas models, tachyonic models discussed above, could end up in either an infinitely accelerating expansion state of de Sitter type or in a Big Brake singularity depending on initial conditions, as they put it [52].

The aforementioned tachyonic cosmological model where the Big Brake singularity naturally occurs has been confronted against supernovae data in [53] and has successfully passed this cosmological fitting.

Furthermore, as shown by Dabrowski et al. in [40] the earliest time when a Big Brake singularity could occur in the future of a tachyonic model is 1 Gyr and the latest time is 44 Gyr. The authors in [40] claim that although these events happen in a very distant future, they could potentially serve as a dark energy candidate.

Moreover, the type IV singularity is given the name, the Big Sepa-

ration in [40]. We will discuss one aspect of this type of singularity as noted by Dabrowski and Denkiewicz who came up with the name “Big Separation” further below.

Going back to the issue of the classification of singularities, after the above classification, Cattoen and Visser [42] classified these “cosmological milestones”, as they call them, in terms of generalised power series expansion of the scale factor and studied them kinematically. In addition they also considered their dynamical behaviours through the Friedmann equation to analyse the energy conditions in the vicinity of these events. As will be talked about later in §2.2.1, energy conditions are no longer as physically reasonable as they were when they were first introduced but nonetheless as Cattoen and Visser [42] put it, they can make a good first guess at determining the strangeness of the cosmological events under study.

Fernandez-Jambrina and Lazkoz then considered the behaviour of causal geodesics in classifying cosmological singularities to complement previous classifications [37]. As they argue, Cattoen and Visser [42] only analyse the singularities in terms of the curvature and curvature is a static concept. They claim rightly that what would be more enlightening in the study of singularities is to dynamically follow observers’ trajectories along causal geodesics, which are subject to gravitational forces only, up to the singularity. Whether or not causal geodesics can be extended beyond a singularity can be an indication of the strength of the singularity under study. Briefly, that is, singularities beyond which the geodesics can be extended are regarded as weak singularities and those where the geodesics halt are strong singularities. In the former case the spacetime is said to be geodesically complete and in the latter geodesically incomplete. Fernandez-Jambina and Lazkoz [37] therefore classified singularities according to

their strengths as well. This issue of the strength of singularities is further discussed and more carefully analysed in the case of sudden singularities in §2.2. We only note in passing that they are regarded as weak singularities in the scheme.

In one of their latest works, [54], Fernandez-Jambrina and Lazkoz continue further to classify singularities in terms of the generalised power series expansion of the equation of state.

Fernandez-Jambrina and Lazkoz's approach in [38] to the issue of exotic singularities in modified gravity theories is a rather interesting one. They present a compact form for modifications to the Friedmann equation which comprises modified gravity theories such as the $f(R)$ theory and braneworld models. They then classify the kind of exotic singularities that occur in various modified gravity models.

In [40] a list of exotic singularities which could serve as dark energy is presented. The reason why this claim is made by the authors is that many of these extremal events arise naturally in alternative dark energy and modified gravity models which attempt to explain the current acceleration of the universe. For instance, as Dabrowski and Denkiewicz [40] claim, the curious w -singularity (which will be explained towards the end of the section) appears in theories such as $f(R)$ gravity, scalar field gravity and in brane gravity models. Moreover, sudden singularities plague loop quantum cosmology.

Dabrowski and Denkiewicz in [40] specifically discuss the following extremal events: the Big Rip (type I), the SFS (type II), the FSF (Finite Scale Factor, type III), the GSFS (Generalised Sudden Future Singularity), the Big Separation (type IV) and the w -singularity. We mentioned FSF and Big Separation singularities before in the discussion of their respective singularity types of III and IV. As can be seen

there are more names than events.

From these listed singularities, the GSFS and the w -singularity are new types which we will now explain in turn below:

GSFS: Generalised Sudden Future Singularities comprise an infinite family of finite-time singularities arising in isotropically expanding universes where all the energy conditions are satisfied. The singular behaviour at these events occurs in arbitrarily high order derivatives of the pressure with respect to cosmic time [55]. That is to say that the density and pressure remain finite at a GSFS. Another way to look at it is that these singularities can be regarded as moderated forms of sudden future singularities where the singularity occurs in a time derivative of the pressure rather than itself. If the pressure derivative singularity occurs at the r th order, the scale factor singularity will occur at the $(r + 2)$ th order. This relation could be understood by looking at the second Friedmann equation (1.8). One can see that the second time derivative of the scale factor is related to the 0th order time derivative of pressure, i.e. the pressure itself. Hence there are two differentiation orders difference between the scale factor and the pressure which explains the abovementioned relation between the derivatives. These events will be further discussed by the use of the appropriate formulae in §2.2.2. Furthermore, as was mentioned in the type IV singularity discussion, Copeland et al. [43] consider this type of singularity as comprising events where both density and pressure are finite and those where these vanish alongside the divergence of higher order derivatives of H . This will then mean that GSFS with its finite density and pressure could also be thought of as a type IV singularity. And as a final note regarding this type of singularity, Dabrowski and Denkiewicz assert in [40] that by their estimations these singularities take place always further into the future than sudden future

singularities.

The Big Separation is similar to GSFS with the difference that $w \rightarrow \infty$ in the Big Separation case even though the pressure and the density vanish [40]. That is:

$$w = \frac{p}{\rho c^2} \rightarrow \infty \quad \text{as} \quad \rho \rightarrow 0 \quad \text{and} \quad p \rightarrow 0. \quad (2.5)$$

This claim by Dabrowski and Denkiewicz is however not approved by Fernandez-Jambrina [56] who asserts that this fact is not necessarily true for type IV singularities. Nevertheless this issue is not noted in the previous considerations of this type of singularity, but as we will now see below, Dabrowski and Denkiewicz' creation, w -singularities, features the same behaviour for the equation of state.

w-singularity: This type of singularity is similar to type IV singularity but with the difference that the higher derivatives of the Hubble parameter do not diverge [57]. Moreover, w -singularities are different from Big Brake singularities specifically since they do not conform to an anti-Chaplygin gas equation of state. As a w -singularity is approached, i.e. $t \rightarrow t_s$ (where t_s is the time of the singularity), we have:

$$a(0) = 0, \quad a(t_s) = \text{const.} \equiv a_s, \quad \dot{a}(t_s) = 0, \quad \ddot{a}(t_s) = 0,$$

where the subindices, s, correspond to the quantities evaluated at the singularity. These conditions would be interpreted as a Big Bang type beginning, fixed and finite size for the scale factor at t_s , halt of expansion at t_s and end of acceleration at t_s respectively. Requiring the above conditions, Dabrowski and Denkiewicz [57] arrived at a particular form for the scale factor for a model with a w -singularity.

With such a scale factor they then show that the equation of state diverges despite the fact that the pressure and the energy density both vanish. They prove this fact by making use of the l'Hopital's rule of calculus.

In [57] the authors further go on to demonstrate a curious duality between the w -singularity and the Big Bang (BB) singularity which is shown as:

$$p_{BB} \leftrightarrow \frac{1}{p_w}, \quad \rho_{BB} \leftrightarrow \frac{1}{\rho_w}, \quad w_{BB} \leftrightarrow \frac{1}{w_w}.$$

To translate exactly what these relations mean, we have [57]:

$$\begin{aligned} p_{BB} &\rightarrow \infty & \text{and} & & p_w &\rightarrow 0, \\ \rho_{BB} &\rightarrow \infty & \text{and} & & \rho_w &\rightarrow 0, \\ w_{BB} &\rightarrow 0 & \text{and} & & w_w &\rightarrow \infty. \end{aligned}$$

Regarding the strength of this type of singularity, Fernandez-Jambrina's work on w -singularities in [56] shows that they are weak singularities.

Some of the events discussed so far have been tested against observational data and have proven to be viable with the accuracy of the measurements that is available to us today. An example is the Big Rip singularity as mentioned before. Initially sudden future singularities were also thought to be possible when compared against high redshift supernovae data only [1]. What the authors did in [1] was to find out that for a particular set of SFS model parameters the luminosity redshift-magnitude relation matches that of the concordance model very well. Their plot of distance modulus, $\mu = 5 \log d_L + 25$ against

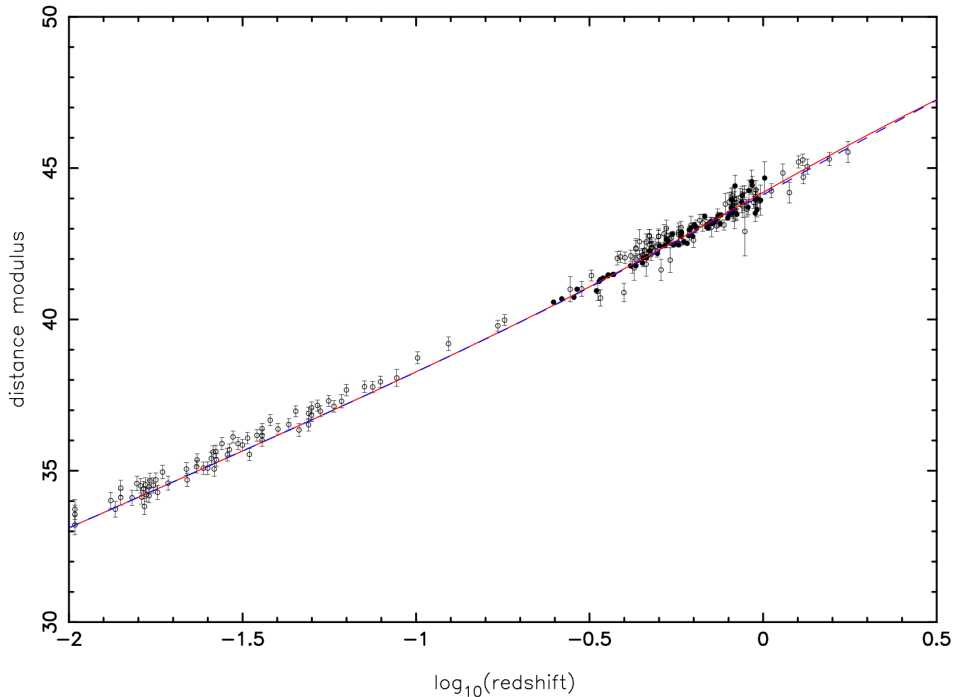


Figure 2.1: Distance modulus against redshift for the concordance model with $H_0 = 72.8 \text{ km s}^{-1} \text{ Mpc}^{-1}$, $\Omega_{m0} = 0.26$ and $\Omega_{\Lambda 0} = 0.74$ (dashed blue curve) and the SFS model with $m = 2/3$, $n = 1.9999$, $\delta = -0.471$ and $y_0 = 0.99936$ (solid red curve). The SNe Ia data shown correspond to the Gold [51] (open circles) and the SNLS [58] (filled circles) datasets. One can see that the concordance and the SFS models are almost indistinguishable. Figure from [1].

redshift is shown in Figure 2.1.

This work demonstrated that if the age of the universe in the SFS model is the same as in the standard concordance model, an SFS could happen in as early as 8.7 million years. Of course we go on to show in this thesis what happens to this conclusion once one considers other available cosmological data like the CMB and the BAO.

2.2 Sudden Future Singularities

After observing where Sudden Future Singularities stand in various currently available classification schemes for exotic singularities in §2.1, here in this section we aim to put Sudden Future Singularities under the microscope and study them in full detail. To do this we will present an overview of Sudden Future Singularities and the models accommodating them, reviewing the key theoretical and physical ideas that have underpinned their development in recent literature.

2.2.1 Sudden Singularities

In 2004 Barrow [41] first published the results of his discovery of the existence of Sudden Future Singularities, which arise in the expanding phase of a standard Friedmann universe and violate the dominant energy condition only [59]. This was an intriguing discovery since until then the theoretical search for expanding universes with possible violent ends had identified only the Big Rip singularity [35] where all the energy conditions of GR are violated. As we have seen before at such an extremal event, which is befittingly named Big Rip, all the matter in the universe down to its smallest constituents is dissociated [35].

Energy conditions are physically reasonable inequalities imposed on the energy-momentum tensor, $T_{\mu\nu}$, which in general is made from many different matter fields. It would be immensely complicated to describe the exact energy-momentum tensor even if one knew precisely what forms of matter were present and what equations of motion governed their behaviour as Hawking explains [60]. Energy conditions are designed to extract as much information as possible about the

energy-momentum tensor through classical GR without assuming any particular form for its equation of state [61]. Recall Einstein's field equations from Equation 1.4:

$$G_{\mu\nu} + \Lambda g_{\mu\nu} = \frac{8\pi G}{c^4} T_{\mu\nu}. \quad (2.6)$$

One sees that with no complete description for the right hand side regarding the energy-momentum tensor, it would not be possible to solve this equation in any way. GR therefore is both a powerful theory in the sense that it allows for any kind of matter field to be considered, and a weak one at that since it does not give much information about the type of matter we ought to have. One should note however that this problem also exists in Newtonian gravity. That is when one considers a falling mass under the force of gravity, a measure of the rate at which the object accelerates says nothing about the nature of the falling mass.

We can therefore see how the energy conditions could be helpful by placing constraints on the energy-momentum tensor that all physically reasonable kinds of matter should satisfy. It should be emphasised that these conditions are still not able to tell us about the type of matter we should be dealing with but they could be utilised in constructing general theorems regarding the strong field behaviours of gravitational fields [62].

A generic feature of matter that we observe is that its energy density is (almost) always positive. The energy conditions of GR are basically different ways of making this quality more precise [62]. The elaboration of these conditions occurred at the same time as when many powerful mathematical theorems were developed. And the construction of different kinds of energy conditions in use today has been

in fact considerably driven by the technical necessity brought about for the derivation of these theorems [62]. These energy conditions have turned out to be sufficient to prove the singularity theorems of Hawking and Ellis [60] which attempt to show in what circumstances gravitation results in singularities. The energy conditions also form the basic foundation for other well-known theorems such as the topological censorship theorem, which postulates that no observer could determine the topology of space-time, and the no-hair theorem, which asserts that all black holes are describable by only the three quantities of mass, electric charge and angular momentum.

The energy conditions can be fundamentally expressed in terms of the components of the energy-momentum tensor [62] but for FRW universes these conditions specialise to the following inequalities in terms of the pressure, p , and density, ρ , of a perfect fluid (where c is the speed of light):

- The null energy condition (NEC): $\rho c^2 + p \geq 0$.
- The weak energy condition (WEC): $\rho c^2 \geq 0$ and $\rho c^2 + p \geq 0$.
- The strong energy condition (SEC): $\rho c^2 + p \geq 0$ and $\rho c^2 + 3p \geq 0$.
- The dominant energy condition (DEC): $\rho c^2 \geq 0$, $-\rho c^2 \leq p \leq \rho c^2$.

Physically these conditions, and their violation or otherwise, may be interpreted as follows:

NEC: The density drops as the universe expands [62]. The violation of the NEC results in super acceleration of the scale factor as occurs in phantom models [63]. Not violating this condition corresponds to allowing dark energy to exist in the form of quintessence.

WEC: This condition embodies the NEC and further adds to it the fact that the energy density is positive [62].

SEC: Gravity is an attractive force. The violation of this condition comes through negative energy density or a large negative pressure [60] which could occur in inflationary processes such as that in the early universe. Not violating the SEC results in a decelerating universe. Moreover, the SEC provides a lower bound on the energy density [62].

DEC: Matter cannot travel faster than light [64]. The DEC provides an upper bound on the energy density [62]. This energy condition is interpreted as expressing the same conditions as the WEC plus the fact that pressure should not exceed energy density [60].

Given all that we said about the energy conditions, we note that their validity has been challenged over the years since they were first set. In particular the SEC is in fact almost completely abandoned now since it corresponds to a decelerating universe. The other conditions are also beginning to lose their validity. More fundamentally, there exist quantum effects that are capable of violating the NEC, which is the weakest of the energy conditions whose violation results in the violation of all the energy conditions [65]. Furthermore, there are serious classical violations of the energy conditions [65]. An example of an energy condition completely abandoned now is the trace energy condition (TEC). This condition asserted that the trace of the energy-momentum tensor should be negative (or positive, depending on the metric conventions). But as Barcelo and Visser [65] discuss, the real-

isation that stiff equations of state similar to those found in neutron stars violate this energy condition, resulted in the rejection of this assertion.

Nevertheless, despite the situation we are in with the energy conditions today, for the lack of more successful replacements, these conditions are still widely used in the GR community [65]. And indeed although we know these conditions are not truly fundamental, as Barcelo and Visser put it, they provide us with a good first pass at the problem of determining how strange physics may get at the vicinity of cosmological milestones, a term coined by Cattoen and Visser [42].

Now to apply these conditions to the main subject of this chapter, we see that at an SFS all the energy conditions except for the DEC are satisfied. It should be noted that this fact is true only when one considers a positive diverging pressure. In such a case one could therefore argue that SFSs appear to be very odd indeed by complying with the SEC and not the DEC. In other words at these events one has deceleration along with superluminal speeds for the matter! Nonetheless, again compared to the Big Rip singularity they could be thought of as less pathological perhaps since they violate only one energy condition in comparison with Big Rip singularity that violates all.

In [40] Dabrowski et al. show how the occurrence of exotic singularities could be linked to the blow up of the statefinders. Statefinders are observational parameters which are made from time derivatives of the scale factor like the well-known Hubble parameter and the deceleration parameter. Dabrowski in [66] specifically demonstrates that the occurrence of the SFS type singularity is accompanied by the blow up of the deceleration parameter and the GSFS, which was introduced earlier in §2.1, is accompanied by the divergence of what is known as the *jerk* parameter which is one order higher than the deceleration

parameter:

$$j = \frac{1}{H^3} \frac{\ddot{a}}{a} = \frac{\ddot{a} a^2}{\dot{a}^3}. \quad (2.7)$$

In the same way as for the Hubble constant and the deceleration parameter, the jerk parameter has also been observationally investigated. Using supernovae data it has been shown that, $j_0 > 0$ [67] which is equivalent to saying that the evolution of the universe changed from a decelerating phase to an accelerating one.

Dabrowski further discusses in [66] how the classic energy conditions may be modified to higher-order versions related to the statefinders, making up *more sophisticated energy conditions*, as he puts it, which could prohibit the occurrence of exotic singularities. Such discussions regarding the modification of the energy conditions are also presented in e.g. Barrow and Tsagas' work [55].

The name Sudden Future Singularities was chosen by Barrow for these singularities as they are temporal singularities and occur in a finite future comoving proper time. Barrow considers sudden future singularities as belonging to the larger group of 'big rip' singularities as they were discovered while searching for possible violent ends to the universe at a finite future time. And indeed what got researchers interested in sudden future singularities following Barrow's work was most importantly the fact that they resembled the Big Rip singularity in many ways but at the same time were much milder and not catastrophic at all as we will see shortly.

In discovering such singularities Barrow sets out by searching for any type of singularity in which a physical scalar becomes infinite in a finite future comoving proper time while the scale factor and the Hubble

expansion rate remain finite. Consider the Friedmann equations in the following form:

$$\rho = \frac{3}{8\pi G} \left(\frac{\dot{a}^2}{a^2} + \frac{kc^2}{a^2} \right), \quad (2.8)$$

$$p = -\frac{c^2}{8\pi G} \left(2\frac{\ddot{a}}{a} + \frac{\dot{a}^2}{a^2} + \frac{kc^2}{a^2} \right), \quad (2.9)$$

where ρ is the energy density, p the pressure, a the scale factor, k the curvature index, c the speed of light, G the gravitational constant and an overdot represents derivative with respect to time. Barrow found that by keeping the scale factor and the Hubble expansion rate finite one will also necessarily maintain a finite density, but that the pressure can still diverge. The divergence of pressure is accompanied by the blow up of the acceleration, as can be seen from Equation 2.9, which leads to a scalar polynomial curvature singularity even when the energy density and the Hubble expansion rate are finite and the scale factor is finite and non-zero [41].

The standard definition of scalar polynomial curvature singularities appears in [60] where they are prescribed as types of singularities where any of the scalar polynomials of the curvature tensor diverges.

To very briefly explain this, these kinds of singularities were created due to the fact that to consider an unboundedly large curvature for a singularity would require specification of a coordinate system. However a way round this problem would be by looking at scalar polynomials in the curvature tensor. In this way one has a scalar polynomial curvature singularity when any of these scalar polynomials diverges. Furthermore, we consider the scalar curvature term in an FLRW background cosmology as given by e.g. [43]:

$$R = 6 \left(\frac{\ddot{a}}{a} + \frac{\dot{a}^2}{a^2} + \frac{k}{a^2} \right), \quad (2.10)$$

where a is the scale factor, k is the curvature constant and an overdot denotes derivative with respect to Comoving time. We can see clearly that the diverging acceleration at an SFS would naturally result in a scalar curvature singularity.

Barrow shows in [68] that similar sudden singularities (moderated forms of the type discussed here) are possible in modified gravity theories where the divergence of the pressure is accompanied by the divergence of higher order derivatives of the scale factor. Furthermore, an SFS of the sort studied here happens regardless of the curvature of the universe [41].

Shortly after their discovery, Nojiri and Odintsov [69, 70] showed that these singularities may be avoided (or moderated) when quantum effects are taken into account. As they argue in [69], as a singularity is approached curvature invariants grow and energies increase which signals the beginning of the dominance of quantum effects on the system. They then explain conformal anomaly back-reaction in investigating how these quantum effects influence the evolution towards a singularity.

The fate of these singularities along with the other four types of exotic singularities mentioned before in §2.1 are also investigated in effective dynamics of quantum cosmology by Sami et al. in [71]. As they explain, the existence of future singularities in an FRW cosmology marks the beginning of the end of the validity of GR at such events. They show that sudden singularities again may be avoided depending on the magnitude of the density at the singularity and in such a framework an oscillating universe without a sudden singularity is created.

We can see that the divergent behaviour of the pressure at an SFS cannot be linked explicitly to that of the energy density, which remains finite, or we will not have an SFS. Hence we need to release the assumption of an equation of state which imposes a link between these two quantities. Of course then in order to avoid an SFS one would just need to impose an equation of state which will bound the pressure. Or as Barrow puts it, to avoid an SFS, it would be sufficient to require $dp/d\rho$ to be continuous or p/ρ to be finite [41].

Sudden future singularities are similar to another type of singularity termed Finite Density singularities which are spatial singularities and happen in inhomogeneous models of the Universe. It should be noted that an SFS can occur also in inhomogeneous models [72] where they may violate all energy conditions. The isotropy of the Universe is not a requirement for the occurrence of such singularities either and they may take place in anisotropic models as well [41]. Barrow and Tsagas in [55] show in fact that finite-time singularities feature in a wide class of cosmological solutions to Einstein equations irrespective of special symmetries. Sudden singularities are also immune to quantum particle production as investigated by [73] which could not be the case for the Big Rip singularity.

Similar to sudden singularities are the so called ‘quiescent’ singularities which occur in braneworld models [74]. These are a type of sudden singularities whereby the pressure remains finite alongside the density and the Hubble parameter while higher derivatives of the scale factor diverge. Alam and Sahni confronted braneworld models with quiescent singularities with SNe Ia and BAO data in [75] and concluded that they would not fit observations.

Furthermore the exact same sudden future singularity with the divergent pressure occurs in nonlocal cosmology as found by Koivisto [76].

Such models attempt to provide an explanation for the current accelerating expansion of the universe through modifications of Einstein's gravity which take the form of nonlocal distortions of the Einstein tensor in addition to possessing other properties. The accelerating universe in this model will lead it towards an SFS rather than a de Sitter type epoch. Koivisto however shows that these singularities may be avoided by a slight modification of the nonlocal model.

Other works where it has been shown that sudden singularities arise in various other models include Abdalla et al.'s study of modified $f(R)$ gravity models where the current dark energy dominance is explained simply by the universe's expansion [77]. Finite-time sudden future singularities naturally occur in such gravitational dark energy models as they put it. These may however be removed by quantum effects just as it was shown by Nojiri and Odintsov [69] to be the case for the sudden singularities in Barrow's model. In general if we had a complete theory of quantum gravity, we would be able to resolve the problem of singularities in cosmology but of course such a theory does not yet exist [78]. As the authors argue in [78], finite-time future singularities plague current black hole and stellar astrophysics. Specifically, they show that in general modified gravity dark energy theories are more immune to singularities than the general exotic fluid dark energy.

Furthermore, GCG models, that were talked about before in the context of Big Freeze singularity, also allow the occurrence of sudden singularities [79]. Another example is the oscillating equation of state dark energy which as Nojiri and Odintsov in [80] show if the universe is dominated by phantom energy now, the oscillating dark energy may allow all known four types of singularities introduced earlier in §2.1. Moreover, sudden singularities occur in dark energy models with the equation of state, $p = -\rho - A\rho^\alpha$ where A and α are real parameters,

as Stefancic shows in [81]. Type III and Big Rip type singularities also occur in this dark energy model for appropriate choices of model parameters.

Physically sudden future singularities manifest themselves as momentarily infinite peaks of tidal forces. That is, they are temporal singularities happening everywhere in the universe at the same moment. The peaks of tidal forces occur in the derivatives of the tidal forces in general sudden future singularities (GSFS) which were introduced before. Sudden future singularities therefore fall into the category of curvature singularities and specifically as was mentioned before they are scalar polynomial curvature singularities. Since curvature is associated with gravity, curvature singularities in general occur either in the case of infinite energy density (like the Big Bang) or infinite tidal forces (like in black holes) where in both cases gravity is infinite [82].

It should be noted however that curvature singularities of the SFS form could be classified as weak curvature singularities [36] according to Tipler and Krolak's definitions. The idea of the *strength* of singularities and analysing their physical behaviours was first put forward by Ellis and Schmidt [83] who argued that a singularity is considered weak if an object falling into it arrives intact at the singularity and otherwise it would be strong. These works were then further refined by Tipler [84] and Krolak [85] independently. When Fernandez-Jambrina and Lazkoz [36] evaluated the strength of sudden singularities as was prescribed by Tipler and Krolak, they concluded that sudden singularities are weak singularities both in the sense of Tipler's definition and that of Krolak's.

In comparison with strong curvature singularities this should therefore mean that the weak sudden singularities are geodesically complete but nevertheless this issue is still up for debate among cosmologists. The

geodesic completeness is the standard definition for the nonexistence of singularities in GR, implying the eternal existence of the universe in question.

Fernandez-Jambrina shows in [36] that causal geodesics in universes where an SFS occurs at a finite future time do not see these singularities but the geodesic deviation equation, which diverges at an SFS, does feel them. This would mean that point-like objects pass through such singularities without noticing them and even extended objects like classical strings may survive these weak singularities and cross through them [86]. As a result in-falling observers or detectors are not destroyed by the instantaneous infinite tidal forces. According to Newton's second law, infinite force is equivalent to infinite acceleration/deceleration. Therefore, to reiterate the moving car analogy, the momentary infinite tidal forces act in the same way as the sudden braking of the car. Hence no damage is caused to even finite objects at these singularities which act only momentarily.

In this view a universe with an SFS will continue its expanding evolution beyond such weak singularities until for example the occurrence of a more serious singularity that is geodesically incomplete like the Big Rip singularity which can end the universe [1]. In [37] the authors specifically regard sudden singularities as not real singularities. The discovery of the weak nature of SFS and the fact that the evolution of the universe will not come to an end at these events were made after Barrow made the statement that SFS can halt the expansion before an expansion maximum is reached in closed models in [41]. Furthermore, he stated that closed models are prevented from recollapsing to a second singularity of Big Crunch type, which is of course a conclusion one can make following the first idea of the halt of expansion. It should be noted that here the recollapse in closed models is talked

about with no mention of a dark energy influence and this idea follows solely from the discussion of geometry which Barrow seems to have chosen to consider.

Notwithstanding Fernandez-Jambrina and Lazkoz' works, Cotsakis and Klaoudatou show in [87] that sudden singularities are indeed geodesically incomplete. The two points of views have their proponents and as mentioned before this issue is still open for question. In fact, through a recent private communication, Dr Cotsakis reaffirmed the situation concerning SFS models and their debatable nature with regard to the issue of geodesic completeness.

2.2.2 Sudden Future Singularity Models

As was mentioned earlier, the divergence of the pressure at an SFS is accompanied by infinite acceleration (or more correctly, deceleration). Therefore in searching for a model that accommodates an SFS one needs to look for one where the scale factor and its first derivative or the Hubble expansion rate remain finite at some finite future time t_s while the second derivative blows up.

Barrow constructs an example SFS model where the scale factor takes the form:

$$a(t) = A + Bt^m + C(t_s - t)^n, \quad (2.11)$$

where $A > 0$, $B > 0$, $m > 0$, C and $n > 0$ are free constants to be determined.

Barrow also constructs the most general form of the solution for the scale factor [68] which takes the following form:

$$a(t) = \left(\frac{t}{t_s}\right)^q (a_s - 1) + 1 - (t_s - t)^n \left\{ \sum_{j=0}^{\infty} \sum_{k=0}^{N_j} a_{jk} (t_s - t)^{j/Q} (\log^k[t_s - t]) \right\}, \quad (2.12)$$

where the quantity in $\{\dots\}$ brackets is a convergent double Psi-series which tends to zero as $t \rightarrow t_s$; a_{jk} are constants, $N_j \leq j$ are positive integers and $Q \in \mathbb{Q}^+$ [68].

Barrow then shows that if we take n to lie in the range $(N, N + 1)$ for $N \geq 2$ where $N \in \mathbb{Z}^+$ we can create a singularity where,

$$\frac{d^{N+1}a}{dt^{N+1}} \rightarrow \infty, \quad (2.13)$$

but

$$\frac{d^r a}{dt^r} \rightarrow 0, \text{ for } r \leq N \in \mathbb{Z}^+. \quad (2.14)$$

He then explains that through the above formulation for the scale factor in Equation 2.12 one will be able to obtain a pressure singularity that is accompanied by higher time derivatives of the scale factor in Friedmann equations of higher-order gravity theories. This will then mean that in these theories, higher-order curvature corrections to the Friedmann equation are not able to remove singularities but they can make them milder.

Let us now go back to the specific form for the scale factor in Equation 2.11 that was first proposed by Barrow. In order to be able to assess a model with such a scale factor in light of the data, we first need to familiarise ourselves with the parameters of this model. The next section is devoted to such considerations.

2.2.2.1 Model parameters

We now return to the special form of the solution for the scale factor first considered by Barrow given in Equation 2.11, which is the one considered in this work following its earlier investigation in Dabrowski et al. [1]. In [1] the authors confronted an SFS model with a scale factor of this form with the luminosity distance redshift relation for a sample of high redshift supernovae.

By fixing the zero of time, i.e. setting $a(0) = 0$, and the time of the singularity, $a(t_s) = a_s$, the scale factor may be written in the equivalent form:

$$a(t) = A + (a_s - A)\left(\frac{t}{t_s}\right)^m - A\left(1 - \frac{t}{t_s}\right)^n. \quad (2.15)$$

Dabrowski et al. [1] changed the original parametrisation for the scale factor by using $A = \delta a_s$, to obtain:

$$a(t) = a_s[\delta + (1 - \delta)y^m - \delta(1 - y)^n] \quad , \quad y = \frac{t}{t_s}, \quad (2.16)$$

where a_s , n , m , δ and t_s are constants to be determined. This way they created a non-standardicity parameter, δ , which, as it tends to zero, recovers the standard Friedmann limit (i.e. a model with no SFS). We therefore note that the proposed SFS scale factor is only an approximate solution to the Friedmann equation which becomes exact only when $\delta \rightarrow 0$.

Now, writing the expression for the r th derivative of the scale factor:

$$\begin{aligned}
a^{(r)} = a_s & \left[\left(\frac{m(m-1)\dots(m-r+1)}{t_s^r} \right) (1-\delta)y^{m-r} \right. \\
& \left. + (-1)^{r-1}\delta \left(\frac{n(n-1)\dots(n-r+1)}{t_s^r} \right) (1-y)^{n-r} \right], \quad (2.17)
\end{aligned}$$

which is related to the pressure derivative $p^{(r-2)}$, shows that in general one can have a pressure derivative $p^{(r-2)}$ singularity which is accompanied by the blowing up of the r th derivative of the scale factor $a^{(r)}$.

From Equation 2.17 one can see that for a pressure derivative singularity to occur we need:

$$r - 1 < n < r \quad , \quad r = \text{integer}. \quad (2.18)$$

We note that, for $r \geq 3$, all energy conditions are fulfilled. These singularities are Generalised Sudden Future Singularities (GSFS) [1] as talked about in §2.1 and they may occur in theories with higher-order curvature corrections [39]. For an SFS however we need $r = 2$ which means that $1 < n < 2$. Furthermore, we note that in Barrow's definition $\delta = A/a_s$ should be positive but Dabrowski et al. [1] argue that δ should be allowed to be either positive or negative corresponding to a decelerating or an accelerating universe respectively if one considers Equation 2.17. We shall return to this point later on in this section when we present our method of determining a suitable range for the possible values for this parameter.

To obtain the asymptotic behaviour of scale factor close to an SFS we perform a change of coordinates and place the singularity at $t = 0$ and Taylor expand the scale factor around it to get:

$$a(t) = a_s(1 + m(1 - \delta)(y - 1)) + \dots \quad (2.19)$$

An important requirement is that the asymptotic behaviour of the scale factor close to the Big Bang singularity follows a simple power law $a_{BB} = y^m$ which will simulate the behaviour of flat $k = 0$ barotropic fluid models with $m = 2/3(w + 1)$. This will ensure that all the standard observed characteristics of the early universe such as the CMB, density perturbations and Big Bang nucleosynthesis are preserved. Additionally we realise that all the energy conditions are satisfied if we require m to lie in the range,

$$0 < m < 1. \tag{2.20}$$

Therefore in accordance with Equation 2.20 if for a standard dust-dominated universe we take $m = 2/3$ our SFS model will reduce to the Einstein-de Sitter universe at early times. As discussed before, an Einstein-de Sitter universe is one which is a flat matter-dominated ($\Omega_m = 1$) universe where the evolution of the scale factor can be shown to take the following form:

$$a(t) \propto t^{2/3}. \tag{2.21}$$

The other parameters of the model that we should consider are: a_s , t_s and δ . The parameter a_s , which sets the physical size of the universe at the time of the SFS, will cancel out in the equations of the standard cosmological probes we have used to test the model. Thus we do not need to consider this parameter further.

For constraining the time, t_s , when an SFS might occur, we can introduce the dimensionless parameter $y_0 = t_0/t_s$, where t_0 is the current age of the universe. Since the singularity is assumed to be in the future, it follows that $0 < y_0 < 1$.

The current acceleration obtained in the SFS model, as a result of the particular form adopted for the scale factor, leads to a divergence of the pressure at sometime in the future evolution of the model. Dabrowski et al. [40] refer to the cause of this late time acceleration in the SFS model as a ‘pressure-driven dark energy’.

With the parameters n , m and y_0 having definite values or ranges, it remains to identify a suitable range of investigation for the non-standardicity parameter δ . In [1] negative values of δ were associated with acceleration, but we revisited this question in order to check rigorously the range of values of δ which should be considered, taking into account all relevant physical constraints. We came to find out about some of these conditions through experimentation with the codes written to calculate some required functions of the scale factor. For instance we realised we have to check that the scale factor is positive at all times or else the code would crash. Another example is the physical condition that positive and negative redshifts should correspond to past and future events respectively. Now one does not normally consider the unbounded future but in our case we have a milestone in the future, namely, a hypothetical SFS. Therefore, by future we really mean the time until an SFS. Therefore we checked the redshift conditions and also the sign of the scale factor up to such an event at $y = 1$.

Interestingly, through these considerations we discovered something quite unusual about the parametrisation of the scale factor for the SFS model we are investigating. If we look at the SFS scale factor again,

$$a(t) = a_s[\delta + (1 - \delta)y^m - \delta(1 - y)^n] \quad (2.22)$$

we can see that for $y > 1$ which corresponds to a time after an SFS, the term $(1 - y)^n$ where $1 < n < 2$, is in fact complex! That is because for

$y > 1$, $(1 - y)$ is negative which when raised to a decimal power, n in this case, it will be complex. Nevertheless, since we are not concerned with times after an SFS, this should not affect our investigations.

Furthermore, we imposed the established observational facts that both the first and second derivatives of the scale factor are currently positive. That is to say, we rejected any combination of SFS model parameters for which $\dot{a}_0 \leq 0$ or $\ddot{a}_0 \leq 0$ corresponding to current contraction and deceleration.

Finally, we checked the sign of \dot{a} throughout the evolution of the SFS model and rejected parameter combinations that would predict a contracting universe (where $\dot{a} < 0$) at any point in the interval $0 \leq z \leq 1$, where the Hubble diagram of Type Ia supernovae over this range of redshifts securely confirms the expansion of the universe. However, we did not require that the expansion history of the universe outside of this range continues in the same manner. Neither did we make assumptions about the future evolution of the universe and therefore we did not exclude parameter combinations that would predict e.g. future contraction of the universe.

Thus by fixing $m = 2/3$, as previously discussed, and varying n and y_0 over their theoretically permitted ranges, we set out to identify those values of δ which were consistent with the above physical constraints. However, it quickly became apparent that this task was not possible analytically. Therefore we carried out a numerical exploration of the 3-dimensional parameter space (n, y_0, δ) . This then told us that δ should not be positive. Although we have arrived at the same result as was first given by Dabrowski et al. [1], our result stands on a much firmer footing as we have extended our requirements to the satisfaction of various other necessary physical conditions which were not discussed before.

2.2.3 Conclusions

In this chapter we have examined some of the possibilities discussed in the literature for the fate of the universe and exotic singularities in non-standard cosmologies. After monitoring where Sudden Future Singularities stand in the current classifications of exotic singularities, we then solely focused on Sudden Future Singularities and the models containing them and presented a selective overview of the literature on the subject. We started from the motivation behind the creation of Sudden Future Singularities which was to do with the energy conditions of GR. We then talked about the energy conditions and their debatable applicability today. Then we went on to talk about the SFS from the viewpoint of the statefinders, which we briefly explained. Moreover, we discussed how exactly Barrow came up with the idea of this kind of singularity. Quantum effects near SFSs and how they can remove sudden singularities were also briefly touched upon together with various other non-standard models where SFSs might arise. Furthermore, SFS removal was discussed as possible in modified gravity theories. We then moved on to detail at length the specific SFS model of Barrow which we investigated in this thesis. It now remains to be seen how well this particular SFS model fits the available data, an investigation which we will begin in Chapter 3.

Chapter 3

Data Analysis Methodology

“Data analysis is simply a dialogue with the data.”

Stephen F. Gull, Cambridge 1994

What use is a hypothesis if it is not to conform to the data? Indeed if we are to make progress in our understanding of nature we must be able to test our hypothetical models with the data and hence consequently make modifications to our models accordingly and repeat this process until we reach a coherent model whose accurate predictions we can rely on. We can think of data as our only guiding light in the dark of our quest to discover. Therefore we need to be able to take as much as possible from it in correct ways to ensure that we are being guided in the right way. Data analysis methodology provides us with the necessary tools and skills needed to allow us speak to the data, as Gull puts it.

In the context of cosmology, where our guiding light is indeed light itself, data analysis techniques play a more significant role today than ever before with the increasing bulk of ever more precise data that is becoming available through state of the art experiments such as

the Planck [26] satellite for measuring temperature anisotropies in the CMB. With no sign of letting up of this trend, such a situation calls for not only reliable data analysis techniques but also ones that are cleverly designed to tackle large datasets ever more efficiently. This is because with the computing power available to us today we simply cannot afford brute-force and exhaustive searches.

With regards to the data in general, since we are limited by accuracy and we can never be certain that we have a complete set of data, our inference about nature is therefore inevitably probabilistic [88]. We therefore require to base our investigations on a probability theory and try to find the most probable models that describe our data. Now, there are two different frameworks where the notion of probability takes on different definitions. These two paradigms are known as *frequentist* and *Bayesian*. In the frequentist regime, the probability of an event is measured through in principle infinitely many repetitions of the same experiment. Then the event with the highest frequency of occurrence is assigned the highest probability and others are allocated probabilities according to their relative frequencies. In the second Bayesian approach however, probability is interpreted as our degree of belief that something is true which is based on our prior knowledge and background information, modified in the light of any new data that we acquire. Frequentists argue that the Bayesian approach is subjective as it depends on background information and our logical reasoning. But indeed probability itself is subjective since by nature it depends on the available information. What is crucial to note in the Bayesian way of thinking is that given the same background information, different Bayesian analyses should produce the same probabilities. This is where objectivity in the Bayesian approach shows itself. Bayesian probability theory which is basically probabil-

ity theory as logic, is becoming increasingly popular in physics and astronomy today [88].

Cosmology is perhaps an extreme example of a physical phenomenon where in order to understand it, a Bayesian analysis would seem to be the only option and hence essential. This is seen by realising that we have only one universe of which to make sense. In other words, our inability to start over another universe to investigate its properties tells us that we ought to rely on plausible reasoning rather than on the frequency of occurrence. And indeed the Bayesian framework is the one we adopt in this work too.

3.1 Bayesian Inference

Bayesian inference, named after Thomas Bayes (whose ideas were published after his death in 1763 by his student) is a method of assessing the viability of a certain hypothesis, H , according to the available observational data, D , through calculating the probability of the hypothesis given the data and any prior information, I , that we might have concerning the hypothesis and the data. We write this probability as $p(H|D, I)$, which reads as the probability that the hypothesis, H , is true given the data, D , and any prior information, I . Bayesian inference follows specific rules for combining probabilities. These are:

The sum rule:

$$p(H|I) + p(\overline{H}|I) = 1. \tag{3.1}$$

Here \overline{H} denotes the negation of H . This rule implies that the total probability is divided between the possible different outcomes. Here

we have two possible outcomes: H or \overline{H} .

The product rule:

$$p(H, D|I) = p(H|I)p(D|H, I). \quad (3.2)$$

This rule states that the probability that both H and D are the outcomes is the product of the individual probabilities given that H has already happened. An equal statement is that the probability that both H and D are the outcomes is the product of their individual probabilities given that D has happened before, that is: $p(H, D|I) = p(D, H|I)$, where:

$$p(D, H|I) = p(D|I)p(H|D, I). \quad (3.3)$$

We can now solve for $p(H|D, I)$ by equating Equation 3.2 and Equation 3.3 to get:

$$p(H|D, I) = \frac{p(H|I)p(D|H, I)}{p(D|I)}. \quad (3.4)$$

This is Bayes' theorem which is one of the most important rules for calculations in Bayesian inference [88]. The terms in Equation 3.4 are described below:

- $p(H|I)$ is called the *prior probability* of H and it arises from the knowledge we already have about the hypothesis regardless of the data. If we do not have much prior information we often set this probability equal to a constant.
- $p(H|D, I)$ is the *posterior probability* which calculates the probability of the hypothesis after the data are taken into account

together with our prior knowledge and therefore calculates our state of knowledge about the hypothesis.

- $p(D|H, I)$ is called the *likelihood* of H and it gives the probability that the data is obtained given the hypothesis and our prior knowledge. In effect the likelihood function modifies the prior in light of the data to yield the posterior.
- $p(D|I)$ is called the *evidence* which can be treated as the normalisation factor when we realise that the sum of the posterior probability over all the parameters of the hypothesis should equal 1, that is in the continuum limit:

$$\int_{\Delta H} p(H|D, I)dH = 1, \quad (3.5)$$

where ΔH indicates the range of integration for the hypothesis parameter space. Therefore, since the evidence does not depend on the hypothesis parameters, in the context of parameter estimation for a given hypothesis we can ignore it and hence present Bayes' theorem as a proportional relation:

$$p(H|D, I) \propto p(D|H, I)p(H|I). \quad (3.6)$$

Therefore putting together the above we see that what Bayes's theorem does is to combine what new data have to say about the hypothesis through the likelihood, together with our prior knowledge on it in the prior probability, to give us an updated knowledge of the hypothesis in the form of the posterior probability. And hence, it can be seen how the Bayes' theorem describes a learning process whereby the probability of the hypothesis is updated in light of new data. In doing so for every new data the old posterior probability becomes the new prior and so on.

3.1.1 Parameter Estimation

Now assuming that the hypothetical model under study is correct, we then want to determine its parameters from data through using Bayes' theorem. This is called *parameter estimation*. If we are dealing with continuous parameter spaces, the parameters we are looking for are in a *probability density function* or a pdf. But a more general name for a pdf is a probability distribution function which also includes discrete parameter spaces. To reiterate the definition of parameter estimation more correctly, we use Bayes' theorem to determine the full posterior pdf of the parameters rather than one single parameter value. Then to describe the pdf and make sense of it in relation to the parameter we are seeking, we quote the *posterior mode* (the most probable value for the parameter) or the *posterior mean* (these two match for a normal distribution) as our “best-fit” parameter together with error bars. We will explain these quantities and how to obtain them in the next section.

As a final discussion in this section, we will talk about *marginalisation* which is an essential and useful calculation tool that lets us infer more relevant information from our full posterior pdf. In many problems we might be confronted with situations where a particular set of model parameters are more important to us than the rest. In these circumstances we integrate out the uninteresting parameters, which are called *nuisance parameters*. This integration procedure is called *marginalisation* and the resulting posterior pdf is called the *marginal posterior pdf* for the interesting parameters. To see an example of this explicitly, if we have a model, M , with parameters α and β , where we are interested to know more about the latter, we integrate the full posterior pdf over the former. That is:

$$p(\beta|D, M) = \int p(\beta, \alpha|D, M)d\alpha. \quad (3.7)$$

Next in §3.1.2 we will talk about parameter estimation methods which follow from Bayes' theorem discussed in this section.

3.1.2 Maximum Likelihood and χ^2 Fitting

We employed the χ^2 test for comparing our SFS model with the data which, in the case of normally distributed likelihood function, is equivalent to applying the principle of maximum likelihood. Following from Equation 3.6 if we further assume that the prior probability takes on a uniform distribution (i.e. $p(H|I) = \text{constant}$) implying that we have no *a priori* information regarding our hypothesis (which is safe choice and indeed what we often need to do in practice) we can rewrite Bayes' theorem as:

$$p(H|D, I) \propto p(D|H, I) = \mathcal{L}. \quad (3.8)$$

And therefore we have the posterior probability proportional to the likelihood. This means that maximising the likelihood is equivalent to maximising the posterior probability. Hence we can now work with the likelihood, which we assume to be a Gaussian distribution, and determine which sets of SFS model parameters are most likely to produce the observed data. To this end, we maximise the likelihood function such that its first derivative is zero and its second derivative is negative i.e. for Θ_0 representing the maximum likelihood set of parameters of the model under study:

$$\left. \frac{d\mathcal{L}}{d\Theta} \right|_{\Theta_0} = 0 \quad \text{and} \quad \left. \frac{d^2\mathcal{L}}{d\Theta^2} \right|_{\Theta_0} < 0. \quad (3.9)$$

This will define the best-fit value of the parameter. Then in order to determine the reliability of our best guess, we need to find the error on this value. The error is a measure of the spread of the likelihood function around the best-fit value. We can work this out by Taylor expanding the likelihood function about our best guess. Instead of working with the likelihood function which could consist of sharp peaks, it is better that we work with the logarithm of it which varies more slowly with the parameter(s) and so can be better approximated. Therefore, for $\ln \mathcal{L}$ expanded about the best-fit value of Θ_0 we have:

$$\ln \mathcal{L}(\Theta) = \ln \mathcal{L}(\Theta_0) + \left. \frac{1}{2} \frac{d^2 \ln \mathcal{L}}{d\Theta^2} \right|_{\Theta_0} (\Theta - \Theta_0)^2 + \dots, \quad (3.10)$$

where at the maximum likelihood parameter(s), Θ_0 we have:

$$\left. \frac{d \ln \mathcal{L}}{d\Theta} \right|_{\Theta_0} = 0. \quad (3.11)$$

The second linear term which in addition to the first derivative term (3.11) also involves $(\Theta - \Theta_0)$ (both of which are zero at Θ_0) is therefore missing in the expansion in Equation 3.10 [89]. And with the first term a constant which does not say anything about the function and also ignoring all the higher order terms, we are left with:

$$\mathcal{L}(\Theta) \approx C \exp \left(\left. \frac{1}{2} \frac{d^2 \ln \mathcal{L}}{d\Theta^2} \right|_{\Theta_0} (\Theta - \Theta_0)^2 \right), \quad (3.12)$$

where C is a normalisation constant. This takes the form of the well-

known Gaussian distribution and demonstrates that adopting a Gaussian likelihood function from the beginning is a natural choice and is indeed well-justified provided we neglect the higher order terms. Now writing the Gaussian function in a more familiar form, we have:

$$p(x|\mu, \sigma) = \frac{1}{\sigma\sqrt{2\pi}} \exp\left[-\frac{(x - \mu)^2}{2\sigma^2}\right], \quad (3.13)$$

where the maximum occurs at $x = \mu$ with the width of the function proportional to σ . When we now compare this general Gaussian function with the function we arrived at in Equation 3.12 we see that as expected the maximum occurs at Θ_0 , the normalisation constant is $C = \frac{1}{\sigma\sqrt{2\pi}}$ and that σ corresponds to:

$$\sigma = \left(-\frac{d^2 \ln \mathcal{L}}{d\Theta^2} \Big|_{\Theta_0} \right)^{-1/2}. \quad (3.14)$$

Hence, we have now derived the spread of our likelihood function which tells us about the errors on our best-fit values and therefore their reliability. The two quantities of the best-fit and a measure of the spread of our likelihood function well-summarise the likelihood function we were looking for. We present this summary of the likelihood function in the following form:

$$\Theta = \Theta_0 \pm \sigma. \quad (3.15)$$

With the best-fit and error we have effectively determined what are called the first and second moments of our likelihood function which are enough to describe a Gaussian likelihood function. In general, one can determine the shape of a likelihood through its moments. Obviously, the more peaked the distribution is at the maximum value, the

more confidence we have that we have estimated the correct parameter values. The central r th moment of a probability density function, $p(x)$ with a mean of μ , where the “central” refers to taking the mean as the origin, is:

$$\langle (x - \mu)^r \rangle = \int_{-\infty}^{+\infty} (x - \mu)^r p(x) dx. \quad (3.16)$$

As mentioned previously a Gaussian distribution is described only by the first and second moments and since we have assumed a Gaussian likelihood function we are interested in these two, which are:

First central moment (the mean):

$$\langle (x - \mu) \rangle = \langle x \rangle - \mu = 0. \quad (3.17)$$

Second central moment (the variance):

$$\text{var}(x) = \sigma^2 = \langle (x - \mu)^2 \rangle. \quad (3.18)$$

To see the above, we expand it to get:

$$\begin{aligned} \langle (x - \mu)^2 \rangle &= \langle (x^2 - 2\mu x + \mu^2) \rangle = \langle x^2 \rangle - 2\mu \langle x \rangle + \mu^2 \\ &= \langle x^2 \rangle - 2\mu^2 + \mu^2 = \langle x^2 \rangle - \mu^2 = \langle x^2 \rangle - \langle x \rangle^2 \\ \sigma^2 &= \langle x^2 \rangle - \langle x \rangle^2. \end{aligned} \quad (3.19)$$

This is the definition of the variance which is the square of σ , the *standard deviation*, that gives a good measure of the spread of the pdf. We can express the spread of the pdf in multiples of the standard

deviation, i.e. 1σ , 2σ and 3σ where if we are farther than 3σ from the true value then we do not have such reliable results. In a Gaussian likelihood function these levels correspond to 68.3%, 95.4% and 99% of the posterior pdf respectively. We will see below how we can calculate these so-called *credible regions* for our parameters. They are called credible regions, since we can say that we are e.g. 68.3% confident that the true value lies in a certain fraction of the posterior pdf.

We now show how exactly the above procedure is done in practice. If we assume that our data are independent, we can write their joint pdf as the product of the individual pdfs (which recall we are assuming are Gaussian):

$$\mathcal{L}(\Theta) = \prod_{i=1}^n \frac{1}{\sigma_i \sqrt{2\pi}} \exp \left[-\frac{(D_i - f_i(\Theta))^2}{2\sigma_i^2} \right], \quad (3.20)$$

where D_i is an independent datum with an uncertainty of σ_i and $f_i(\Theta)$ is our model predicted value for the i th datum, D_i . We can now write the likelihood function in the form:

$$\mathcal{L}(\Theta) \propto \exp \left[-\frac{1}{2} \chi^2 \right]. \quad (3.21)$$

where,

$$\chi^2 = \sum_{i=1}^n \left(\frac{D_i - f_i(\Theta)}{\sigma_i} \right)^2, \quad (3.22)$$

which is the sum of the normalised residuals, being the differences between the model predicted values and the data divided by the errors on the data, i.e. $(D_i - f_i(\Theta))/\sigma_i$. And indeed this quantity is called the χ^2 since provided the residuals are drawn from a normal distribution

$\Delta\chi^2$ as a Function of Confidence Level and Degrees of Freedom						
p	ν					
	1	2	3	4	5	6
68.3%	1.00	2.30	3.53	4.72	5.89	7.04
90%	2.71	4.61	6.25	7.78	9.24	10.6
95.4%	4.00	6.17	8.02	9.70	11.3	12.8
99%	6.63	9.21	11.3	13.3	15.1	16.8
99.73%	9.00	11.8	14.2	16.3	18.2	20.1
99.99%	15.1	18.4	21.1	23.5	25.7	27.8

Figure 3.1: As the title reads, the table is showing $\Delta\chi^2$ values as a function of confidence level and degree of freedom or the number of parameters of the model, ν . Table from: <http://apps.nrbook.com/c/index.html>.

then this quantity follows a χ^2 distribution.

Looking at Equation 3.21 we can see that to find the maximum likelihood parameters we need to minimise χ^2 . This method is known as the *least squares fitting* method which is the most popular and most widely used method in data analysis [89]. To recapitulate, such a simple and effective method results directly from Bayes' theorem and the assumptions of constant prior and Gaussian likelihood pdf.

Now to return to our credible regions discussion, we can calculate contours of constant probability which enclose a certain percentage of the posterior pdf by calculating $\Delta\chi^2$ values which are measured from χ_{\min}^2 . These $\Delta\chi^2$ values can be calculated for different numbers of degrees of freedom (model parameters). These values are shown in the table in Figure 3.1

As a final note in this section, it may be possible to minimise the χ^2 analytically in some fitting problems, but this is usually done numerically in practice. That is, we either go through all the parameter space in an n -dimensional grid, which is computationally viable only for low values of n , or use MCMC methods which provide a fast and efficient

way of generating samples from the posterior probability for high dimensional parameter spaces. We will explain the MCMC method in detail in the next section but briefly, in this method a random walk is carried out in the parameter space which moves around according to the probabilities of different regions, identifying and exploring the most probable areas much faster than exhaustive grid searches.

3.2 Markov Chain Monte Carlo

In this section we will introduce a very efficient mathematical tool for estimating posterior distributions for high-dimensional models for which direct and exhaustive calculations are not computationally feasible at least at the current time [88]. This powerful method is called *Markov Chain Monte Carlo* (MCMC). The method's principal use is in evaluating multi-dimensional integrals. The way this method works is by generating random walks through the parameter space, constructing Markov chains that will explore the distribution under study. This procedure is led by suitable algorithms. Instead of drawing independent samples from the posterior pdf, these algorithms create random walks in the parameter space with the sampling probability proportional to the posterior probability, $p(H|D, I)$. Therefore what all MCMC algorithms do and indeed what makes them so efficient is the fact that they direct the walker towards more probable areas of the parameter space and therefore waste less time and computational power in low probability areas. This advantage is what a Monte Carlo method, which gives equal attention to all points in the parameter space, lacks.

The algorithm that we use which is the most popular one is the Metropolis-Hastings algorithm. More precisely we use its special case

where the proposal density is symmetric which is the Metropolis algorithm. This algorithm works in two stages. Firstly, one samples a tentative point in the parameter space, say x' using a *proposal density* which is typically chosen to be Gaussian with the mean of the previous sample, x in the chain and a standard deviation which can be adjusted to yield more efficient sampling. Secondly, one will decide whether to accept or reject the new sample based on the ratio of probabilities, r :

$$r = \frac{p(x'|D, I)}{p(x|D, I)}, \quad (3.23)$$

where $p(x'|D, I)$ is the probability at x' and $p(x|D, I)$ the probability at x . If $r \geq 1$ then x' is accepted as the next link in the chain. If $r < 1$, x' is accepted with probability $= r$. The way this is done is by generating a random number, say y from a uniform distribution between 0 and 1. Then the probability of y being less than r is exactly r , so we accept the new point in the chain provided y is less than r , otherwise the new sample in the chain is a copy of the old point i.e. x . The Markov chain is therefore constructed such that each new sample depends on the previous one based on a transition probability. When the process is completed, the constructed Markov chain's sequence of x 's will then be a full representative sample of the posterior pdf after an initial *burn-in* period has been discarded. The burn-in period comprises the initial samples which are not to be trusted that are drawn from the desired posterior pdf since the MCMC chain has not come to stabilise at the beginning.

It should be noted that by only accepting points in the chain for which $r \geq 1$ we would only be going uphill in the likelihood function but by also accepting points for which $r < 1$ with probability r we are allowing the chain to explore the neighbourhood of the maximum as

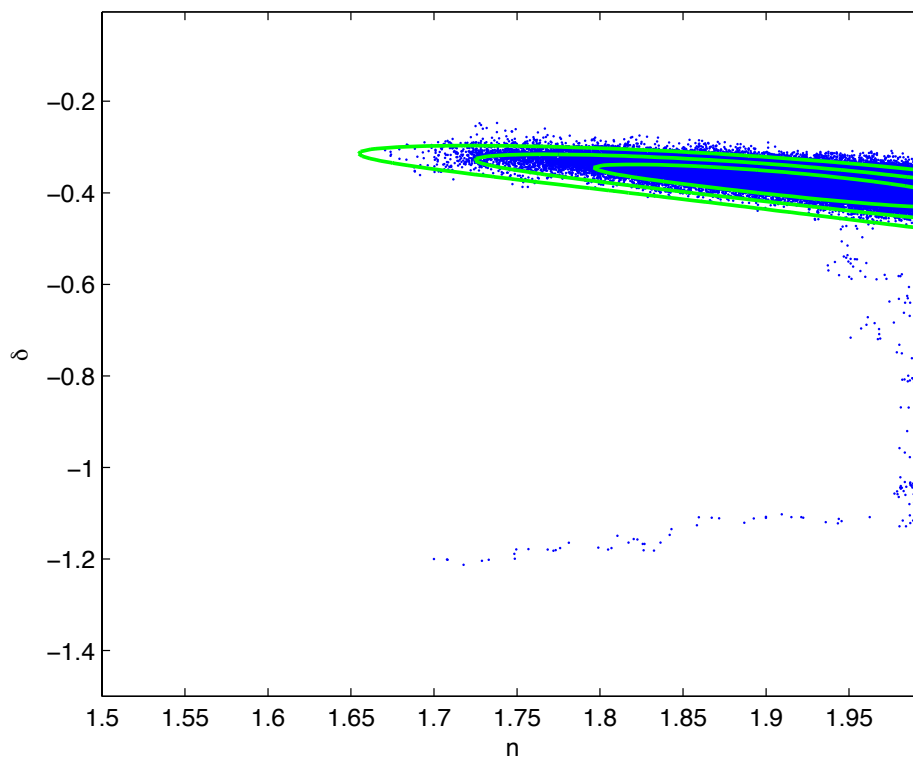


Figure 3.2: Example plot of an MCMC exploration of in this case the parameter space of (n, δ) in light of SNe Ia data. The chain starts from the point with coordinates $n = 1.7$ and $\delta = -1.2$ and after an initial burn-in period it reaches the desired posterior pdf. The chain presented here is 10^5 steps long and the proposal density chosen for this MCMC search is a Gaussian with a width of 0.01 for both parameters. The green contours have been calculated through a grid-based search over a 100×100 grid. To demonstrate the numerical consistency between the two methods we note that the grid-based search results in: $n = 1.951 \pm 0.036$ and $\delta = -0.37 \pm 0.02$ and the MCMC method gives: 1.943 ± 0.041 and $\delta = -0.37 \pm 0.02$. One can see how well the methods agree with each other.

well to map out this area. This is valuable information as it will let us determine errors on the maximum likelihood parameters.

One other very useful property of the MCMC method is to do with the way the marginalised likelihoods of the parameters of the posterior distribution are obtained. This is simply the sequence of the coordinates of the samples, x 's, explored by the chain. Furthermore in this method, we can easily determine what regions correspond to required fractions of the sample, which is now the posterior pdf. To do this, when we are certain that our chain has converged, we order the random chain points based on their likelihood values and then find the points which correspond to 68.3%, 95.4% and 99% of the chain. These fractions will then be good estimators of the 1σ , 2σ and 3σ credible regions of the likelihood function.

In Figure 3.2 we show an example of an MCMC chain exploring the posterior pdf of in this case the SFS parameters, n and δ in light of the SNe Ia data. It can be seen how well the chain identifies the set of contours calculated through a grid search starting from $n = 1.7$ and $\delta = -1.2$. One can clearly see the burn-in period before the chain reaches the posterior pdf and stabilises. This demonstration is for a 2-dimensional problem but of course the real power of the MCMC method become apparent in higher dimensional problems as we will see later in Chapter 6.

3.3 Conclusions

In this chapter we have discussed the Bayesian data analysis techniques we used to confront our SFS model with the data we will talk about in Chapter 4. We started by introducing the Bayes' theorem

and then talked about our parameter estimation method based on the principle of maximum likelihood. We showed that in effect we used least squares fitting in our analysis in producing contour plots for the various kinds of data we will employ in the parameter space search of our SFS model. Finally, we talked about the MCMC method and how efficiently it works to construct our sought for pdfs. We used both MCMC and exhaustive grid-based search methods in exploring our parameter space in our analysis, the results of which are presented in the next two chapters.

Chapter 4

Cosmological Constraints

In §1.4 we discussed the most important cosmological observations that have helped shape the standard model of cosmology. Here in this chapter we will talk in detail about the specific observational probes derived from those ground breaking observational discoveries, which we employed in our data analysis.

4.1 SNe Ia Luminosity Distance-Redshift Relation

By far the most common and indeed historical cosmological constraint used in model fitting is the luminosity distance-redshift relation as probed by SNe Ia. One can place constraints on one's model parameters by comparing the luminosity distances as predicted by their model with the observed values. What we actually do in practice is work with the distance modulus, μ which gives the relation between the flux of the source that we can observe and its intrinsic luminosity, expressed in terms of m (apparent magnitude) and M (absolute magnitude) respectively. The relation reads as:

$$\mu = m - M = 5 \log d_L + 25, \quad (4.1)$$

where d_L is the luminosity distance (in units of Mpc) to the source. The luminosity distance is defined as the distance to a source of luminosity L with an observed flux F :

$$F = \frac{L}{4\pi d_L^2}. \quad (4.2)$$

But this relation only holds in a static universe with Euclidean geometry. To consider luminosity distance first in an expanding universe, we need to invoke the comoving distance, r and multiply it by the scale factor, $a(t)$ at the time of observation which is now hence $a(t_0) = a_0$. Therefore we can now write:

$$F = \frac{L}{4\pi a_0^2 r^2}. \quad (4.3)$$

Now we need to take into account the effect of expansion on the energy of the photons. This works in two ways. Firstly the number of photons per unit time is diminished by a factor of $(1 + z)$ since the space has got bigger and secondly the energy of photons is redshifted by the expansion by an additional factor of $(1 + z)$, hence:

$$F = \frac{L}{4\pi a_0^2 r^2 (1 + z)^2}. \quad (4.4)$$

Therefore we have the luminosity distance in a flat expanding universe as:

$$d_L = a_0 r (1 + z). \quad (4.5)$$

Now, to also take into account the geometry of the space-time considered, we know that the comoving distance is defined as:

$$r(z) = \frac{c}{a_0 H_0 \sqrt{|\Omega_k|}} S \left(\sqrt{|\Omega_k|} \int_0^z \frac{dz'}{E(z')} \right), \quad (4.6)$$

where, $S(x) = \sin(x), x, \sinh(x)$ for a closed, flat and open universe, Ω_k is the curvature density parameter, $E(z)$ is the Hubble function as introduced before in §1.3 and c and H_0 are the speed of light and the Hubble constant as usual and hereafter. Assuming flatness, we now arrive at the luminosity distance relation we presented in Equation 1.23, i.e.:

$$d_L(z) = \frac{c(1+z)}{H_0} \int_0^z \frac{dz'}{E(z')}. \quad (4.7)$$

Although as mentioned in the previous section an SFS could occur regardless of the curvature of the universe, to make our calculations simpler, and also to be consistent with the present observational data, we considered only a flat universe which bears an SFS. Furthermore, since $E(z) = \frac{H(z)}{H_0}$ and $H(z) = \frac{\dot{a}}{a}$, as discussed previously, we expressed $E(z)$ as a function of the SFS scale factor, as given in Equation 2.19, and its first derivative in our d_L calculation.

We used 557 supernovae from the Union2 dataset as compiled by [17] which is the largest published SNe Ia sample to date and it consists of SNe Ia in the redshift range, $0.015 < z < 1.4$. A sample of these data are shown in the table in Figure 4.1.

Moreover, in our analysis we treated the Hubble constant as a nuisance parameter, marginalising over a range of values using as a prior distribution the most recent (at the time) results from the Hubble

SN	z_{CMB}	m_B^{max}	x_1	c	μ	sample	cut
1993ah	0.0285	16.86(0.19)	-2.26(0.93)	0.23(0.09)	34.61(0.23)	1	...
1993ag	0.0500	17.79(0.05)	-1.09(0.24)	0.12(0.02)	35.95(0.17)	1	...
1993o	0.0529	17.60(0.05)	-1.03(0.14)	-0.01(0.02)	36.09(0.16)	1	...
1993b	0.0701	18.43(0.04)	-0.53(0.21)	0.09(0.02)	36.71(0.16)	1	...
1992bs	0.0627	18.25(0.05)	-0.27(0.23)	0.02(0.02)	36.75(0.16)	1	...
1992br	0.0876	19.19(0.11)	-2.97(0.38)	-0.04(0.07)	37.50(0.19)	1	...
1992bp	0.0786	18.27(0.04)	-1.27(0.20)	-0.02(0.02)	36.76(0.16)	1	...
1992bo	0.0172	15.75(0.13)	-2.68(0.18)	0.03(0.02)	33.93(0.20)	1	...
1992bl	0.0422	17.30(0.08)	-1.95(0.24)	0.02(0.04)	35.61(0.17)	1	...
1992bh	0.0453	17.58(0.05)	-0.02(0.25)	0.10(0.02)	35.91(0.17)	1	...
1992bg	0.0365	16.71(0.09)	-0.66(0.22)	0.01(0.03)	35.18(0.17)	1	...
1992bc	0.0196	15.07(0.11)	0.51(0.10)	-0.05(0.01)	33.86(0.18)	1	...
1992aq	0.1009	19.27(0.05)	-1.36(0.43)	-0.02(0.03)	37.73(0.17)	1	...
1992al	0.0135	14.44(0.16)	-0.41(0.13)	-0.05(0.01)	33.10(0.22)	1	z
1992ag	0.0273	16.26(0.09)	-0.13(0.21)	0.19(0.02)	34.35(0.18)	1	...
1992ae	0.0746	18.39(0.04)	-0.68(0.21)	0.01(0.03)	36.86(0.16)	1	...
1992p	0.0265	16.03(0.09)	0.70(0.58)	-0.02(0.02)	34.75(0.19)	1	...
1990af	0.0499	17.75(0.05)	-2.65(0.26)	0.07(0.02)	35.84(0.16)	1	...
1990o	0.0306	16.19(0.08)	0.39(0.29)	-0.00(0.03)	34.82(0.17)	1	...
1992bk	0.0589	18.04(0.13)	-2.11(0.32)	-0.04(0.08)	36.35(0.17)	1	p
1992au	0.0603	18.12(0.11)	-1.80(0.53)	0.01(0.09)	36.33(0.17)	1	p
1992j	0.0461	17.70(0.09)	-1.86(0.27)	0.15(0.05)	35.55(0.16)	1	p
1991ag	0.0139	14.37(0.17)	0.77(0.22)	0.02(0.03)	32.88(0.22)	1	p,z
1991u	0.0324	16.40(0.09)	0.23(0.22)	0.11(0.03)	34.62(0.17)	1	p
1991s	0.0561	17.71(0.07)	0.24(0.23)	0.02(0.03)	36.17(0.15)	1	p
1990y	0.0387	17.38(0.08)	-0.33(0.26)	0.25(0.03)	35.17(0.17)	1	p
1990t	0.0397	17.18(0.07)	-0.59(0.16)	0.08(0.03)	35.38(0.16)	1	p
2001cz	0.0163	15.02(0.14)	0.04(0.14)	0.12(0.01)	33.31(0.14)	2	...
2001cn	0.0154	15.26(0.14)	-0.79(0.12)	0.22(0.01)	33.20(0.15)	2	...
2001bt	0.0144	15.26(0.15)	-1.14(0.11)	0.26(0.01)	33.06(0.16)	2	z
2001ba	0.0305	16.19(0.07)	0.00(0.14)	-0.04(0.01)	34.87(0.09)	2	...
2000ca	0.0245	15.53(0.09)	0.35(0.20)	-0.07(0.01)	34.33(0.10)	2	...
2000bh	0.0240	15.92(0.10)	-0.55(0.17)	0.08(0.03)	34.24(0.11)	2	...
1999gp	0.0260	16.00(0.09)	1.64(0.21)	0.06(0.02)	34.63(0.11)	2	...
1999dk	0.0139	14.81(0.16)	0.29(0.27)	0.11(0.02)	33.14(0.17)	2	z
1999cp	0.0104	13.93(0.21)	-0.05(0.25)	-0.01(0.02)	32.54(0.22)	2	z
1999cl	0.0087	14.81(0.25)	-0.36(0.20)	1.20(0.01)	30.35(0.26)	2	z
2000ce	0.0165	17.02(0.14)	0.65(0.24)	0.61(0.03)	34.03(0.15)	2	p

Figure 4.1: A sample of the Union2 SNe Ia dataset consisting of supernovae in the redshift range $0.015 < z < 1.4$ used in the redshift-magnitude fit. Table from [17].

Space Telescope (HST) Key Project [30], which assume no underlying cosmology in measuring this parameter. The most recent value of the Hubble constant, as we have mentioned before is given by [7], but the shift in the new value is small compared to the size of the error bar. Hence in practice this would not make a difference to our results and so we did not redo our calculations with the most updated value for H_0 .

For our SNe Ia likelihood function (similar to all the other probes' likelihood functions) we adopt a Gaussian model with the corresponding χ^2 quantity given by:

$$\chi^2 = \sum^n \frac{(\mu_{\text{obs}} - \mu_{\text{pred}})^2}{\sigma_{\text{phot}}^2 + \sigma_{\text{int}}^2}, \quad (4.8)$$

where μ_{obs} and μ_{pred} denote the observed and model predicted distance moduli respectively, σ_{phot} is the measurement uncertainty tabulated for each supernova (a sample of this is shown in the table in Figure 4.1) and σ_{int} is the scatter intrinsic to every supernova because they are not perfect standard candles. These two errors are added in quadrature since they are uncorrelated with one another. We take σ_{int} to be 0.15 as advocated by Kowalski et al. [90] which is an average value derived from consideration of recent analyses.

Figure 4.2 shows the distance modulus as a function of redshift for the SFS model and the concordance model for their respective best-fitting parameters and how they compare with the best SNe Ia dataset available. One can see that the SFS model fits the data very well and that it is almost distinguishable from the concordance model over the redshift range probed by the Union2 sample.

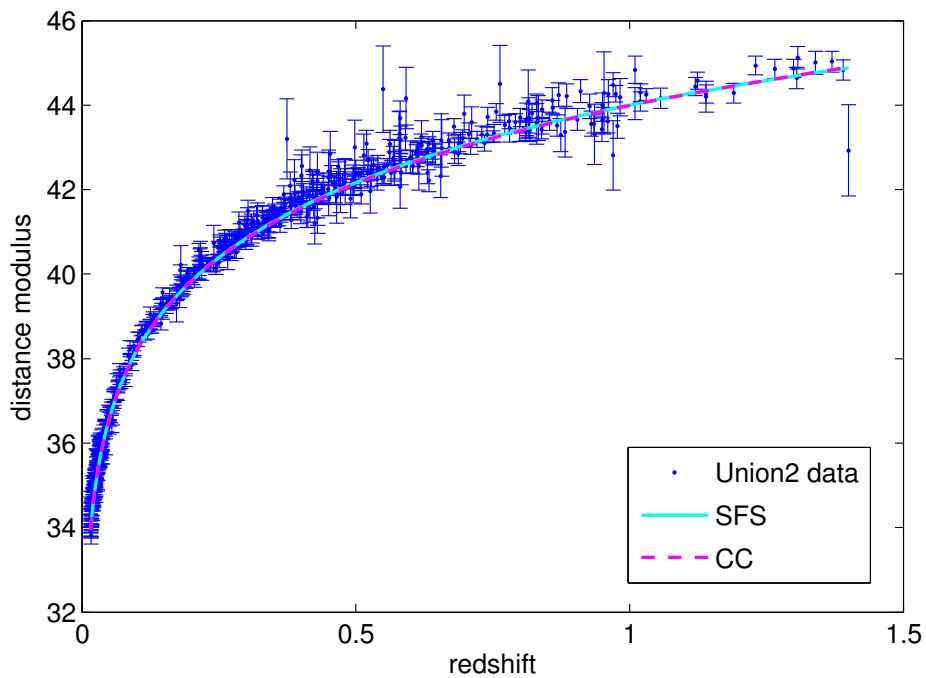


Figure 4.2: The predicted distance modulus plotted against redshift for the SFS model and Concordance Cosmology standard model (CC). The SFS model prediction is shown as the solid cyan line and is for parameters $n = 1.995$, $\delta = -0.5$, $y_0 = 0.805$. (These are the best-fitting SFS parameters for the Union2 SNe Ia dataset). The concordance model prediction is shown as the dashed pink line and is for parameters $\Omega_m = 0.2725$, $\Omega_\Lambda = 0.7275$ (from the WMAP7 results [18]). Both sets of calculations assume $H_0 = 74.2 \text{ km s}^{-1} \text{ Mpc}^{-1}$ from the HST Key Project results [30]. Also shown are the observed data points (with quoted $1\text{-}\sigma$ errors) for the Union2 SNe Ia dataset. One sees that the SFS model fits the data very well and that the fit is almost indistinguishable from that for the concordance model. Figure from [91].

4.2 Cosmic Microwave Background Distance Priors

In order to test a model against the cosmic microwave background (CMB) data one would ideally calculate the full angular power spectrum of the temperature anisotropies for the model, and compare it with the observed angular power spectrum. However, since this process is rather computationally intensive and complex, a simpler approach is instead to calculate the distance scales to which the power spectrum is very sensitive. The positions of the peaks and troughs of the CMB power spectrum, which can be measured precisely, provide a measure of the distance to the decoupling epoch. The distance ratios measured by the CMB are given below.

4.2.1 Acoustic Scale, l_a

This is defined as the angular diameter distance to the last scattering surface (at redshift z_{CMB} , which we take to be 1089), $d_A(z_{\text{CMB}})$, divided by the sound horizon size at the decoupling epoch, $r_s(z_{\text{CMB}})$ which is quantified by the ‘*acoustic scale*’ and is defined by:

$$l_a = \frac{\pi d_A(z_{\text{CMB}})}{r_s(z_{\text{CMB}})}, \quad (4.9)$$

where $d_A(z_{\text{CMB}})$ and $r_s(z_{\text{CMB}})$ given as comoving quantities are:

$$d_A(z_{\text{CMB}}) = \frac{c}{H_0} \int_0^{z_{\text{CMB}}} \frac{dz'}{E(z')}. \quad (4.10)$$

and

$$r_s(z_{CMB}) = \int_{z_{CMB}}^{\infty} \frac{c_s dz'}{E(z')} \quad \text{with} \quad c_s = \frac{1}{\sqrt{3(1 + \bar{R}_b a)}}, \quad (4.11)$$

where $E(z) = H(z)/H_0$ as defined before and c_s is the speed of sound with $\bar{R}_b = \frac{3\rho_b}{4\rho_\gamma}$, where ρ_b is the baryon density and ρ_γ is the photon density, is the baryon to photon ratio given by: $\bar{R}_b = 31500\Omega_b h^2 (\frac{T_{CMB}}{2.7k})^{-4}$, where $T_{CMB} = 2.7\text{K}$ is the temperature of the CMB [92, 28]. To see what the inclusion of baryon to photon density means physically, we can think that in the early universe the sound speed is lowered by \bar{R}_b since the baryons effectively weigh down the fluid.

4.2.2 Shift Parameter, R

This distance ratio is defined as the angular diameter distance to the last scattering surface divided by the Hubble horizon size at the decoupling epoch, which is called the ‘*shift parameter*’, R , and is given by:

$$R(z_{CMB}) = \frac{\sqrt{\Omega_m H_0^2}}{c} d_A(z_{CMB}), \quad (4.12)$$

where Ω_m is the matter density parameter. The shift parameter is defined as the ratio of the position of the first peak in the CMB temperature anisotropy angular power spectrum in a given model to the same position in a reference flat model with the same baryonic and dark matter densities. Therefore the shift parameter is a measure of the amount by which the first peak ‘shifts’ with respect to a reference model. The power spectra of the Λ CDM model and its corresponding reference model (SCDM) are shown in Figure 4.3 It can be seen how the first peak has shifted in the Λ CDM model with respect to SCDM.

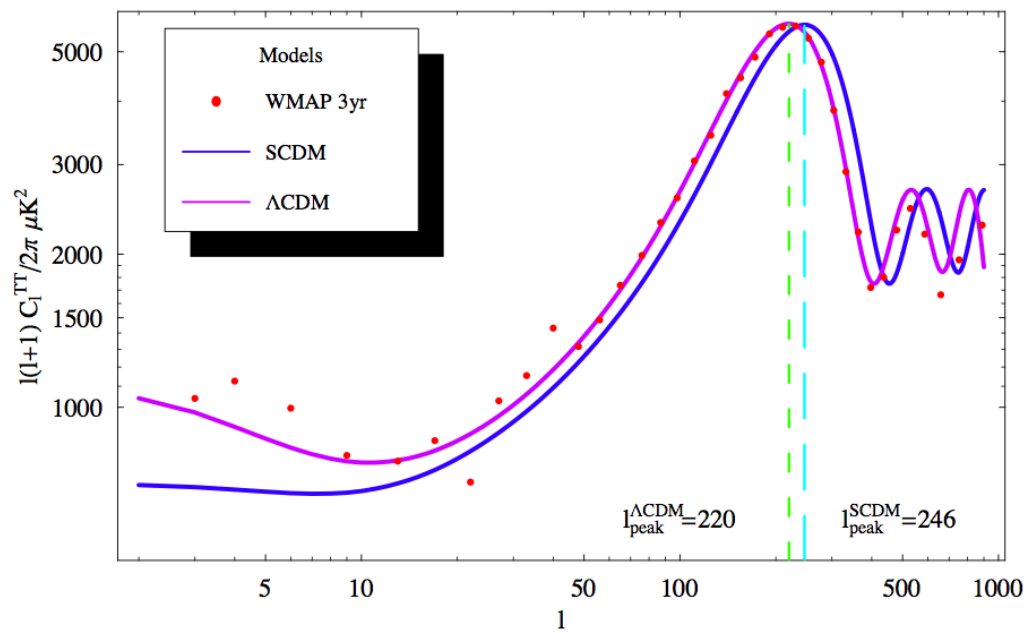


Figure 4.3: Definition of shift parameter: The CMB anisotropy angular power spectrum of Λ CDM model and the corresponding reference flat model (SCDM) with the same physical dark matter and baryon densities are shown together with the WMAP3 data. One can see the shift in the location of the first peaks of the two models. Figure from [93].

It was shown by Wang and Mukherjee [92] that using these two parameters together is necessary in order to place tight CMB constraints on the parameters of the model of interest. They found that models with the same parameter R but different values for l_a , and vice versa, in general gave different CMB angular power spectra. Furthermore, Wang and Mukherjee show that R and l_a are almost uncorrelated with one another even though they are taken from the same dataset of the CMB. This therefore means that we can safely write down the following χ^2 expressions for the shift parameter and the acoustic scale respectively as:

$$\chi_R^2 = \frac{(R^{\text{obs}} - R^{\text{pred}})^2}{\sigma_R^2}, \quad (4.13)$$

$$\chi_{l_a}^2 = \frac{(l_a^{\text{obs}} - l_a^{\text{pred}})^2}{\sigma_{l_a}^2}, \quad (4.14)$$

where R^{obs} and l_a^{obs} are the observed shift parameter and acoustic scale and R^{pred} and l_a^{pred} are the respective model predicted values.

The observed values for these quantities: $R = 1.725 \pm 0.018$ and $l_a = 302.09 \pm 0.76$, are obtained from the WMAP7 data and given by Komatsu et al. [18]. However, as pointed out by Elgaroy and Multamaki [94], the shift parameter is not a directly measurable quantity and it is in fact derived from the CMB data assuming a specific cosmological model. Care therefore needs to be taken when using this quantity as a cosmological constraint.

The value for the shift parameter quoted above, as [95] explains, has been derived assuming a standard FLRW universe with matter, radiation, curvature and dark energy components. The SFS model we are considering is also a standard Friedmann model but it assumes no

explicit dark energy component; instead cosmic acceleration is driven by the divergence of pressure resulting from the particular form of scale factor adopted in the model. Matter is also permitted in the SFS model and in fact since we require our model to reduce to the Einstein-de Sitter case at early times, we adopt the same matter content as that in the concordance model. Concerning the radiation and curvature components, we follow [95] and ignore these in the shift parameter calculation.

Turning to the dark energy component, here we followed the approach of Elgaroy and Multamaki [96] and expressed our SFS model in a form equivalent to an evolving dark energy model by computing its effective equation of state, $w_{\text{eff}}(z)$. To derive the required expression we note that a dark energy component with equation of state parameter $w(a)$, will correspond to a density that varies with the scale factor according to:

$$\rho(a) = \rho_0 \exp \left(-3 \int_1^a \frac{da}{a} [1 + w(a)] \right). \quad (4.15)$$

The standard Friedmann equation for a flat model will therefore take the form:

$$E(a)^2 = \frac{\Omega_m}{a^3} + (1 - \Omega_m) \exp \left(-3 \int_1^a \frac{da}{a} [1 + w(a)] \right), \quad (4.16)$$

where, $E(a)$ is the same Hubble function as introduced before, in terms of the scale factor a here. Now, rewriting the above using $a = (1+z)^{-1}$ (where we have assumed $a_0 = 1$) we have:

$$E(z)^2 = \Omega_m(1+z)^3 + (1 - \Omega_m) \exp\left(3 \int_0^z \frac{1+w(z)d(z)}{1+z}\right), \quad (4.17)$$

which means:

$$\int_0^z \frac{1+w(z)d(z)}{1+z} = \frac{1}{3} \ln\left(\frac{E(z)^2 - \Omega_m(1+z)^3}{1 - \Omega_m}\right). \quad (4.18)$$

Now, differentiating both sides gives, where $' \equiv \frac{d}{dz}$:

$$w(z) = -1 + (1+z) \left(\frac{2/3 E(z)E'(z) - 3\Omega_m(1+z)^2}{E(z)^2 - \Omega_m(1+z)^3}\right). \quad (4.19)$$

We note also that if we consider a flat universe we can have an analytic form for the equation of state parameter of the SFS model:

$$w(t) = \frac{p}{\rho c^2} = \frac{1}{3}[2q(t) - 1], \quad (4.20)$$

where $q(t) = -\ddot{a}a/\dot{a}^2$ is the deceleration parameter as introduced before. We emphasise here that this w_{eff} would work for a single ‘‘SFS fluid’’ with pressure, p and energy density, ρ . One therefore does not expect to necessarily see the same behaviour for the two definitions of w_{eff} given above. This is because in the first case one assumes a dark matter component along with an SFS dark energy term, while in the second case there is one single SFS fluid which to comply with observations should behave like matter in the early universe and like a dark energy in the current epoch. In [97] we attempt to formulate the the function $E(z)$ in such a way that it includes the one SFS fluid talked about here, which behaves in the standard way in the early and late universes. Please refer to Appendix A for a discussion on this issue.

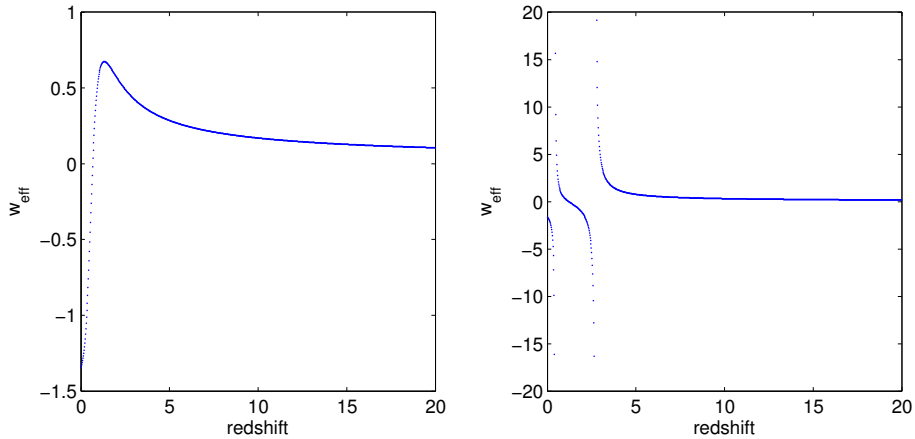


Figure 4.4: The evolution of w_{eff} as a function of redshift in the SFS model, for two representative sets of model parameters. Both plots show generic behaviour as $z \rightarrow 0$ and $z \rightarrow \infty$ which is in good agreement with current observations, although plot (b) also shows ‘fake’ singularities due to the parametrisation of w_{eff} . It is noteworthy that qualitatively similar behaviour was obtained using the w_{eff} expression in Equation 4.20.

Now to continue with our w_{eff} discussion, we investigated the evolution of the effective equation of state as given in Equation 4.19 numerically to see how it compared with the observed behaviour.

Figure 4.4 shows the evolution of the effective equation of state (using the expression in Equation 4.19) over the redshift range $0 < z < 20$, for two representative sets of SFS model parameters and an Ω_m of 0.24 as in the standard concordance model.

In both cases we see the same general features: $w_{\text{eff}} \simeq -1$ as $z \rightarrow 0$ and $w_{\text{eff}} \rightarrow 0$ for large z . These limiting behaviours are in good agreement with current observations. Note, however, that in 4.4(b) the particular SFS model parameters result in the divergence of w_{eff} at certain redshifts, which is caused by the denominator in the expression on the right hand side of Equation 4.19 tending to zero at these redshifts.

This behaviour is discussed in [98] where they make the case that in models where dark energy is not treated as an explicit fluid or a field, the equation of state cannot be used as a fundamental quantity and

indeed an effective equation of state may display unusual properties like singularities.

Again the same divergent behaviour in w_{eff} was found e.g. by Sola and Stefancic [99] in computing an effective equation of state for their evolving Λ model; indeed those authors refer explicitly to each divergent feature as a ‘fake singularity, which is nothing but an artefact of the EOS (equation of state) parametrisation’. In our case too the divergence of w_{eff} is not seen as an indication of a fundamental physical problem with the model. Nevertheless the general similarity of the limiting behaviour of w_{eff} to that of the concordance model gives us confidence, following Elgaroy and Multamaki [94], that it remains appropriate to use the ‘observed’ value of the shift parameter when investigating our SFS model.

4.3 Baryon Acoustic Oscillations Distance Parameter

Baryon acoustic oscillations which originate from the excitation of sound waves in the early universe photon-baryon plasma through cosmological perturbations are useful distance indicators at the current epoch. We can use this to constrain very well the following quantity, termed as the ‘*distance parameter*’, using the current data:

$$A = \frac{\sqrt{\Omega_m}}{E(z_{\text{BAO}})^{1/3}} \left[\frac{1}{z_{\text{BAO}}} \int_0^{z_{\text{BAO}}} \frac{dz}{E(z)} \right]^{2/3}, \quad (4.21)$$

where Ω_m is the matter density parameter, $E(z)$ is the Hubble function as introduced before and z_{BAO} is the effective redshift of the galaxy sample used to measure the distance parameter and is equal to $z = 0.35$ for the SDSS galaxy sample [19]. For the BAO distance parameter

constraint we adopt:

$$\chi_{\text{BAO}}^2 = \frac{(A_{\text{obs}} - A_{\text{pred}})^2}{\sigma_A^2}, \quad (4.22)$$

where A_{obs} and A_{pred} are the observed and model predicted values of A . Here the observed value for the distance parameter has been taken from the latest SDSS results which is: $A = 0.469(n/0.98)^{-0.35} \pm 0.017$ [28]. We used the value of $n = 0.963$ for the spectral index from WMAP7 results [18].

We find that the BAO distance parameter is not immune to the model dependency issue in its derivation either. This issue is considered in detail in e.g. Carneiro et al. [100] who, following Eisenstein et al. [101], identify two (implicitly assumed) conditions which should be valid in order that the BAO distance parameter is applicable. For the model in question firstly the evolution of matter density perturbations during the matter dominated era must be similar to the concordance cosmology case, and secondly the comoving distance to the horizon at the epoch of matter-radiation equality should scale inversely with $\Omega_m H_0^2$. While these conditions are *not* met for the Carneiro et al. [100] model of a time varying cosmological constant, we can assume that they are met in our case.

4.4 Age of the Universe

Using the standard Friedmann equation for calculating the age of the universe we have:

$$t_0 = t_H \int_0^\infty \frac{dz'}{(1+z')E(z')}, \quad (4.23)$$

where $t_H = \frac{1}{H_0}$ is the Hubble time and $E(z)$ is defined as before. In our Gaussian likelihood function for this constraint we used the χ^2 expression:

$$\chi_{\text{age}}^2 = \frac{(t_0^{\text{obs}} - t_0^{\text{pred}})^2}{\sigma_{\text{age}}^2}. \quad (4.24)$$

where t_0^{pred} is the age of the universe predicted in our SFS model, as computed from Equation 4.23. For t_0^{obs} , the observed age of the universe, we followed e.g. Balbi et al. [102] and used the best current estimate derived from various astrophysical probes, including globular cluster ages, that have been determined without assuming a particular cosmological model. We adopt $t_0 = 12.6_{-2.2}^{+3.4}$ Gyr with an asymmetric error distribution corresponding to 95% upper and lower confidence limits, as reported in [103]. In practice however, we simplified this analysis and used a symmetric standard deviation of $(3.4 + 2.2)/2$. We reasoned that the small systematic change that would be caused by this simplification would be negligible considering the weak constraining power of the age due to its large error bars.

4.5 Hubble Constant

The Hubble constant, derived from nearby observations of the cosmic expansion, is the final constraint which we employed in our analysis. Indeed the Hubble constant already features indirectly in the SNe Ia and age constraints, since it enters into our calculations of the predicted values for those two probes, we considered it would be useful also to compare directly the observed value of H_0 with its predicted value calculated for our SFS model. Therefore, for H_0 in the SFS model we have:

$$H_0^{\text{pred}} = \left(\frac{\dot{a}}{a}\right)_0 = \left(\frac{m(1-\delta)y^{(m-1)} + n\delta(1-y_0)^{(1-n)}}{\delta + (1-\delta)y_0^m - \delta(1-y_0)^n}\right). \quad (4.25)$$

We thus computed a likelihood function for this constraint using the χ^2 quantity:

$$\chi_{H_0}^2 = \frac{(H_0^{\text{obs}} - H_0^{\text{pred}})^2}{\sigma_{H_0}^2}, \quad (4.26)$$

where H_0^{pred} is the model predicted Hubble parameter and $H_0^{\text{obs}} = 74.2 \pm 3.6 \text{ km s}^{-1}\text{Mpc}^{-1}$, i.e. the (cosmology-independent) HST Key Project value discussed earlier.

4.6 Conclusions

In this chapter a detailed list of all the cosmological probes we have employed in our SFS model investigations was presented. These were, the supernovae Type Ia redshift-magnitude relation, the cosmic microwave background distance priors known as the shift parameter, R and the acoustic scale, l_a , the baryon acoustic oscillation distance parameter, A , the age of the universe and the Hubble constant, H_0 . In Chapters 5 and 6 we will now present the results of employing these cosmological probes in confronting our SFS model with the data.

Chapter 5

Results with Fixed m

In this chapter we will present the results of the first part of our investigations of the particular SFS model we introduced in Chapter 2. Specifically, we keep the parameter m constant in this chapter, which as will be discussed, is a simplifying assumption that follows a reasonable physical motivation. We shall explain in detail the methods by which we tackled the various problems that arose along the way of this exploration of our SFS model. We will then seek to physically interpret the results often presented in the form of contour or scatter plots.

To begin with, let us recapitulate the characteristics of our SFS model. In Chapter 2 we introduced the SFS scale factor to be of the form:

$$a(t) = a_s[\delta + (1 - \delta)y^m - \delta(1 - y)^n] \quad , \quad y = \frac{t}{t_s}, \quad (5.1)$$

with the free parameters of, a_s , δ , n , m and t_s . Furthermore, we introduced the dimensionless parameter $y_0 = t_0/t_s$ to account for the time when an SFS might happen in the future, which meant that:

$$0 < y_0 < 1. \tag{5.2}$$

Moreover, we saw how the parameters n and m are theoretically constrained to be in the following ranges:

$$1 < n < 2 \quad \text{and} \quad 0 < m < 1. \tag{5.3}$$

It remains to mention the parameter known as the non-standardicity parameter, δ , which was so called because when it was set to 0, our SFS model would follow a standard Friedmann limit where the universe had no SFS. In Chapter 2, we discussed how we attempted to redetermine a prior range for this parameter through the consideration of all the basic and established physical observational facts such as the observed current expansion along with the acceleration of our universe. The latter was the only condition which was assumed for this problem by Dabrowski et al. [1]. Please refer to §2.2.2.1 for a complete discussion of this issue and a full list of the physical conditions considered. From such investigations we can firmly say that δ should only take on negative values.

We can see now that we have 4 free parameters to work with in determining the posterior pdfs of the SFS model parameters under study. We started this task by simplifying the problem slightly and fixing the parameter m to take the value of $2/3$, which as discussed previously will ensure that our SFS model corresponds to an Einstein-de Sitter type universe at early times. By fixing m we are in fact continuing Dabrowski et al.'s work in [1] where they first confronted SFS models with SNe Ia data only. Later on we shall allow m to vary from $2/3$ but for now we will start our investigations with the 3-dimensional parameter space of (n, δ, y_0) .

In addition to keeping m fixed to start with, we keep one other parameter fixed to assist us in our investigations and to better interpret our results as will be discussed. This in turn is split into two different paths of investigation: one with the parameter y_0 kept constant and the other with the parameter δ fixed. We start our discussion from the fixed y_0 case, which is indeed where we started from in practice too.

5.1 Fixing y_0

Initially we chose to keep the parameter y_0 constant since then every fixed value of y_0 would correspond to an SFS at a particular time in the future. We had therefore 2-dimensional (n, δ) spaces to search over.

For every value of y_0 considered we searched a grid of regularly spaced n and δ values, computing χ^2 values, both separately and jointly, corresponding to the following three probes: the SNe Ia luminosity distance-redshift relation, the CMB shift parameter, R and the BAO distance parameter, A . This list of cosmological probes is certainly not the complete one talked about in Chapter 4 since at the time we had not considered the acoustic scale. Moreover, generally we wished to keep the problem as simple as possible initially by considering only the most important probes.

The joint χ^2 statistic corresponding to the likelihood functions of all of our cosmological probes' χ^2 's would read as:

$$\chi_{\text{total}}^2 = \chi_{\text{SN}}^2 + \chi_{\text{CMB}}^2 + \chi_{\text{BAO}}^2. \quad (5.4)$$

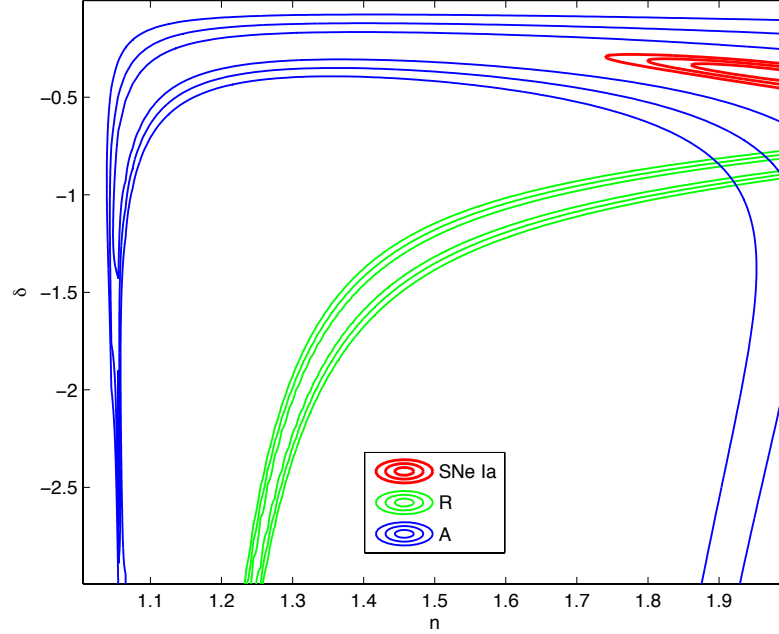


Figure 5.1: The contours show conditional 68%, 95% and 99% credible regions in the (n, δ) parameter space at fixed $y_0 = 0.99936$ corresponding to an SFS in 8.7 million years. The contours are calculated using the probes: SNe Ia redshift-magnitude relation (red), CMB shift parameter, R , (green) and BAO distance parameter, A , (blue).

Note that χ_{total}^2 can be written in this way since the considered probes are independent from each other.

We therefore sought the minimum of the χ^2 statistic for both the individual probes and also their sum. Note that in the latter case the minimum χ^2 will not in general occur at the same location in the parameter space as the minimum χ^2 for each individual probe.

Now to illustrate the results of this first investigation, we will present a series of conditional ‘slices’ through our 3-dimensional posterior distribution. We present these conditional contour plots in Figures 5.1 - 5.6 (The contours presented in these plots and throughout have been calculated on grids with a 100×100 resolution.).

We started from $y_0 = 0.99936$ in Figure 5.1, which was the value

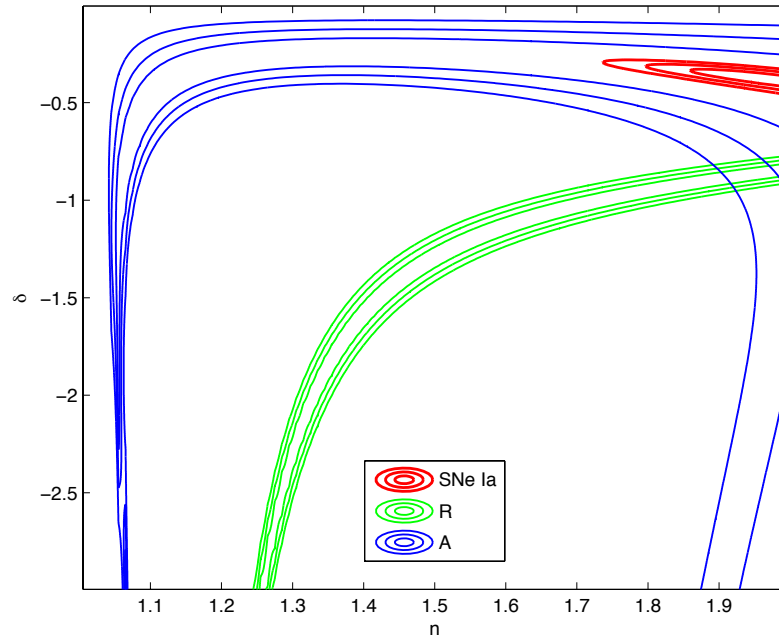


Figure 5.2: The contours show conditional 68%, 95% and 99% credible regions in the (n, δ) parameter space at fixed $y_0 = 0.999$ corresponding to an SFS in 13.7 million years.

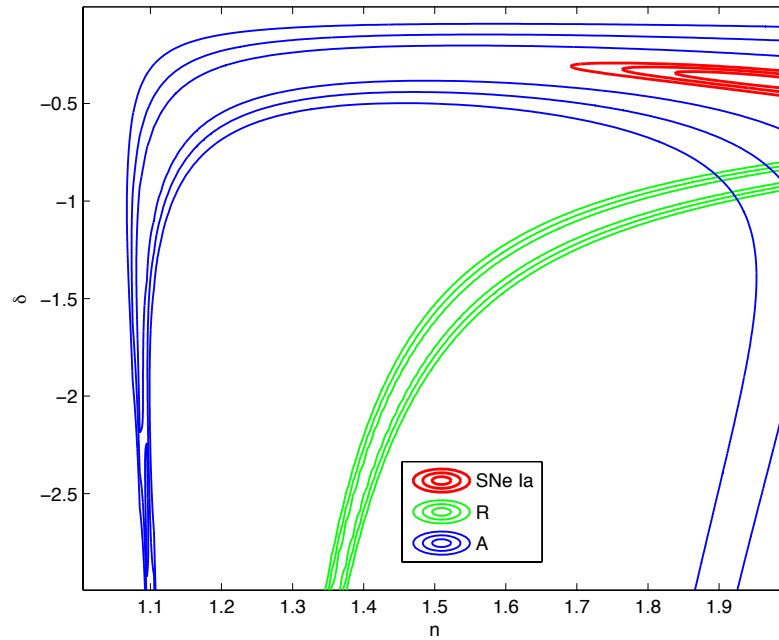


Figure 5.3: The contours show conditional 68%, 95% and 99% credible regions in the (n, δ) parameter space at fixed $y_0 = 0.99$ corresponding to an SFS in 138 million years.

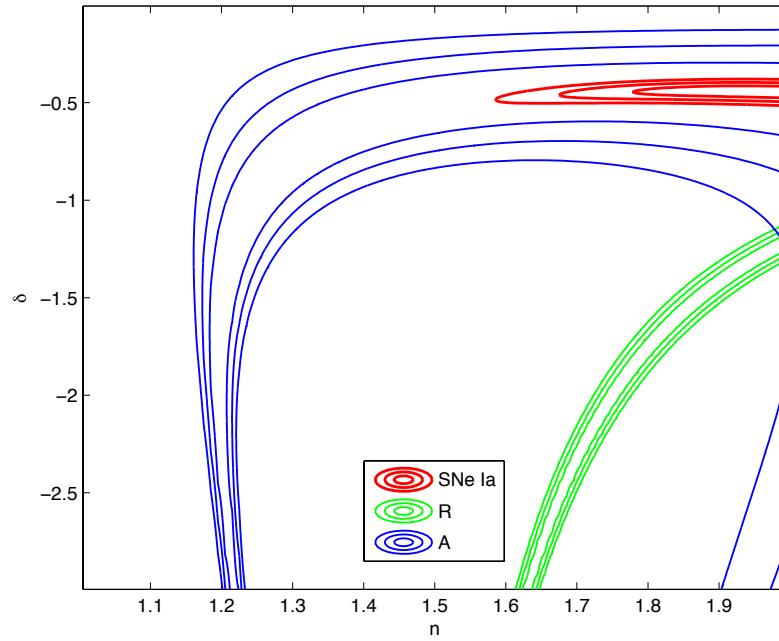


Figure 5.4: The contours show conditional 68%, 95% and 99% credible regions in the (n, δ) parameter space at fixed $y_0 = 0.9$ corresponding to an SFS in 1.5 billion years.

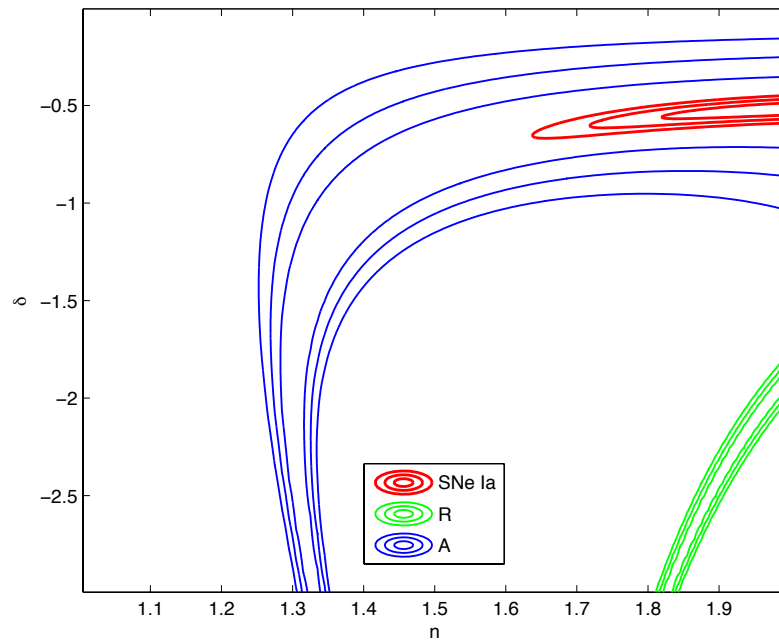


Figure 5.5: The contours show conditional 68%, 95% and 99% credible regions in the (n, δ) parameter space at fixed $y_0 = 0.8$ corresponding to an SFS in 3.4 billion years.

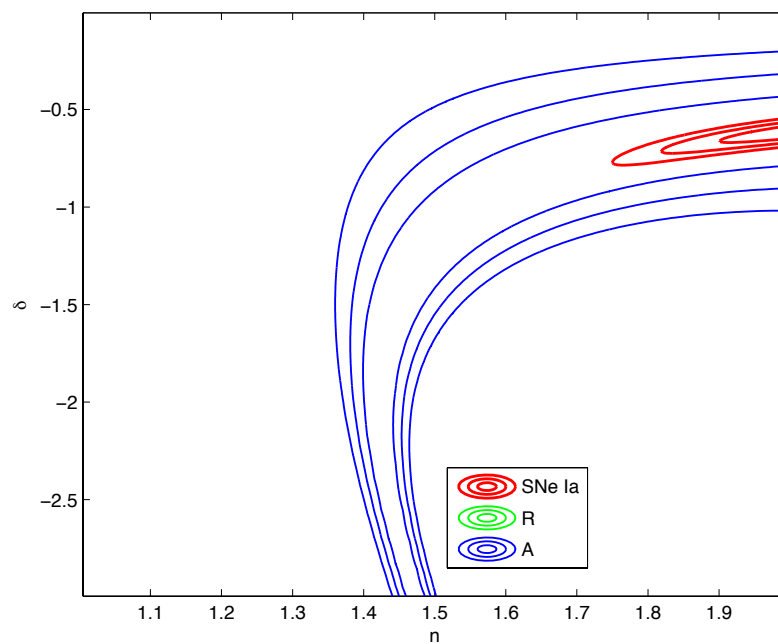


Figure 5.6: The contours show conditional 68%, 95% and 99% credible regions in the (n, δ) parameter space at fixed $y_0 = 0.7$ corresponding to an SFS in 5.8 billion years. Note that the shift parameter contours in this plot occupy a very small region in the lowermost bottom left corner.

for this parameter considered in the work of Dabrowski et al. [1] who showed that the SFS model fits the SNe Ia data at this value of y_0 . And therefore they concluded that an SFS might happen in 8.7 million years corresponding to $y_0 = 0.99936$ if we assume the same age for the universe as in the standard concordance model. However, here we see that although there is a well-defined set of contours for the SNe Ia probe, these contours do not seem to overlap with the shift parameter credible regions at 99% level. Indeed the BAO distance parameter credible regions overlap with those of the SNe Ia, which is to be expected as both probes cover approximately the same range of redshifts.

In Figures 5.2 - 5.6 we decrease y_0 to lower values of 0.999, 0.99, 0.9, 0.8 and 0.7 which correspond to SFSs occurring in 13.7 Myr, 138 Myr, 1.5 Gyr, 3.4 Gyr and 5.8 Gyr respectively. One can see that the same trend continues in these plots showing that there is no common region where all the probes overlap to give a common fit to the data. Furthermore, one can see that the shift parameter contours seem to be moving out of the (n, δ) plane with decreasing y_0 . Of course, it is legitimate to ask why not extend the range of values of δ to more negative values. Indeed we looked at those values as well and found that the shift parameter contours continue to move to lower δ values and hence move further away from the SNe Ia contours.

One might wonder what would happen if we increased the value of y_0 from the value of 0.99936 considered in Figure 5.1, so that the SFS would occur even sooner in the future. Indeed we also investigated those values. Such slices are presented in Figures 5.7 - 5.9. It can be seen that still there appears to be no common overlap between all the probes' contours. Note that in such situations where at least two of the probes disagree at 99% level, calculating the minimum for

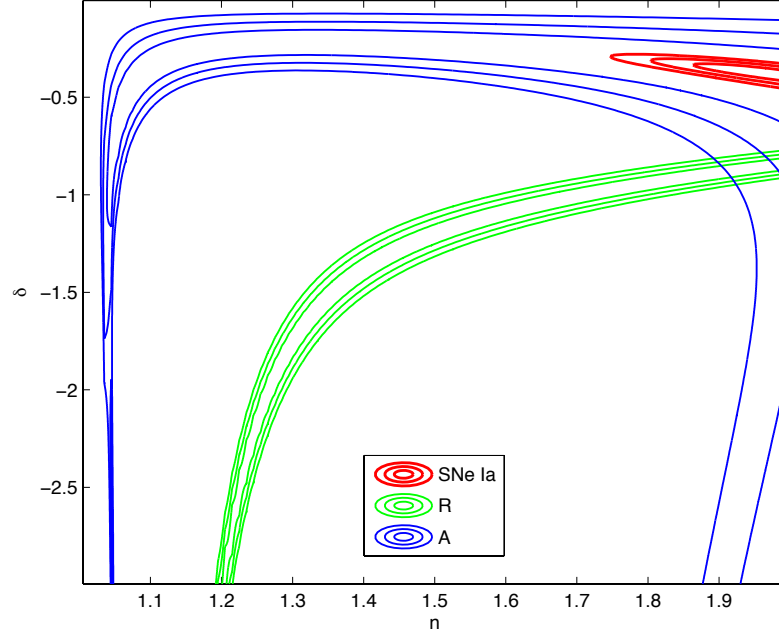


Figure 5.7: The contours show conditional 68%, 95% and 99% credible regions in the (n, δ) parameter space at fixed $y_0 = 0.9999$ corresponding to an SFS in 1.3 million years.

the total χ^2 is not required, since the joint probability for n and δ given the data is clearly negligible at all points in the parameter space considered. Therefore we no longer performed such a calculation.

It would now be interesting to see how our results are affected if we perform a 3-dimensional search of regular grid of values in the (n, δ, y_0) parameter space. To present the results of this investigation, we needed to marginalise the resulting probabilities over every parameter in turn to obtain sets of contours for the different cosmological probes used for pairs of model parameters: (n, δ) , (n, y_0) and (δ, y_0) . As we will see, it will suffice to show the results of this marginalisation over one parameter which we choose to be y_0 in keeping with the theme followed so far. Figure 5.10 shows 68%, 95% and 99% credible regions in the (n, δ) space marginalised over y_0 for the three cosmological probes considered before (which are presented in three separate labelled pan-

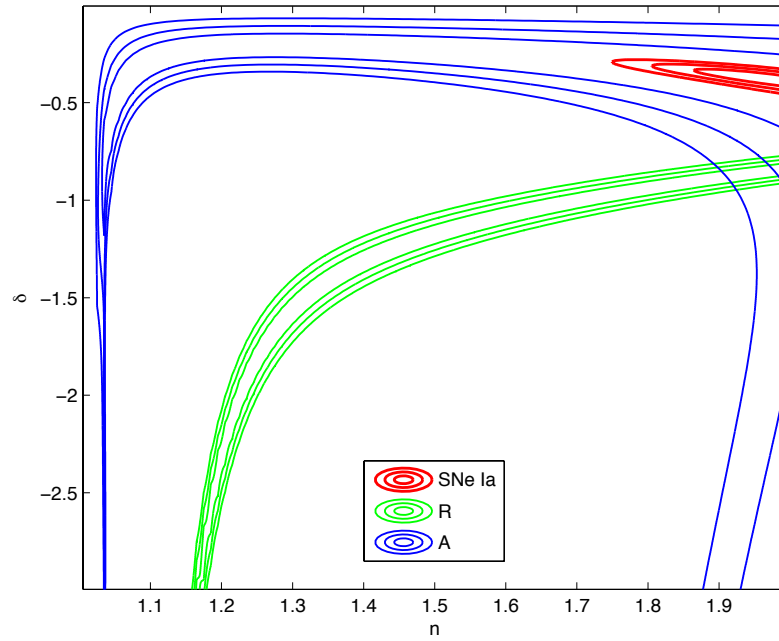


Figure 5.8: The contours show conditional 68%, 95% and 99% credible regions in the (n, δ) parameter space at fixed $y_0 = 0.99999$ corresponding to an SFS in 137 thousand years.

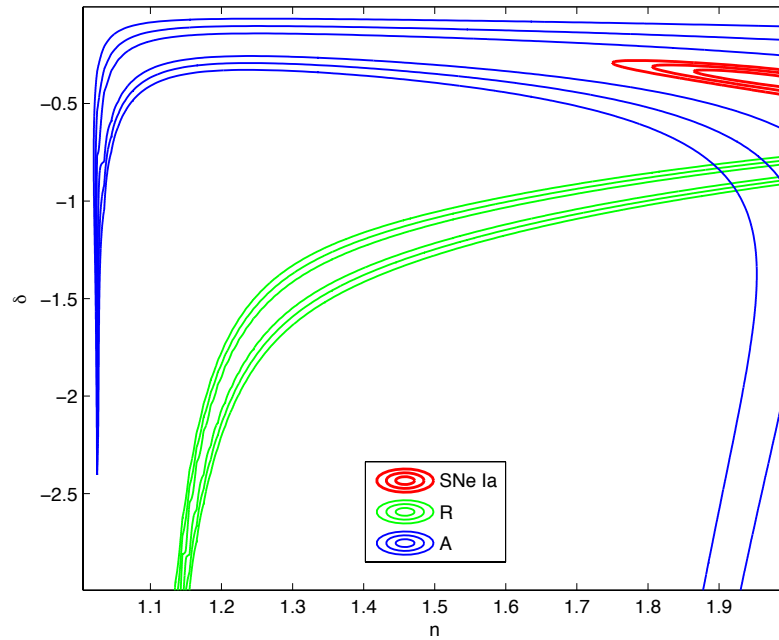


Figure 5.9: The contours show conditional 68%, 95% and 99% credible regions in the (n, δ) parameter space at fixed $y_0 = 0.999999$ corresponding to an SFS in 13,700 years.

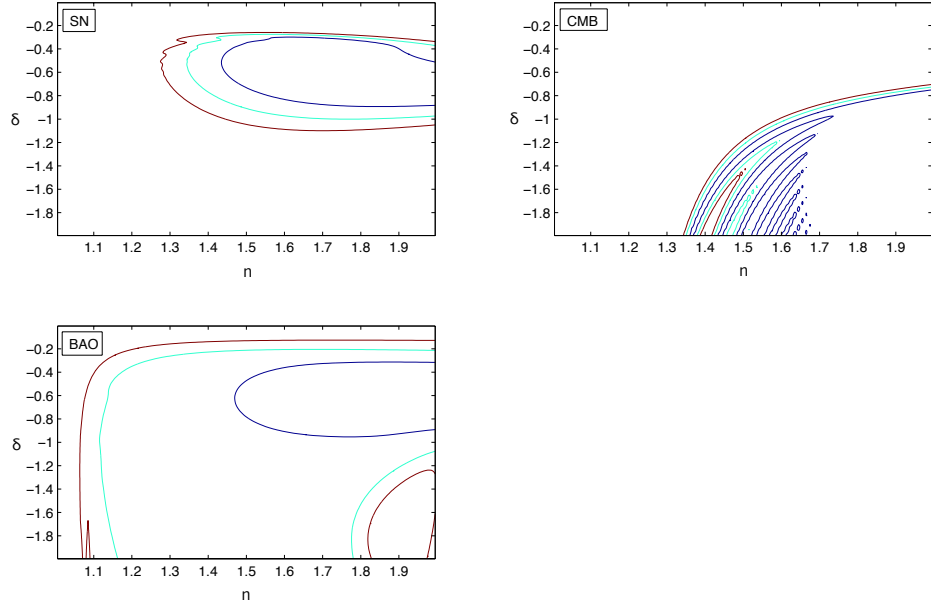


Figure 5.10: The contours show conditional 68%, 95% and 99% credible regions in the (n, δ) space marginalised over y_0 calculated using the cosmological probes: SNe Ia redshift-magnitude relation (labelled SN), CMB shift parameter (labelled CMB) and the BAO distance parameter (labelled BAO).

els). And Figure 5.11 shows the superposition of these marginalised contours.

Looking at the plot in Figure 5.10 and 5.11 one might be led into thinking that there is a fit to all the cosmological data used in the analysis since there seems to be overlaps present among the contours of the different cosmological probes. But this is certainly not the case as we have seen in the 2-dimensional conditional posterior pdfs and indeed the χ^2 values suggest otherwise. In particular we found that at the point where the χ^2_{total} was minimum the other probes' χ^2 's were unacceptable.

To quantify these results we show the reduced χ^2 values for the probes used. The reduced χ^2 is simply the actual χ^2 values divided by $N - \nu - 1$, where N is the number of observations and ν is the number of the parameters of the model. The reduced χ^2 values in this case were

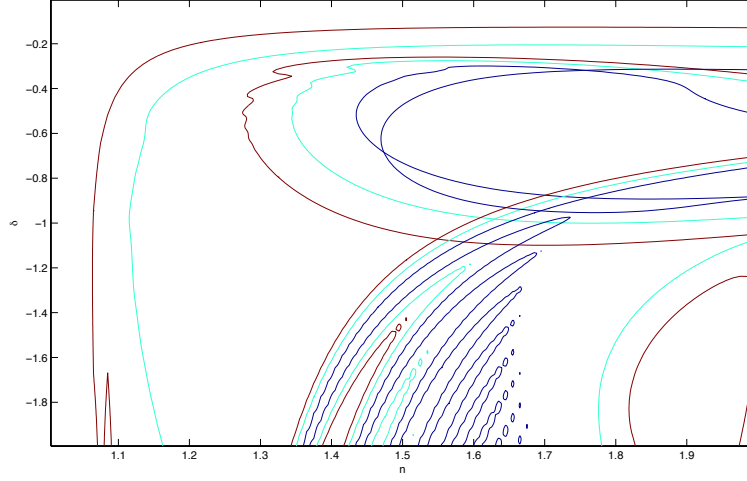


Figure 5.11: The superposition of the contours presented in Figure 5.10. One can see more clearly in this plot that there appears to be an area of overlap between the marginalised credible regions of the probes mentioned in Figure 5.10.

as follows:

$$\chi_{\text{SN}}^2 = 0.917, \quad \chi_{\text{CMB}}^2 = 107.50 \quad \text{and} \quad \chi_{\text{BAO}}^2 = 4.01.$$

We can assess these values using the $\Delta\chi^2$ values table given in Figure 3.1. Since we have marginalised over one of the three parameters we need to look at $\Delta\chi^2$ values corresponding to 2 degrees of freedom. For SNe Ia, we have a reduced χ_{min}^2 of 0.616 which means that at the point of minimum of χ_{total}^2 it has a reduced $\Delta\chi^2$ of $0.917 - 0.616 = 0.3001$, which then means that the actual $\Delta\chi^2$ is $0.3001 \times (N - \nu - 1) = 166.55$ and that it lies well outside the 99% credible region for this probe. If we do the same calculation for BAO we find it lies in the 90%, 2- σ credible region. Also the CMB already has a very large χ^2 that we need not consider its $\Delta\chi^2$ value. We therefore realised that the apparent overlap that shows up in Figure 5.11 must come from a kind of a projection effect that occurs between the non-overlapping sets of

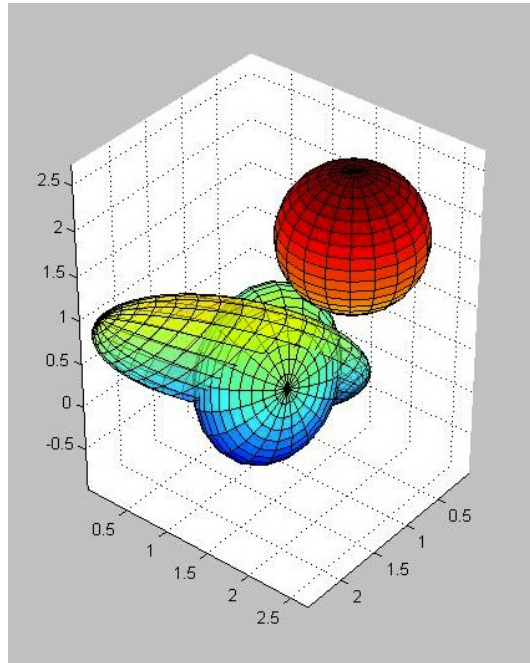


Figure 5.12: An illustrative 3-dimensional plot to demonstrate the idea of the project effect that might follow after marginalisation discussed in the text. Figure from: <http://www.mathworks.com/matlabcentral/fileexchange/16543-plotgaussianellipsoid>.

contours. We can understand this effect schematically by considering the cartoon plot shown in Figure 5.12. Note that the shape of the contours shown serves only as an illustration and bears no relation to the physical probes considered here.

We can see in this figure that there is a clear overlap between the two blue/green ellipsoids but not between the red sphere and the ellipsoids underneath it. However, if we were to marginalise the ellipsoids into 2-dimensional contour plots along the vertical axis, say, it is clear that we would indeed end up with overlapping regions. This projection effect is what we believe is also occurring in the case of the marginalisation of our 3-dimensional SFS parameter space pdfs.

Now, before we move onto the next phase of our ‘fixed m ’ parameter space exploration we point out a final consideration about the SNe Ia contours. As mentioned previously in §4.1 we marginalised over the

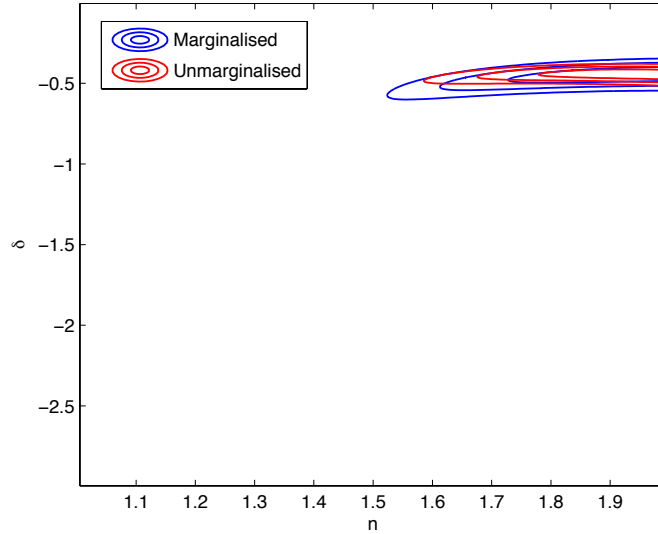


Figure 5.13: Contours showing the SNe Ia conditional 68%, 95% and 99% credible regions in the (n, δ) space at $y_0 = 0.9$ marginalised over the Hubble constant (blue) and unmarginalised (red).

Hubble constant, H_0 , as it could be treated as a nuisance parameter in the luminosity distance fitting. To do this, we adopted a Gaussian prior for H_0 with a mean of 73.8 and a standard deviation of 2.4 in accordance with the latest results of the HST Key Project experiment [7]. That is, for our conditional posterior pdf fixed at y_0 , from Bayes' law we have:

$$p(n, \delta | y_0) = \int p(n, \delta | H_0, y_0) p(H_0) dH_0. \quad (5.5)$$

We show an example plot of the SNe Ia luminosity distance contours in Figure 5.13 where we marginalise over the Hubble constant. It can be seen in Figure 5.13 that the marginalisation does not significantly change the results. Put another way, the marginalisation over H_0 would certainly not be sufficient to produce a consistent fit to the data among the three cosmological probes. Hence for simplicity we choose to omit this marginalisation procedure in what follows.

Furthermore, as will be seen in the next section we include the Hubble constant as a separate probe to take care of the SFS parameter dependences on this constant. That is, one could either only use the SFS parameters that give the correct Hubble constant today in the whole of one's analysis or more simply include the Hubble constant constraint as a separate probe as we did. The two methods are equivalent.

5.2 Fixing δ

The investigations so far have been based on the condition that δ should take on negative values to yield a currently accelerating universe as was claimed in Dabrowski et al. [1]. But as discussed in §2.2.2.1, we decided to revisit the problem of identifying a suitable prior range for δ considering all the observational constraints we have available today (cf. §2.2.2.1 for a comprehensive list). As mentioned before after realising that the solution to this problem was not possible to reach analytically, we resorted to numerical computation. To do this we again sliced our 3-dimensional parameter space but this time over the parameter δ since there was no definite derivable range for its values as was talked about in §2.2.2.1. This way we could check every single parameter combination in the 2-dimensional (n, y_0) space at a fixed δ against the physical conditions. Hence we changed our search through the conditional slices of y_0 to conditional slices of δ .

One might argue that if no overlap has been obtained in the set of contours in one series of conditional 2-dimensional spaces, no such overlap should be present in any other series of 2-dimensional spaces. In other words, it should not matter which way one 'slices' the overall 3-dimensional space. Indeed that is true, but the reason why we decided to look at δ slices was to investigate the effects of the newly

considered physical conditions on the contours. And as mentioned above δ now seemed like the best parameter for this slicing.

At the same time that we became aware of the necessity of the inclusion of the physical conditions, we realised through the work of Elgaroy and Multamaki [94] the potential advantages of using the acoustic scale, l_a , as well as the shift parameter, R , to provide a closer estimate to the full CMB power spectrum fit, as was discussed fully in Chapter 4. We also thought of extending our toolbox of cosmological probes to further include the Hubble constant, H_0 and the age of the universe, t_0 , as was discussed in Chapter 4. Therefore, equipped with six cosmological probes and the physical conditions, we recomputed each model parameter's posterior. Some selected conditional posteriors in the (n, y_0) space have been shown in Figures 5.14 - 5.16. These slices through the 3-dimensional parameter space, are sufficient to illustrate the results obtained, as we will discuss below.

Figures 5.14 - 5.16 show our computed Bayesian 68%, 95% and 99% credible regions for our six cosmological probes in the 2-dimensional (n, y_0) space for a series of fixed δ values. In each figure the contours are shown separately for each cosmological probe in labelled (a) – (f) panels. These correspond to: (a) the SNe Ia redshift-magnitude relation; (b) the CMB shift parameter, R ; (c) the CMB acoustic scale, l_a ; (d) the BAO distance parameter, A ; (e) the Hubble constant, H_0 ; (f) the present age of the universe, t_0 .

Firstly, we see these sets of contours for $\delta = -0.7$ in Figure 5.14. This starting value for δ was chosen since we observed that for larger (i.e. less negative) values of δ the posterior distributions for almost all of the probes were qualitatively similar. However, in the case of the shift parameter at greater values of δ , we found no credible regions for the SFS model parameters at the 99% level. One can see in the shift

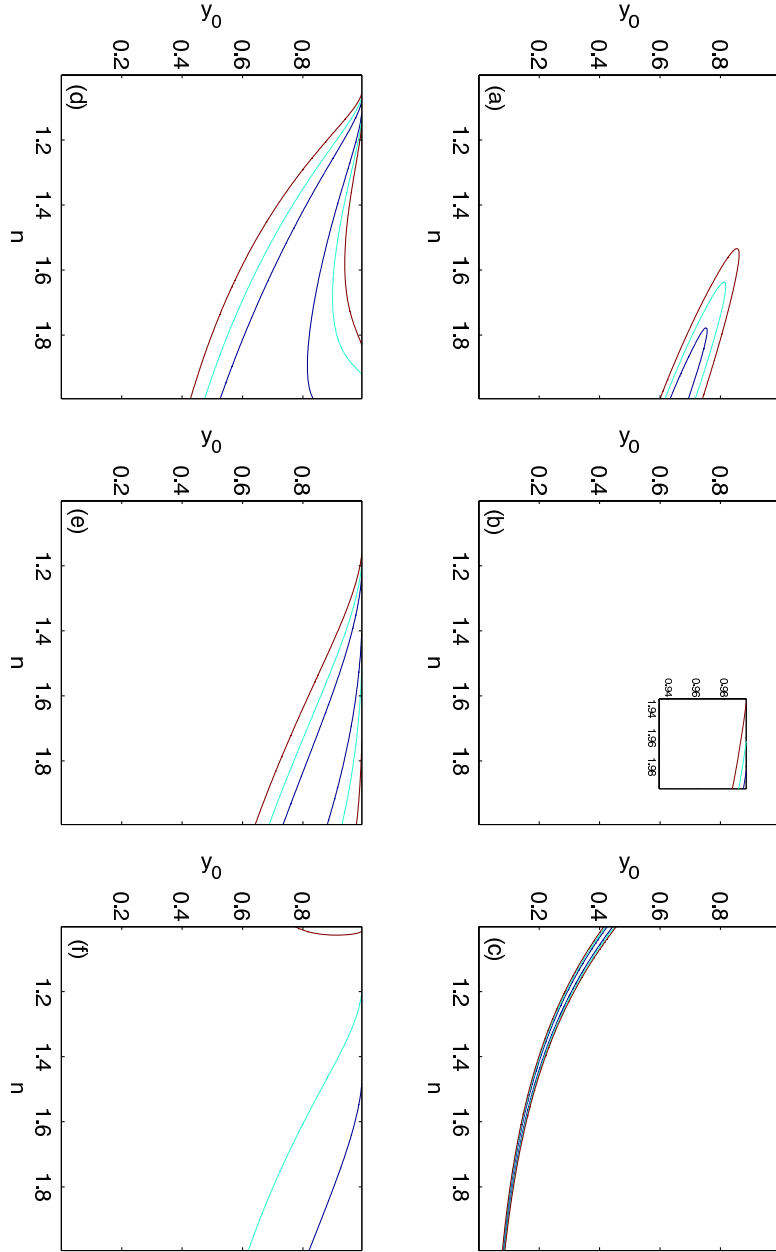


Figure 5.14: The contours show conditional 68%, 95% and 99% credible regions in the (n, y_0) parameter space for a fixed value of $\delta = -0.7$. The plots labelled (a), (b), (c), (d), (e) and (f) correspond to the contours calculated using the probes, SNe Ia redshift-magnitude relation, CMB shift parameter, R , CMB acoustic scale, l_a , BAO distance parameter, A , the Hubble constant and the age of the universe respectively.

parameter contour plot at $\delta = -0.7$ that this situation only starts to improve with the appearance of a very small (hence magnified for greater clarity) set of contours in the top right corner of panel (b). Hence we decided not to present further sets of contours for $\delta > -0.7$.

It is clearly apparent from Figure 5.14 that there is no region of common overlap in the (n, y_0) plane between all the six cosmological probes at the δ value of -0.7 . We can see that there is indeed an overlap between the SNe Ia and BAO contours which is to be expected as both probes explore similar ranges of redshifts and therefore depend on the function $E(z)$ in very much the same way.

Furthermore, the age constraint in panel (f) is shown to be weak and non-constraining which reflects the large uncertainty in its observed value. There appears only a very small area in the top left corner of the contour plot that is excluded at the 99% level which is not very useful as these parameter values are strongly excluded by the other cosmological probes.

To reanalyse the shift parameter contours in panel (b) in terms of some numbers, we note that the minimum χ^2 value in this plot is 21.35 (corresponding to a predicted value of $R = 1.641$) which is already very large and translates into an almost zero likelihood function (and equivalently zero posterior probability) everywhere. As we increased the value of δ to less negative values we observed a progressive increase in the value of the minimum χ^2 , hence our decision to omit the corresponding contours and starting from $\delta = -0.7$.

Another interesting point to draw the attention of the reader to, is the fact that the credible regions of the two CMB constraints R and l_a in panels (b) and (c) respectively, do not show *any* overlap at 99% level with one another. This must come through different model parameter

dependences of the two probes. Recalling Wang and Mukherjee’s discussion [92] as talked about in Chapter 4, R and l_a ought to be used in conjunction with one another for a fit to the CMB data to mimic the full power spectrum fit closely. Here we can see that there is indeed a disagreement between R and l_a themselves so there is definitely no fit to the CMB data alone. Moreover, these contours do not appear to overlap with any of the other four cosmological probes’ contours which means that there is no fit to the data at $\delta = -0.7$.

Now to illustrate the patterns followed by the six different contours, we show these credible regions at two further values of δ : -1 and -1.5 in Figures 5.15 and 5.16. Starting with $\delta = -1$ in Figure 5.15 we see that the contours take the same overall shapes (though slightly shifted from their previous positions in Figure 5.14) where we again have a clear overlap between the contours of SNe Ia, BAO distance parameter, Hubble constant and the age of the universe. These contours however continue to show no overlap with either of the CMB probes’ contours at the 99% level which themselves do not show any sign of tending to overlap with each other.

And lastly, we see the credible regions at $\delta = -1.5$ in Figure 5.16. Again we see the same trend continued with more or less all the contours. The CMB probes’ contours still neither show an overlap with each other nor with the other probes both at 99% level. In addition, one can see that the l_a contours appear to be moving down the (n, y_0) plane, approaching the y_0 lower limit as δ decreases to more negative values, indicating no possible fit to this probe in particular and hence overall to the collection of data employed.

To more clearly demonstrate that there is indeed no overlap among the cosmological probes employed in the analysis, we show in Figure 5.17 the most important contours of SNe Ia, CMB shift parameter,

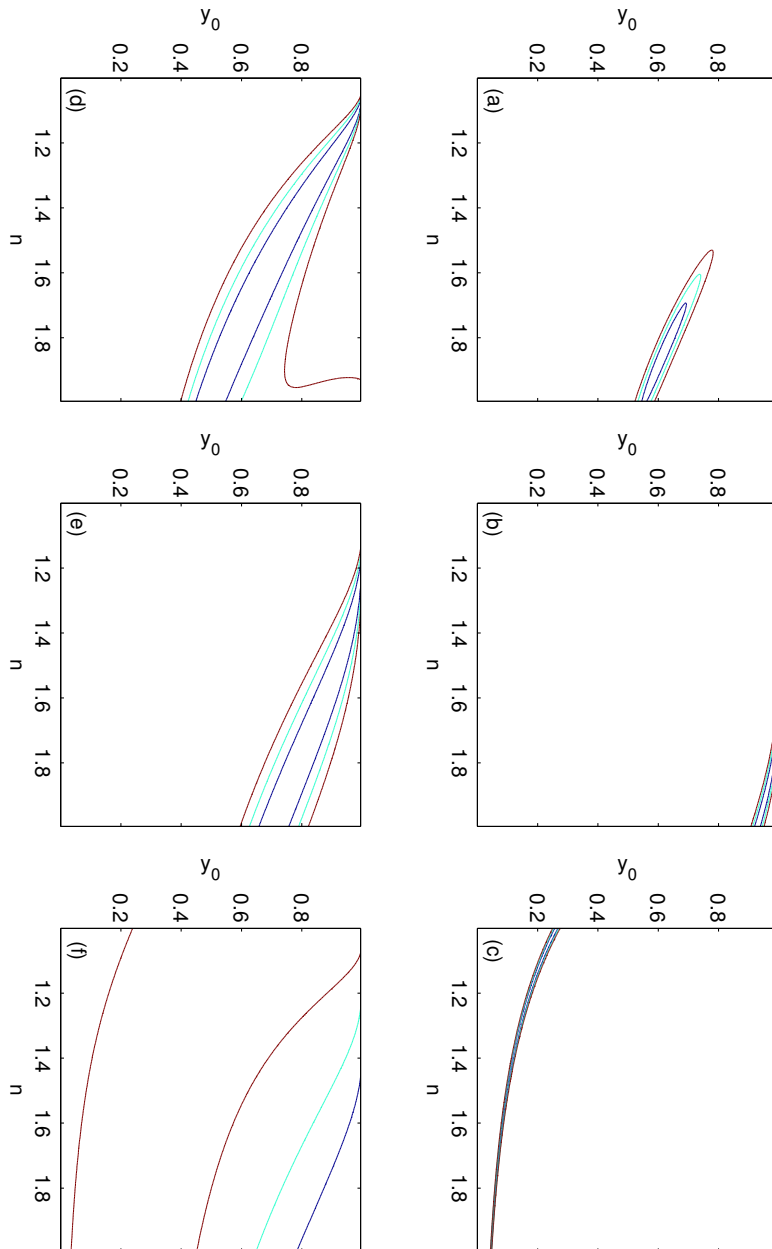


Figure 5.15: The contours show conditional 68%, 95% and 99% credible regions in the (n, y_0) parameter space for a fixed value of $\delta = -1$. The labels are as described in Figure 5.14.

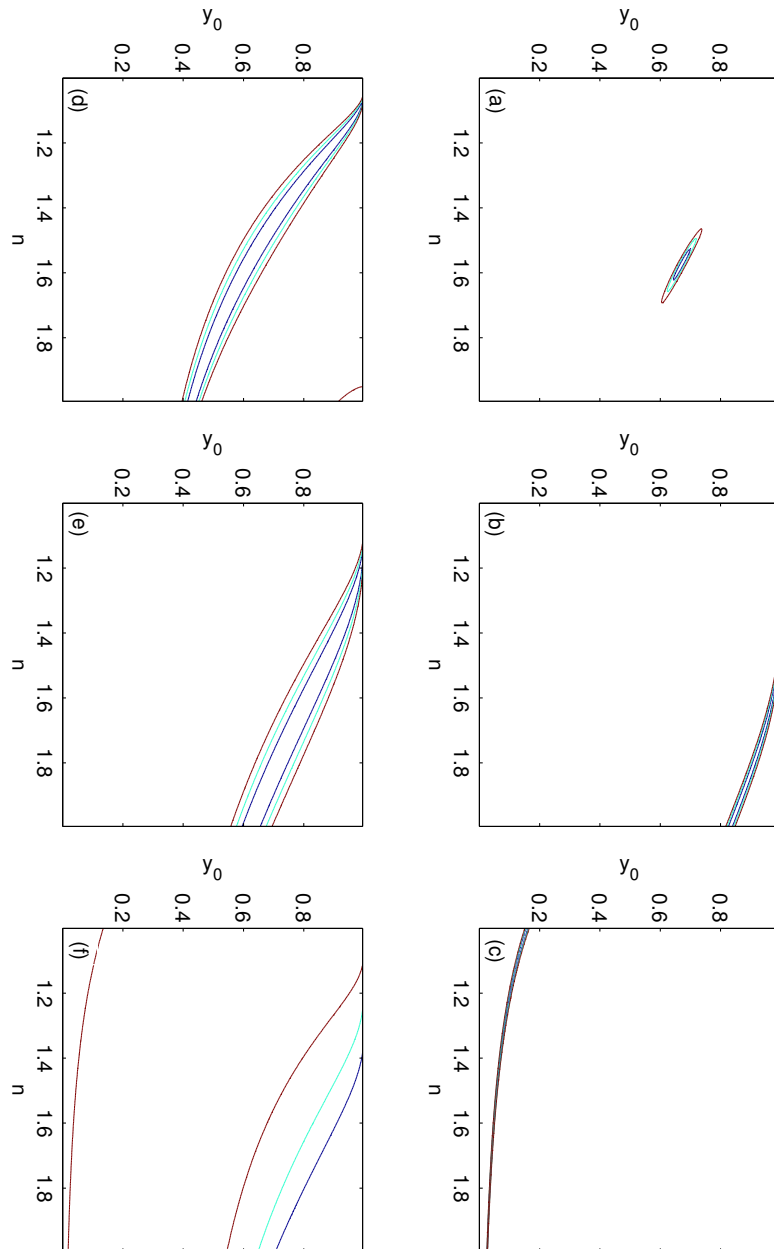


Figure 5.16: The contours show conditional 68%, 95% and 99% credible regions in the (n, y_0) parameter space for a fixed value of $\delta = -1.5$. The labels are as described in Fig. 5.14.

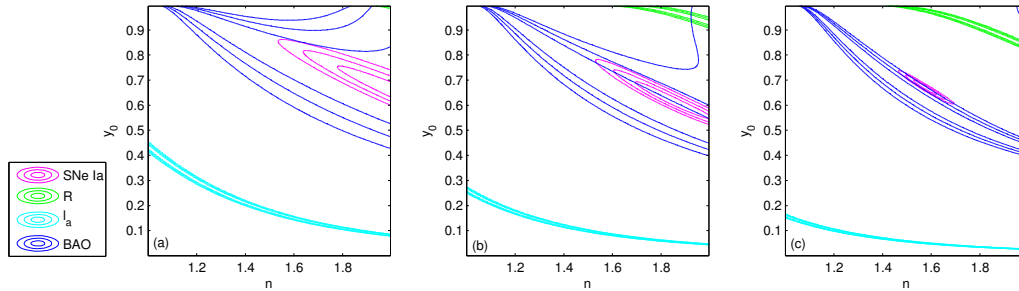


Figure 5.17: The panels show a superposition of the credible regions in the (n, y_0) parameter space derived from the SNe Ia, CMB shift parameter, R , CMB acoustic scale, l_a and BAO distance parameter, A data, for the values of $\delta = -0.7$ (a), $\delta = -1$ (b) and $\delta = -1.5$ (c), as previously illustrated in Figs. 5.14 - 5.16 respectively. Note that in each panel there is no part of the parameter space where all credible regions overlap.

R , CMB acoustic scale, l_a and BAO distance parameter superimposed for values of δ previously considered in Figures 5.14 - 5.16.

Looking at Figure 5.17 one can conclude that although an SFS might happen in a very near future when one considers the SNIa data only, as shown in [1], such a fit is not consistent with the CMB data for the same SFS model parameters.

As discussed earlier, in this second method of investigating our SFS model by slicing the parameter space over δ we incorporated physical conditions in our analysis. However, as we discovered that these conditions did not modify the results, for the purpose of presenting clearer and more easily readable contour plots we omitted these conditions from our calculations that produce Figures 5.14 - 5.17.

To show a typical example of the impact of the physical conditions on the contours, consider the acoustic scale, l_a 's contours in Figure 5.18. It can be seen how these conditions abruptly cut off the contours when they are included in the calculation of the l_a contours here. The condition responsible for the cut off shown in Figure 5.18(b) is the current acceleration of the universe. In other words, the section of the con-

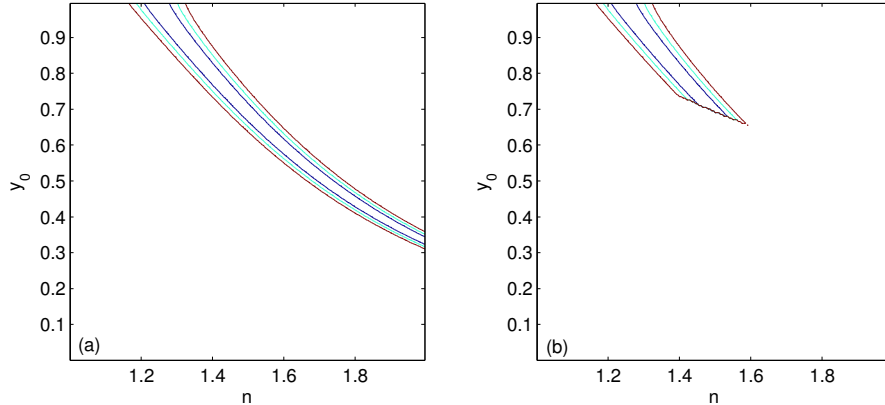


Figure 5.18: The impact of the imposition of the physical conditions discussed in §2.2.2.1 is shown here for the l_a contours. The plot labelled (a) shows these contours not considering the physical conditions while in plot (b) these conditions are included.

tours cut off by the inclusion of the acceleration condition would have given a good fit to the observed value of l_a in a currently decelerating universe. The physical conditions apply to the other probe's contours in the same way but less severely it seems. And since we already get no fit to the data *without* assuming the physical conditions as we have seen, we will not present more figures regarding the effects of the physical conditions.

To see what effect the physical conditions have on the explored (n, y_0) parameter space in Figures 5.14 - 5.16, we present these constraints in Figure 5.19. This figure shows the effect of the physical conditions on the (n, y_0) plane at the three δ values of -0.7 , -1 and -1.5 considered in Figures 5.14 - 5.16. The coloured regions indicate the areas excluded by the physical conditions which in this case turns out to be the current acceleration only. In particular one can see that the l_a contours are completely inside the excluded regions for all the three values of δ and hence are most severely affected. In comparison, the shift parameter contours never reach these forbidden regions.

We superimpose the plots presented in Figure 5.19 in Figure 5.20. We

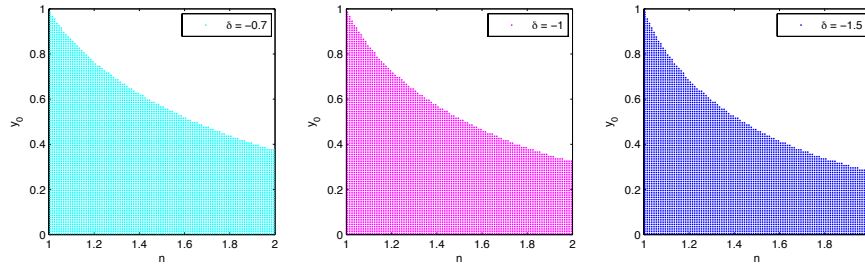


Figure 5.19: The coloured regions show the excluded areas of the (n, y_0) parameter spaces at $\delta = -0.7$, $\delta = -1$ and $\delta = -1.5$ corresponding to parameter combinations resulting in a currently decelerating universe.

can see that there exists a continuous transition between the excluded areas as δ decreases.

5.3 Conclusions

This chapter presented our results and findings about testing our SFS model when the parameter m , which is related to the early universe properties, is kept fixed at the value $2/3$ corresponding to a standard Einstein-de Sitter universe at early times. The result was that we did not find a common set of SFS model parameters which would give a fit to all the considered cosmological probes.

Our results took the form of a series of ‘slices’ through the 3-dimensional parameter space of (n, δ, y_0) . We first carried out this task by slicing over the parameter y_0 where each slice would then correspond to an SFS at a particular time in the future. Thus we looked at (n, δ) slices initially. The cosmological probes considered in this analysis were the SNe Ia redshift-magnitude relation, the CMB shift parameter, R and the BAO distance parameter, A . Furthermore, we extended our cosmological probes to include the acoustic scale, l_a , the Hubble constant, H_0 and the age of the universe t_0 , while this time we sliced over the parameter δ . We found δ was a more suitable choice

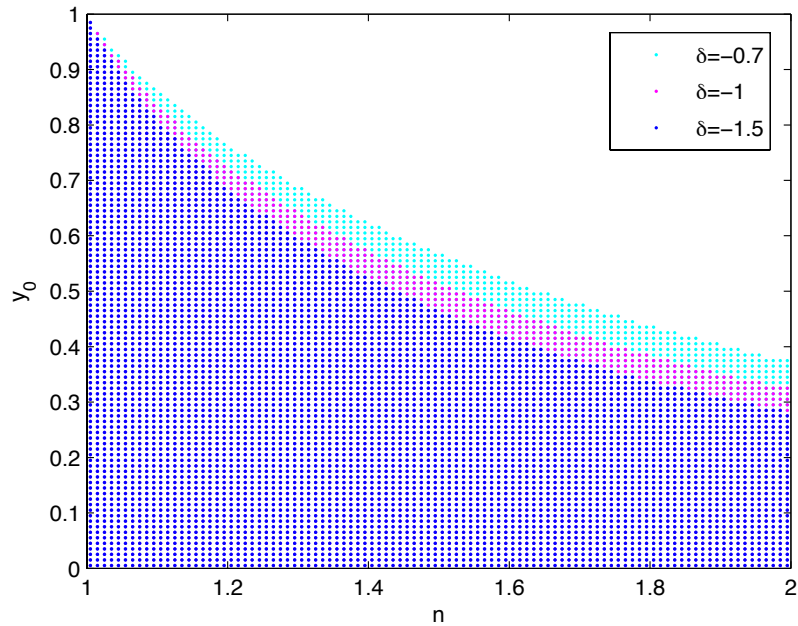


Figure 5.20: The superposition of the excluded areas described in Figure 5.19 displaying a continuous transition between consecutive δ slices.

given its open-ended prior and the realisation that we needed to check each parameter set against a certain list of observational facts such as the expansion and acceleration of the universe. Indeed we ended up with the same result that there was no fit to the data used.

As a final note in this chapter, we checked the results we obtained through our grid-based searches with the MCMC method as well and we got consistent results. We will now demonstrate the usefulness of the MCMC method in the case of the higher dimensional problem we investigate in Chapter 6.

Chapter 6

Results with Varied m

This chapter concerns the effects of relaxing the fixed $m = 2/3$ assumption and letting it vary within its theoretically allowed range of $0 < m < 1$. First of all we should consider the theoretical consequences of relaxing the fixed m assumption. We know that for $m = 2/3$ our SFS model reduces to the matter-dominated Einstein-de Sitter universe. To relax this assumption we therefore need to be prepared to be faced with other unusual properties for the early universe. Such a recent proposal was made by Dabrowski and Denkiewicz and we are currently considering it in detail in [97].

With m a free parameter now, we have a 4-dimensional parameter space to explore. Hence to calculate posterior pdfs for the corresponding parameters we employed the faster MCMC method for this higher dimensional problem. To illustrate the power of this method, in a 4-dimensional grid-based search with reasonable resolution the computer would have to do certain sets of calculations 10^8 times whereas we could reach the same results using the MCMC method by doing the same sets of calculations 10^5 to 10^6 times. The MCMC method therefore outperforms its counterpart grid-based method in high-dimensional problems.

We will utilise the same cosmological probes we employed in our analysis in the previous section for $m = 2/3$ but there is a slight issue here with the acoustic scale, which we think is worth discussing. We saw in §5.2 that after the realisation that the acoustic scale, l_a , should be used together with the shift parameter, R , the former was included in the analysis throughout. It so happened however that the acoustic scale did not have any effects on the final results in the end. Nevertheless using the two probes together, as discussed in Chapter 4 is indeed important in placing tight constraints on one's model using the CMB data. We should however be careful when employing the acoustic scale in our analysis in the investigation of the model now that we are letting m vary from its fixed value of $2/3$. Recalling from Chapter 4, the acoustic scale is defined through two separate distance scales; it is directly proportional to the angular diameter distance, d_A , and inversely proportional to the sound horizon, r_s , both evaluated at the redshift of recombination, z_{CMB} :

$$l_a = \pi \frac{d_A(z_{CMB})}{r_s(z_{CMB})}, \quad (6.1)$$

where the comoving sound horizon is defined as:

$$r_s = \int_{z_{CMB}}^{\infty} \frac{c_s dz'}{E(z')} \quad \text{with} \quad c_s = \frac{1}{\sqrt{3(1 + \bar{R}_b a)}}, \quad (6.2)$$

where $E(z) = H(z)/H_0$ as defined before and c_s is the speed of sound with $\bar{R}_b = 31500\Omega_b h^2 (\frac{T_{CMB}}{2.7k})^{-4}$, $T_{CMB} = 2.7\text{K}$. Now the difficulty in the l_a calculation for the varied m case really comes from the sound speed calculation. As mentioned before, when we let m vary from $2/3$, we no longer have the standard Einstein-de Sitter early universe. Previously in the fixed m case we would interpret the use of the acoustic scale in

the analysis as a distance scale set at the time of recombination in the “standard early universe” which would be measured differently now in an SFS universe due to its particular scale factor and hence history of evolution as taken care of by d_A . But we can no longer use the same reasoning in the case of m varied from $2/3$.

On the one hand, one might argue that it would not be trivial to determine the sound speed in such a non-standard early universe fluid and on the other hand, it could be argued that it is after all standard baryonic physics that sets the required distance scale. Since further investigation of this issue is beyond the scope of this thesis, we let the reader make their own judgement on this matter and will suffice to just present the results of our investigations with and without including the acoustic scale in what follows.

Furthermore, as it was shown in the previous section, the Hubble constant and the age of the universe do not have very constraining effects on the parameter space due to the inevitable relatively large uncertainties in their measurements. We therefore do not consider these any further here.

We employed the same physical conditions discussed in §2.2.2.1 in our MCMC parameter space exploration. We did this such that these conditions would be tested at every point in the chain and then the violation of any of them would result in sampling a new point centred on the last accepted point.

As described before, to carry out an MCMC search one needs to specify a suitable proposal density. We adopted a Gaussian proposal density and through experimentation with the program settled on a proposal density of 0.01 and about 10^5 to 10^6 steps in the chain.

In order to make sense of our MCMC results we needed to marginalise

the posterior pdf over two parameters at a time in order to then obtain 2-dimensional marginal distributions for the other two parameters. As seen in Chapter 3, the marginalisation procedure is done very easily in the MCMC method and without the need to integrate the full posterior pdf as is the case for the grid-based search. In the MCMC method one only needs to take the required coordinates of the chain points to arrive at the corresponding marginalised distributions. Therefore in our case we needed to plot 2 of the coordinates of the chain to obtain 2-dimensional marginalised posterior pdfs to be able to display the results in 2-dimensional plots.

Furthermore, to determine 1σ , 2σ and 3σ credible regions in our 2-dimensional parameter spaces, we carried out the procedure as prescribed in Chapter 3. That is we ordered the chains from the highest to lowest likelihoods. Then for a properly converged chain which is a representative sample of the full target pdf, we took the top 68% of the ordered chain to correspond to the 68% (1σ) credible region of the pdf. Similarly, 95% and 99% of the chain would correspond to 2σ and 3σ credible regions.

First let us consider the three classic probes of SNe Ia redshift-magnitude relation, CMB shift parameter and BAO distance parameter. In Figure 6.1 we present the marginalised credible regions obtained for these cosmological probes. We plot the chains calculated using each of the cosmological probes separately in different colours, where the marginal distributions for SNe Ia, the CMB shift parameter, R and the BAO distance parameter, A are red, green and blue respectively. To clarify how we intend to show that there is an overlap between the chains of different probes, we show these chains in separate plots in Figure 6.2 for the (m, y_0) plane in Figure 6.1. By looking at Figure 6.2 we note that the region explored by the CMB probe is

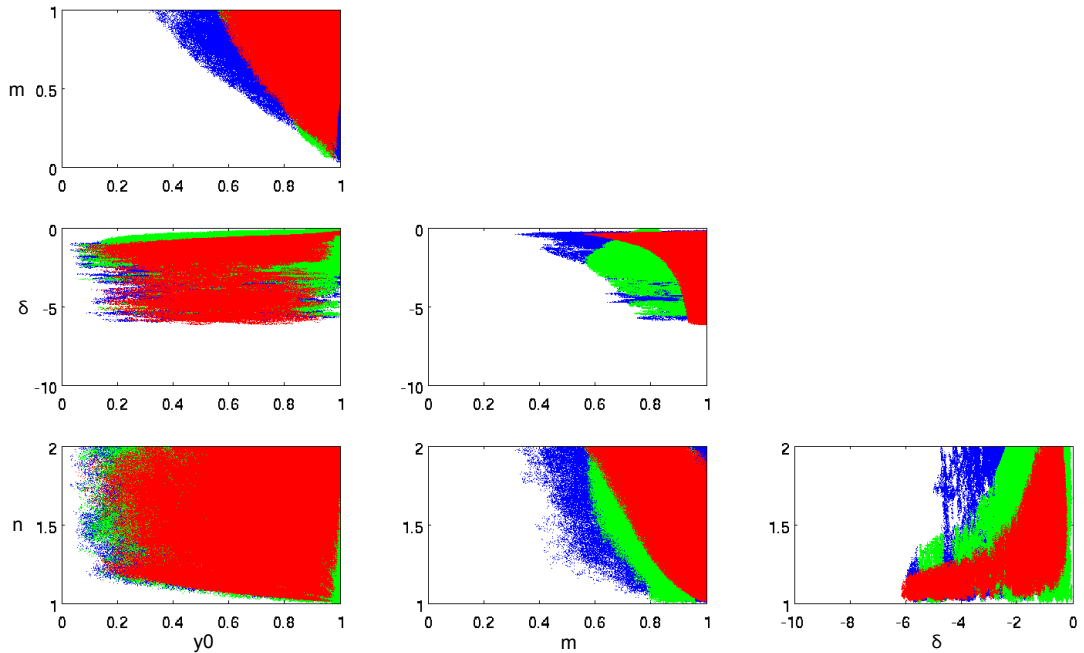


Figure 6.1: A series of overlay plots of 2-dimensional marginalised MCMC chains calculated separately for each cosmological probe used which were: SNe Ia redshift-magnitude relation (red), CMB shift parameter (green) and BAO distance parameter (blue).

slightly smaller than that of the SN probe, which lies on top of it in Figure 6.1. But we found that this is only the case in the (m, y_0) plane and therefore decided that the order of the BAO (blue), underneath all, CMB (green), in the middle and SN (red), on the top, as presented in Figure 6.1 is the best way to illustrate the results. This way the largest region would be placed underneath and the smallest would be on the top hence clearly demonstrating overlaps.

Looking at the plots in Figure 6.1 we can see that there appears to exist regions in all the 2-dimensional marginal distributions where all the probes overlap, thus indicating a possible fit to the data used. However, we should remember that we are looking at marginal plots and hence we could indeed be dealing with the same projection effect we saw earlier in Chapter 5. Therefore we decided to carry out some more rigorous numerical checks. To do this we selected one of the

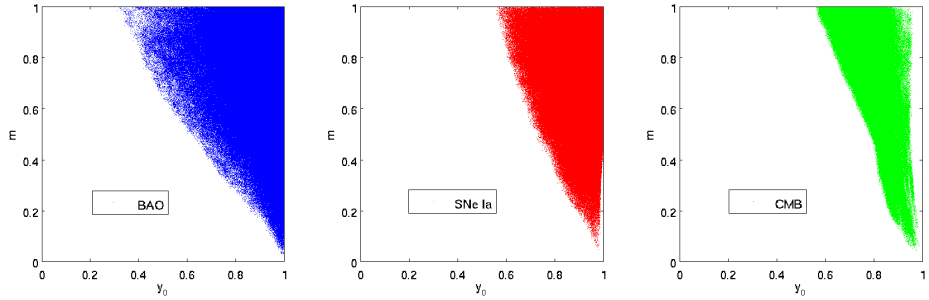


Figure 6.2: The (m, y_0) plane of Figure 6.1 separated out into the three probes' marginals to illustrate the relative sizes of these. As labelled, the colours blue, red and green correspond to the marginals of the probes BAO, SNe Ia and CMB shift parameter respectively.

probes (e.g. the CMB shift parameter) and ordered its MCMC chain by descending likelihood, in order to identify the $\Delta\chi^2$ corresponding to the top 68% of the chain. We called this $\Delta\chi^2$ the critical $\Delta\chi^2$ which, for a fully converged chain (as we believe our chain was) would correspond to the 1σ credible region of the posterior pdf.

Then for all the points in the top 68% of the other two chains of SNe Ia and BAO we calculated the CMB shift parameter $\Delta\chi^2$'s. By doing this we could examine whether or not these $\Delta\chi^2$'s were smaller than the critical shift parameter $\Delta\chi^2$ and thus also lie within the 1σ credible region of the CMB shift parameter posterior pdf. In this way we could make absolutely sure whether an overlap in the 68% credible regions existed.

In effect, we “thinned” our SNe Ia and BAO chains to only include those point (if any) which lay within the 1σ credible region of the CMB shift parameter.

The result of this investigation was positive and we can firmly say that we could obtain a fit to the SNe Ia, CMB shift parameter and the BAO distance parameter by relaxing the fixed m assumption. In Figure 6.3 we attempt to show this result by presenting our thinned

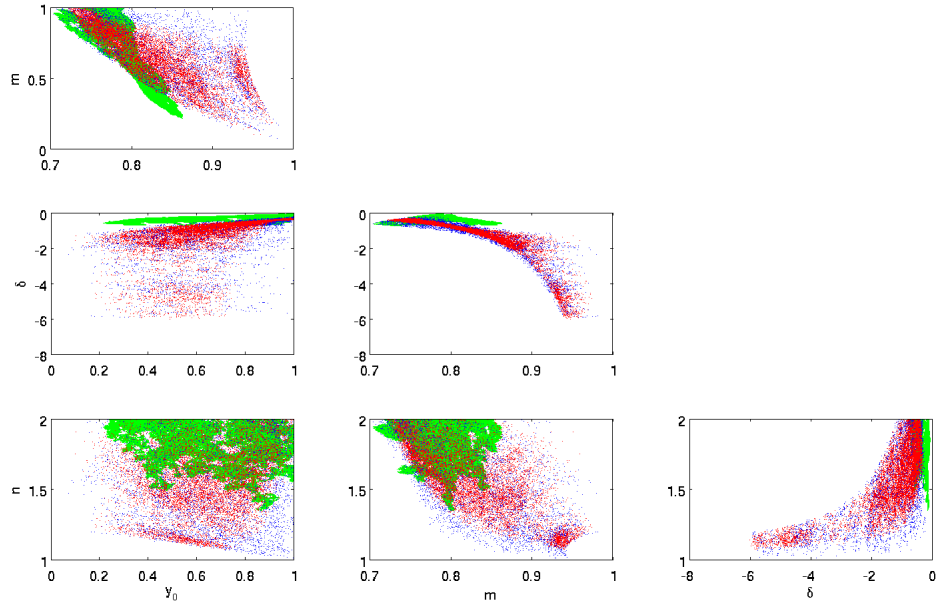


Figure 6.3: A series of overlay plots of 2-dimensional marginalised “thinned” MCMC chains of SNe Ia (red) and BAO (blue) probes in light of the CMB shift parameter. Also shown is the top 68% of the CMB shift parameter chain (green). By “thinning” it is meant that only the points in the SNe Ia and BAO chains which lie within the 68% of the CMB shift parameter chain are shown. To better illustrate the overlap, the CMB shift parameter chain is underneath the other two chains, the BAO chain is in the middle and the SNe Ia chain lies on the top.

out marginal SNe Ia (red) and BAO (blue) chains together with the marginal top 68% of the CMB shift parameter chain (green). Looking at Figure 6.3 one can see that there exists an overlap between the three probes’ chains hence indicating a fit.

As promised we will also show the results with the acoustic scale included in the analysis. The resulting plots are shown in Figure 6.4, where the yellow chains of acoustic scale have been laid on top of the rest.

One can see the same apparent overlapping of the different probes’ marginals. Therefore we performed the same checks as in the previous case to reach definite results. The results of this check was however negative. That is, we did not find any points in the acoustic scale

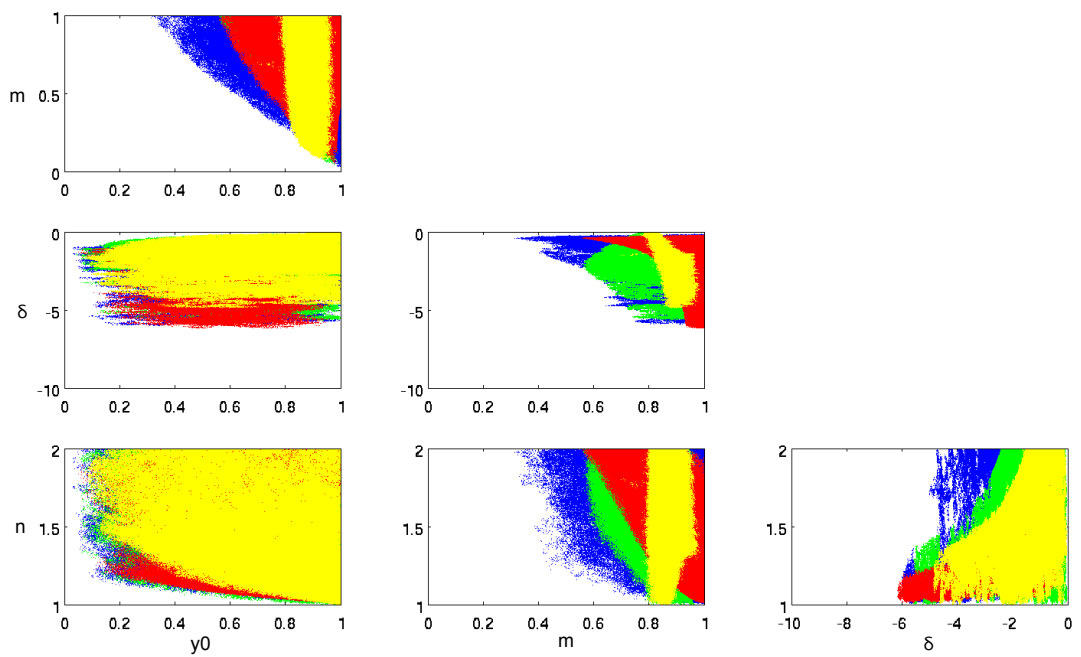


Figure 6.4: A series of overlay plots of 2-dimensional marginalised MCMC chains calculated separately for each cosmological probe used which were: SNe Ia redshift-magnitude relation (red), CMB shift parameter and acoustic scale (green and yellow respectively) and BAO distance parameter (blue).

chain that laid within the 1σ credible region of the shift parameter.

Thus, we have found out that when one includes the acoustic scale in confronting the SFS model with the data when one relaxes the fixed m assumption, one does not obtain a fit.

6.1 Conclusions

This chapter concerned the consequences of varying the parameter m from its fixed value of $2/3$ which was the assumption in Chapter 5 and which ensured that the SFS model reduced to the standard Einstein-de Sitter universe at early times. Hence we discussed the physical interpretation of letting m vary and also questioned the applicability of the acoustic scale for this investigation since this probe is related to the standard early universe properties which is arguably not the case when one allows m to take up values other than $2/3$. We then presented the results of our investigations of the problem and showed that in the varied m case one indeed obtains a fit to the SNe Ia, CMB shift parameter and the BAO distance parameter but not the acoustic scale.

Chapter 7

Concluding Remarks

Current observations of SNe Ia, the CMB and the large scale structure have shown not to be able to exclude the possibility that dark energy could be in the form of phantom energy with an equation of state $w < -1$ [17, 18, 19]. The value of w could have drastic consequences for the final state of the universe and in particular in the case of phantom dark energy ($w < -1$) leads the universe towards a Big Rip singularity where the universe down to its smallest constituents is ripped apart by the phantom-driven super acceleration. The possibility of occurrence of such a fate for the universe prompted cosmologists to look for various other exotic end days for the universe. The Sudden Future Singularity is one such fate which was first proposed by Barrow [41].

In addition to discovering such a possible event for the future evolution of the universe, Barrow constructed an example model which could accommodate such an event. Indeed a theoretical model bears no value if it does not conform to observational data. And this is exactly what Dabrowski et al. [1] thought regarding the SFS model. Hence they confronted it with SNe Ia data and showed that there exist a set of model parameters for which a fit to the data is obtained and which

corresponds to an SFS occurring in 8.7 million years' time. What we have done in this thesis has been to go one step (or perhaps more than one!) further to investigate whether the SFS model of Barrow indeed conforms to other available datasets from the CMB to the large scale structure.

In Chapter 2 we introduced the theory behind the SFS model examining its characteristics and discussing its free parameters. In particular we gave details of our scrutinising of the model parameters in light of established observational facts like the current expansion and acceleration of the universe. We then discussed our data analysis methodology in Chapter 3, where we made the case that a Bayesian framework was indeed the suitable choice for our analysis, being in the cosmological context and hence limited to observations from only one universe. Furthermore, in Chapter 4 we gave a detailed account of the observational data we employed in our investigations taking care to clarify the justification of using each probe i.e. the applicability of each to our non-standard model fitting. The cosmological probes we employed were: The SNe Ia redshift-magnitude relation, CMB shift parameter, R , acoustic scale, l_a , the BAO distance parameter, A , the Hubble constant, H_0 and the age of the universe, t_0 . Finally, we presented the results of our investigations in Chapters 5 and 6.

In summary our findings indicate that the SFS model does not appear to fit all the cosmological probes employed in our analysis when we fix the parameter $m = 2/3$, which ensures that our model reduces to the standard Einstein-de Sitter model at early times. We noted that while one could obtain a fit to the Union2 SNe Ia [17] and the SDSS BAO data [19] the same model parameters did not fit the CMB data of WMAP7 [18]. These results were given in Chapter 5. In Chapter 6 we considered the case of allowing the value of m to vary within

its theoretically allowed range, $0 < m < 1$. Whether it is physically justifiable to vary m from $2/3$ i.e. to change the standard Einstein-de Sitter early universe to some other “non-standard” one remains an open question. Nonetheless, we carried out the same tests as in the $m = 2/3$ case. We found that indeed an overall fit to the SNe Ia, CMB shift parameter and the BAO distance parameter may be achieved but not when we include the acoustic scale in this analysis. To recap from Chapter 4, Wang and Mukherjee [92] found that in order to place tight constraints on one’s model from the CMB data, one ought to use the shift parameter and the acoustic scale in conjunction with one another. With this in mind, one can see that there is no overall fit to the data in the varied m case with the predicted acoustic scale not showing a fit to the data while the shift parameter does.

As a final note in this section we would like to point out once again the remark made in the beginning of Chapter 3, that if a theoretical model does not reproduce the observed data its usefulness in progressing our knowledge of nature may be questioned.

A P P E N D I X A

SFS Hubble Function

Here we will continue our discussion of the special form of the function $E(z)$ proposed for the SFS. Denkiewicz et al. in [97] show that such a $E(z)$ could take the form:

$$E(z)^2 = \Omega_{\text{SFS}}(1+z)^3 \exp \left[\int_0^z dz \frac{2q(z) - 1}{1+z} \right], \quad (\text{A.1})$$

where Ω_{SFS} is the density parameter of the SFS fluid. To compare this expression with the standard form of this function, we recall $E(z)$ in the standard model as:

$$E(z)^2 = \Omega_m(1+z)^3 + \Omega_\Lambda(1+z)^{3(w+1)}, \quad (\text{A.2})$$

where the Ω_m and Ω_Λ correspond to the dark matter and dark energy density parameters and the radiation and curvature terms are neglected.

One can check the behaviour of the function in Equation A.1 e.g. in early and late time cosmological epochs of matter domination and dark energy domination respectively. We know that for a universe with dark matter and dark energy the deceleration parameter takes

the form:

$$q(z) = \frac{\Omega_m}{2} - \Omega_\Lambda, \quad (\text{A.3})$$

where Ω_m and Ω_Λ are the dark matter and dark energy density parameters. In the early matter dominated era (i.e. in an Einstein-de Sitter universe), we have $\Omega_m = 1$ and $\Omega_\Lambda = 0$ therefore $q(z) = 1/2$ which when substituted back into Equation A.1 yields:

$$E^2(z) = \Omega_{\text{SFS}}(1+z)^3. \quad (\text{A.4})$$

This is exactly the type of evolution we have in the standard matter dominated universe. Furthermore for the late Λ -dominated universe, (i.e. in a de Sitter universe) we have $\Omega_m = 0$ and $\Omega_\Lambda = 1$, we get $q(z) = -1$ which when substituted into Equation A.1 we obtain the following:

$$E^2(z) = \Omega_{\text{SFS}}. \quad (\text{A.5})$$

This is again the type of evolution we would expect to see in a dark energy dominated universe.

Bibliography

- [1] M. P. Dabrowski, T. Denkiewicz, and M. A. Hendry. How far is it to a sudden future singularity of pressure? *Phys. Rev.*, D75:123524, 2007.
- [2] D. Scott. The standard cosmological model. 2005. <http://arxiv.org/abs/astro-ph/0510731>.
- [3] A. Liddle. *An Introduction to Modern cosmology*. John Wiley & Sons, 2003.
- [4] M. S. Turner. Cosmology solved? Maybe. *Nucl. Phys. Proc. Suppl.*, 72:69, 1999.
- [5] E. Hubble. A Relation between Distance and Radial Velocity among Extra-Galactic Nebulae. *Proceedings of the National Academy of Science*, 15, 1929.
- [6] M. Rowan-Robinson. *Cosmology*. Oxford University Press, 4th edition, 2004.
- [7] A. G. Riess et al. A 3% Solution: Determination of the Hubble Constant with the Hubble Space Telescope and Wide Field Camera 3. *Astrophys. J.*, 730:119, 2011.
- [8] P. J. E. Peebles. *Principles of Physical Cosmology*. Princeton University Press, 1993.

-
- [9] W. L. Freedman et al. Final Results from the Hubble Space Telescope Key Project to Measure the Hubble Constant. *Astrophys. J.*, 553:47–72, 2001.
- [10] S. Dodelson. *Modern cosmology*. Academic Press, 2003.
- [11] A. G. Riess et al. Observational Evidence from Supernovae for an Accelerating Universe and a Cosmological Constant. *Astron. J.*, 116:1009–1038, 1998.
- [12] S. Perlmutter et al. Measurements of Omega and Lambda from 42 High-Redshift Supernovae. *Astrophys. J.*, 517:565–586, 1999.
- [13] V. Sahni and A. A. Starobinsky. The Case for a Positive Cosmological Lambda-term. *Int. J. Mod. Phys.*, D9:373–444, 2000.
- [14] C. Armendariz-Picon, V. F. Mukhanov, and P. J. Steinhardt. A dynamical solution to the problem of a small cosmological constant and late-time cosmic acceleration. *Phys. Rev. Lett.*, 85:4438–4441, 2000.
- [15] C. Armendariz-Picon, V. F. Mukhanov, and P. J. Steinhardt. Essentials of k-essence. *Phys. Rev.*, D63:103510, 2001.
- [16] G. W. Gibbons. Cosmological evolution of the rolling tachyon. *Phys. Lett.*, B537:1–4, 2002.
- [17] R. Amanullah et al. Spectra and Light Curves of Six Type Ia Supernovae at $0.511 < z < 1.12$ and the Union2 Compilation. *Astrophys. J.*, 716:712–738, 2010.
- [18] E. Komatsu et al. Seven-Year Wilkinson Microwave Anisotropy Probe (WMAP) Observations: Cosmological Interpretation. *Astrophys. J. Suppl.*, 192:18, 2011.

-
- [19] W. J. Percival et al. Baryon Acoustic Oscillations in the Sloan Digital Sky Survey Data Release 7 Galaxy Sample. *Mon. Not. Roy. Astron. Soc.*, 401:2148–2168, 2010.
- [20] Supernova Cosmology Project. <http://supernova.lbl.gov/>.
- [21] R. A. Knop et al. New Constraints on Ω_M , Ω_Λ , and w from an Independent Set of Eleven High-Redshift Supernovae Observed with HST. *Astrophys. J.*, 598:102–137, 2003.
- [22] R. A. Alpher, H. Bethe, and G. Gamow. The origin of chemical elements. *Phys. Rev.*, 73(7):803–804, 1948.
- [23] A. A. Penzias and R. W. Wilson. A Measurement of Excess Antenna Temperature at 4080 Mc/s. *Astrophys. J.*, 142:419–421, 1965.
- [24] G. F. Smoot et al. Structure in the COBE differential microwave radiometer first-year maps. *Astrophys. J.*, 396:L1–L5, 1992.
- [25] G. Hinshaw et al. Five-Year Wilkinson Microwave Anisotropy Probe (WMAP) Observations: Data Processing, Sky Maps, & Basic Results. *Astrophys. J. Suppl.*, 180:225–245, 2009.
- [26] *The Scientific programme of planck*. 2006. <http://arxiv.org/abs/astro-ph/0604069>.
- [27] S. Cole et al. The 2dF Galaxy Redshift Survey: Power-spectrum analysis of the final dataset and cosmological implications. *Mon. Not. Roy. Astron. Soc.*, 362:505–534, 2005.
- [28] D. J. Eisenstein et al. Detection of the Baryon Acoustic Peak in the Large-Scale Correlation Function of SDSS Luminous Red Galaxies. *Astrophys. J.*, 633:560–574, 2005.
- [29] Sloan Digital Sky Survey. <http://www.sdss.org/>.

-
- [30] A. G. Riess et al. A Redetermination of the Hubble Constant with the Hubble Space Telescope from a Differential Distance Ladder. *Astrophys. J.*, 699:539–563, 2009.
- [31] R. Frost 1916. *Fire and Ice*, from Collected Poems of Robert Frost. Published by Holt & Co., 1930.
- [32] L. M. Krauss and M. S. Turner. Geometry and destiny. *Gen. Rel. Grav.*, 31:1453–1459, 1999.
- [33] R. R. Caldwell. A Phantom Menace? *Phys. Lett.*, B545:23–29, 2002.
- [34] R. R. Caldwell, Rahul Dave, and Paul J. Steinhardt. Cosmological Imprint of an Energy Component with General Equation-of-State. *Phys. Rev. Lett.*, 80:1582–1585, 1998.
- [35] R. R. Caldwell, M. Kamionkowski, and N. N. Weinberg. Phantom Energy and Cosmic Doomsday. *Phys. Rev. Lett.*, 91:071301, 2003.
- [36] L. Fernandez-Jambrina and R. Lazkoz. Geodesic behaviour of sudden future singularities. *Phys. Rev.*, D70:121503, 2004.
- [37] L. Fernandez-Jambrina and R. Lazkoz. Classification of cosmological milestones. *Phys. Rev.*, D74:064030, 2006.
- [38] L. Fernandez-Jambrina and R. Lazkoz. Singular fate of the universe in modified theories of gravity. *Phys. Lett.*, B670:254–258, 2009.
- [39] S. Nojiri, S. D. Odintsov, and S. Tsujikawa. Properties of singularities in (phantom) dark energy universe. *Phys. Rev.*, D71:063004, 2005.

-
- [40] M. P. Dabrowski and T. Denkiewicz. Exotic-singularity-driven dark energy. *AIP Conf. Proc.*, 1241:561–570, 2010.
- [41] J. D. Barrow. Sudden Future Singularities. *Class. Quant. Grav.*, 21:L79–L82, 2004.
- [42] C. Cattoen and M. Visser. Necessary and sufficient conditions for big bangs, bounces, crunches, rips, sudden singularities, and extremality events. *Class. Quant. Grav.*, 22:4913–4930, 2005.
- [43] E. J. Copeland, M. Sami, and S. Tsujikawa. Dynamics of dark energy. *Int. J. Mod. Phys.*, D15:1753–1936, 2006.
- [44] S. Nojiri and S. D. Odintsov. The final state and thermodynamics of dark energy universe. *Phys. Rev.*, D70:103522, 2004.
- [45] M. Bouhmadi-Lopez, P. F. Gonzalez-Diaz, and P. Martin-Moruno. Worse than a big rip? *Phys. Lett.*, B659:1–5, 2008.
- [46] A. V. Yurov, P. Martin-Moruno, and P. F. Gonzalez-Diaz. New ‘Bigs’ in cosmology. *Nucl. Phys.*, B759:320–341, 2006.
- [47] M. Bouhmadi-Lopez, P. F. Gonzalez-Diaz, and P. Martin-Moruno. On the generalised Chaplygin gas: worse than a big rip or quieter than a sudden singularity? *Int. J. Mod. Phys.*, D17:2269–2290, 2008.
- [48] A. Yu. Kamenshchik, U. Moschella, and V. Pasquier. An alternative to quintessence. *Phys. Lett.*, B511:265–268, 2001.
- [49] M. C. Bento, O. Bertolami, and A. A. Sen. The revival of the unified dark energy - dark matter model? *Phys. Rev.*, D70:083519, 2004.

-
- [50] A. V. Yurov, A. V. Astashenok, and P. F. Gonzalez-Diaz. Astronomical bounds on future big freeze singularity. *Grav. Cosmol.*, 14:205–212, 2008.
- [51] A. G. Riess et al. New Hubble Space Telescope Discoveries of Type Ia Supernovae at $z > 1$: Narrowing Constraints on the Early Behavior of Dark Energy. *Astrophys. J.*, 659:98–121, 2007.
- [52] V. Gorini, A. Yu. Kamenshchik, U. Moschella, and V. Pasquier. Tachyons, scalar fields and cosmology. *Phys. Rev.*, D69:123512, 2004.
- [53] Z. Keresztes, L. A. Gergely, V. Gorini, U. Moschella, and A. Yu. Kamenshchik. Tachyon cosmology, supernovae data and the Big Brake singularity. *Phys. Rev.*, D79:083504, 2009.
- [54] L. Fernandez-Jambrina and R. Lazkoz. Equation of state and singularities in FLRW cosmological models. *J. Phys. Conf. Ser.*, 229:012037, 2010.
- [55] J. D. Barrow and C. G. Tsagas. New Isotropic and Anisotropic Sudden Singularities. *Class. Quant. Grav.*, 22:1563–1571, 2005.
- [56] L. Fernandez-Jambrina. w -cosmological singularities. *Phys. Rev.*, D82:124004, 2010.
- [57] M. P. Dabrowski and T. Denkiwicz. w -singularities. *Phys. Rev.*, D79:063521, 2009.
- [58] J. D. Neill et al. The Supernova Type Ia Rate Evolution with SNLS. *AIP Conf. Proc.*, 924:421–424, 2007.
- [59] K. Lake. Sudden future singularities in FLRW cosmologies. *Class. Quant. Grav.*, 21:L129, 2004.

-
- [60] S. W. Hawking and G. F. R Ellis. *The Large Scale Structure of Space-Time*. Cambridge University Press, 1973.
- [61] M. Visser. General Relativistic Energy Conditions: The Hubble expansion in the epoch of galaxy formation. *Phys. Rev.*, D56:7578–7587, 1997.
- [62] M. Visser and C. Barcelo. Energy conditions and their cosmological implications. *Plenary talk presented at Cosmo99*, 1999. <http://arxiv.org/abs/gr-qc/0001099>.
- [63] P. Schuecker et al. Observational Constraints on General Relativistic Energy Conditions, Cosmic Matter Density and Dark Energy from X- Ray Clusters of Galaxies and Type-Ia Supernovae. *Astron. Astrophys.*, 402:53–64, 2003.
- [64] C. Cattoen and M. Visser. Cosmological milestones and energy conditions. *J. Phys. Conf. Ser.*, 68:012011, 2007.
- [65] C. Barcelo and M. Visser. Twilight for the energy conditions? *Int. J. Mod. Phys.*, D11:1553–1560, 2002.
- [66] M. P. Dabrowski. Statefinders, higher-order energy conditions, and sudden future singularities. *Phys. Lett.*, B625:184–188, 2005.
- [67] A. G. Riess et al. Type Ia Supernova Discoveries at $z < 1$ From the Hubble Space Telescope: Evidence for Past Deceleration and Constraints on Dark Energy Evolution. *Astrophys. J.*, 607:665–687, 2004.
- [68] J. D. Barrow. More general sudden singularities. *Class. Quant. Grav.*, 21:5619–5622, 2004.
- [69] S. Nojiri and S. D. Odintsov. Quantum escape of sudden future singularity. *Phys. Lett.*, B595:1–8, 2004.

-
- [70] S. Nojiri and S. D. Odintsov. The final state and thermodynamics of dark energy universe. *Phys. Rev.*, D70:103522, 2004.
- [71] M. Sami, P. Singh, and S. Tsujikawa. Avoidance of future singularities in loop quantum cosmology. *Phys. Rev.*, D74:043514, 2006.
- [72] M. P. Dabrowski. Inhomogenized sudden future singularities. *Phys. Rev.*, D71:103505, 2005.
- [73] J. D. Barrow, A. B. Batista, J. C. Fabris, and S. Houndjo. Quantum Particle Production at Sudden Singularities. *Phys. Rev.*, D78:123508, 2008.
- [74] Y. Shtanov and V. Sahni. Unusual cosmological singularities in braneworld models. *Class. Quant. Grav.*, 19:L101–L107, 2002.
- [75] U. Alam and V. Sahni. Confronting Braneworld Cosmology with Supernova data and Baryon Oscillations. *Phys. Rev.*, D73:084024, 2006.
- [76] T. Koivisto. Dynamics of Nonlocal Cosmology. *Phys. Rev.*, D77:123513, 2008.
- [77] M. C. B. Abdalla, S. Nojiri, and S. D. Odintsov. Consistent modified gravity: Dark energy, acceleration and the absence of cosmic doomsday. *Class. Quant. Grav.*, 22:L35, 2005.
- [78] S. Nojiri and S. D. Odintsov. Is the future universe singular: Dark Matter versus modified gravity? *Phys. Lett.*, B686:44–48, 2010.
- [79] M. Bouhmadi-Lopez, P. F. Gonzalez-Diaz, and P. Martin-Moruno. On the generalised Chaplygin gas: worse than a big rip or quieter than a sudden singularity? *Int. J. Mod. Phys.*, D17:2269–2290, 2008.

-
- [80] S. Nojiri and S. D. Odintsov. The oscillating dark energy: Future singularity and coincidence problem. *Phys. Lett.*, B637:139–148, 2006.
- [81] H. Stefancic. 'Expansion' around the vacuum equation of state: Sudden future singularities and asymptotic behavior. *Phys. Rev.*, D71:084024, 2005.
- [82] C. Uggla. Spacetime singularities. *Einstein Online*, 2:1002, 2006.
- [83] G. F. R. Ellis and B. G. Schmit. Singular Space-Times. *General Relativity and Gravitation*, 8(11):915–953, 1977.
- [84] Tipler F. J. Singularities in Conformally Flat Spacetimes. *Physics Letters*, 64A(1), 1977.
- [85] Krolak A. Towards the proof of the cosmic censorship theorem. *Class. Quant. Grav.*, 3:267–280, 1986.
- [86] A. Balcerzak and M. P. Dabrowski. Strings at future singularities. *Phys. Rev.*, D73:101301, 2006.
- [87] S. Cotsakis and I. Klaoudatou. Future singularities of isotropic cosmologies. *J. Geom. Phys.*, 55:306–315, 2005.
- [88] P. C. Gregory. *Bayesian Logical Data Analysis for the Physical Sciences*. Cambridge University Press, 2005.
- [89] D. S. Sivia and J. Skilling. *Data Analysis: A Bayesian Tutorial*. Oxford University Press, 2nd edition, 2006.
- [90] M. Kowalski et al. Improved Cosmological Constraints from New, Old and Combined Supernova Datasets. *Astrophys. J.*, 686:749–778, 2008.

-
- [91] H. Ghodsi, M. A. Hendry, M. P. Dabrowski, and T. Denkiewicz. Sudden Future Singularity models as an alternative to Dark Energy? *Mon. Not. Roy. Astron. Soc.*, 414:1517–1525, 2011.
- [92] Y. Wang and P. Mukherjee. Observational Constraints on Dark Energy and Cosmic Curvature. *Phys. Rev.*, D76:103533, 2007.
- [93] S. Nesseris and L. Perivolaropoulos. Crossing the Phantom Divide: Theoretical Implications and Observational Status. *J. Cosmo. Astropart. Phys*, 0701:018, 2007.
- [94] O. Elgaroy and T. Multamaki. On using the CMB shift parameter in tests of models of dark energy. *Astron. Astrophys.*, 471:65–70, 2007.
- [95] E. Komatsu et al. Five-Year Wilkinson Microwave Anisotropy Probe (WMAP) Observations:Cosmological Interpretation. *Astrophys. J. Suppl.*, 180:330–376, 2009.
- [96] O. Elgaroy and T. Multamaki. Cosmic acceleration and extra dimensions: Constraints on modifications of the Friedmann equation. *Mon. Not. Roy. Astron. Soc.*, 356:475–479, 2005.
- [97] T. Denkiewicz, M. P. Dabrowski, H. Ghodsi, and M. A. Hendry. Cosmological tests of sudden future singularities. *Phys. Rev., D*, 2011. In preparation.
- [98] A. Shafieloo, U. Alam, V. Sahni, and A. A. Starobinsky. Smoothing Supernova Data to Reconstruct the Expansion History of the Universe and its Age. *Mon. Not. Roy. Astron. Soc.*, 366:1081–1095, 2006.
- [99] J. Sola and H. Stefancic. Effective equation of state for dark energy: mimicking quintessence and phantom energy through a variable Lambda. *Phys. Lett.*, B624:147–157, 2005.

-
- [100] S. Carneiro, M. A. Dantas, C. Pigozzo, and J. S. Alcaniz. Observational constraints on late-time $\Lambda(t)$ cosmology. *Phys. Rev.*, D77:083504, 2008.
- [101] D. J. Eisenstein and W. Hu. Baryonic Features in the Matter Transfer Function. *Astrophys. J.*, 496:605, 1998.
- [102] A. Balbi, M. Bruni, and C. Quercellini. Lambda-alpha DM: Observational constraints on unified dark matter with constant speed of sound. *Phys. Rev.*, D76:103519, 2007.
- [103] L. M. Krauss and B. Chaboyer. New Globular Cluster Age Estimates and Constraints on the Cosmic Equation of State and The Matter Density of the Universe. 2001. <http://arxiv.org/abs/astro-ph/0111597>.